AD699424

MEMORANDUM 36

REAL-TIME IMPLEMENTATION

OF THE KALMAN FILTER FOR TRAJECTORY ESTIMATION

Distribution:

Gardiner	Salmon
Dressler	Wong
Meier	Eikelman
Ho	Fraser
Kashiwagi	Yabroff
Keckler	Albritton
Korsak	Balote
Lombard	Roscher
Luenberger	Weinstein
Ratner	Branch

Davidson, NXPO
Montgomery, NXPO
Smith, NXPO
Wells, NXPO
Young, NXPO

Prepared by:

Robert M. Dressler
Dale W. Ross
June 1968

Project 5188-305

99

CONTENTS

ILLUSTRATIONS

TABLES

REAL-TIME IMPLEMENTATION OF THE KALMAN FILTER
FOR TRAJECTORY ESTIMATION

I INTRODUCTION

The purpose of this technical memorandum is to describe the results
of a study concerned with real-time implementation of the Kalman filter
for estimating ballistic trajectories. As shown in previous studies[1],[2]*
performed by the Information and Control Laboratory in support of the
NIKE-X system, the performance of the Kalman filter for the trajectory
estimation task is excellent; however, the computation time required
by this filter is relatively large. On the Univac 1108 computer, the com-
putation time per filter iteration is approximately 0.010 sec for endo-
atmospheric estimation; hence, with a data rate of 20 measurements per
second, the filter runs about 5 times faster than real time. For exo-
atmospheric estimation (in which the filter has 6 states instead of 7,
and is programmed in double precision--see Sec. VI), the filter's itera-
tion time is approximately 0.011 sec; hence, with a data rate of one
measurement per second, the filter runs about 100 times faster than real
time.

For real-time estimation of multiple targets, the computation speed
of the Kalman filter may be inadequate (at least for endoatmospheric
trajectory estimation). Thus, it is essential to improve the computa-
tional efficiency of the filtering algorithm; this should be done with
a minimum amount of degradation in filter performance.

In Sec. II, the problem formulation is presented; this consists
of the equations of motion for the ballistic reentry vehicle and the
radar measurement equations. The equations for the extended Kalman
filter and a flow diagram depicting its operation are given in Sec. III.

In Secs. III and IV several approaches that may be used to modify
the Kalman filtering algorithm in order to reduce the computational
requirements are described; these include

---

*References are listed at the end of the report.

1

(1) Use of a precomputed approximation to the weighting matrix in the filter equations (this also eliminates the necessity of calculating the covariance matrices); i.e., the weighting matrix is precomputed off-line, rather than calculated recursively on-line.

(2) Increasing the sample interval (data processing interval) Δt, the computation speed of the filter relative to real time increases as this parameter increases.

(3) Updating the weighting matrix and the covariance matrices at intervals of $\Delta \tau$ sec, where $\frac{\Delta \tau}{\Delta t} = N \geq 1$, i.e., the weighting matrix is only updated every N iterations and is held constant in the filter equations for these iterations, before being updated anew. This computational algorithm will be referred to as the piecewise-recursive Kalman filter.

The first approach was studied extensively in Ref. 1; the other two approaches will be investigated in considerable detail in this report. These approaches were evaluated and compared by estimating the states of a ballistic trajectory based on simulated radar measurements that are corrupted by noise; the simulated trajectories were generated from an accurate model of reentry dynamics. The numerical results that were obtained in this study are presented in Sec. V (for endoatmospheric estimation) and Sec. VI (for exoatmospheric estimation). Estimation errors in position, velocity, and acceleration, and the actual and estimated β are plotted as functions of time for the various computer runs. In addition, the computation times (on the Univac 1108) per iteration for the different filter algorithms are presented.

For real-time estimation of multiple targets, the piecewise-recursive Kalman filter is the most promising approach of those considered in this report. For endoatmospheric estimation, it is possible to filter measurements at a computational speed (on the Univac 1108) that is approximately 20 or 25 times faster than real time (for $\Delta t = 0.05$ sec, $\Delta \tau = 0.5$ sec or $\Delta t = 0.10$ sec, $\Delta \tau = 0.5$ sec, respectively) and yet obtain accuracy approaching that of the fully implemented Kalman filter; for exoatmospheric estimation, the computational speed (on the Univac 1108) is approximately 500 times faster than real time (for $\Delta t = 1.0$ sec, $\Delta \tau = 20$ sec).

2

The last section of the report summarizes the results of this study and indicates areas for future work.

II   PROBLEM FORMULATION

A.   Equations of Motion for the Ballistic Reentry Vehicle

A model for the equations of motion for the ballistic reentry vehicle is taken to be[*]

$$\ddot{x} = -2\omega(\dot{z} \cos \ell - \dot{y} \sin \ell) + \omega^2 x - \frac{1}{2} \frac{\rho g_o}{\beta} V\dot{x} - g \frac{x}{r_1}$$

$$\ddot{y} = -2\omega(\dot{x} \sin \ell) - \omega^2 \sin \ell [(r_o + z) \cos \ell - y \sin \ell] - \frac{1}{2} \frac{\rho g_o}{\beta} V\dot{y} - g \frac{y}{r_1}$$

$$\ddot{z} = 2\omega(\dot{x} \cos \ell) + \omega^2 \cos \ell [(r_o + z) \cos \ell - y \sin \ell] - \frac{1}{2} \frac{\rho g_o}{\beta} V\dot{z} - g \frac{z+r_o}{r_1}, \quad (1)$$

where x, y, z are the radar-centered cartesian coordinates (ft) of the ballistic missile, and

ρ = atmospheric density (slug/ft^3)

β = ballistic coefficient (lb/ft^2)

$V = \sqrt{\dot{x}^2 + \dot{y}^2 + \dot{z}^2}$

    = missile velocity (ft/sec)

$g = g_o \dfrac{r_o^2}{r_1^2}$

    = gravitational acceleration acting upon the missile (ft/sec^2)

g_o = gravitational acceleration at sea level (ft/sec^2)

r_o = earth radius (ft)

$r_1 = \sqrt{x^2 + y^2 + (z + r_o)^2}$

    = distance from center of the earth to the missile (ft)

ω = rotation rate of the earth (rad/sec)

ℓ = latitude of the radar site.

---

[*]A derivation of these equations is presented in Memorandum 37[3] and, hence, will not be repeated here.

The x and y axes point east and north, respectively, and define a plane tangent to the earth at the radar site; the z axis is perpendicular to this plane and gives the vertical direction at the radar site. The density ρ is a function of environmental factors and the altitude h, which is given by

$$h = r_1 - r_o = [x^2 + y^2 + (z + r_o)^2]^{\frac{1}{2}} - r_o \quad . \tag{2}$$

The ballistic coefficient β is a function of altitude, Mach number, and unknown reentry vehicle parameters.

Finally, it should be noted that the above model assumes a rotating, spherical earth with the ballistic missile taken to be a point mass. That is, the model given by Eqs. (1) includes coriolis terms (those containing ω), centripetal terms (those containing ω^2), gravity gradient terms (those containing g), and drag terms (those containing β).

Because β is highly dependent on the characteristics of the missile being tracked, it must be estimated together with the position and velocity state variables. This estimate is also necessary for prediction of the future missile trajectory. As shown in Ref. 1, the performance of the estimator is significantly improved if the quantity ρ/β is estimated, where β is assumed to be locally constant and ρ is assumed to be a locally exponential function of the altitude h, i.e., it is assumed that ρ has an altitude gradient,

$$\frac{\partial \rho}{\partial h} = - K \rho \, , \tag{3}$$

in which K is a specified constant over each of several ranges of altitude (h). Hence, the differential equation that models the behavior of the additional state variable ρ/β is given by

$$\left(\frac{\rho}{\beta} \right)^{\cdot} = - K \dot{h} \left(\frac{\rho}{\beta} \right)$$

$$= - K \frac{x \dot{x} + y \dot{y} + (z + r_o)\dot{z}}{r_1} \left(\frac{\rho}{\beta} \right) \quad , \tag{4}$$

where $\dot{h}$ is obtained from Eq. (2).

4

The state vector $\underline{x}$, which describes the trajectory of the ballistic missile, thus has seven components:

$$
\begin{aligned}
&x_1 = x && x_4 = \dot{x} \\
&x_2 = y && x_5 = \dot{y} && x_7 = \frac{\rho}{\beta} \qquad . \qquad (5)\\
&x_3 = z && x_6 = \dot{z}
\end{aligned}
$$

The nonlinear system equations (1) and (4) can then be written in state-variable form as follows:

$$
\dot{\underline{x}} = \underline{f}(\underline{x}) =
\begin{bmatrix}
x_4 \\[4pt]
x_5 \\[4pt]
x_6 \\[4pt]
-2\omega(x_6 \cos \ell - x_5 \sin \ell) + \omega^2 x_1 - \tfrac{1}{2} x_7 g_o V x_4 - g \dfrac{x_1}{r} \\[10pt]
-2\omega(x_4 \sin \ell) - \omega^2 \sin \ell [(r_o + x_3)\cos \ell - x_2 \sin \ell] - \tfrac{1}{2}x_7 g_o V x_5 - g \dfrac{x_2}{r_1} \\[10pt]
2\omega(x_4 \cos \ell) + \omega^2 \cos \ell [(r_o + x_3)\cos \ell - x_2 \sin \ell] - \tfrac{1}{2}x_7 g_o V x_6 - g \dfrac{x_3 + r_o}{r_1} \\[10pt]
- K x_7 \dfrac{x_1 x_4 + x_2 x_5 + (x_3 + r_o)x_6}{r_1}
\end{bmatrix}, \quad (6)
$$

where $\underline{f}(\underline{x})$ is a seven-dimensional vector function and

$$
V = \sqrt{x_4^2 + x_5^2 + x_6^2}
$$

$$
r_1 = \sqrt{x_1^2 + x_2^2 + (x_3 + r_o)^2}
$$

The nonlinear differential equation (6) is inexact because ρ and β do not exactly satisfy the assumptions made above, and also because the reentry vehicle has additional degrees of freedom that have been neglected. The actual trajectory of the ballistic missile (i.e., the trajectory to be estimated) is generated by a set of equations that are more accurate than the model described in Eq. (6). In order to account

5

for these inaccuracies as well as actual system disturbances, a random forcing function is introduced into Eq. (5), yielding

$$\dot{\underline{x}} = \underline{f}(\underline{x}) + \underline{w}' , \qquad (7)$$

where the seven-dimensional vector $\underline{w}'$ is assumed to be a zero-mean, white Gaussian noise process.

B. Radar Measurement Equations

Measurements of the target vehicle's position are made every Δt_o seconds by means of a phased-array radar. These measurements are made of the angles α, γ, and the range r, which are defined in the radar-face coordinate system of Fig. 1. The radar-face coordinates x_1', x_2', x_3' are related to the ground coordinates x_1, x_2, x_3 (or x, y, z) by the following two rotations: a rotation of $90^o - \tau$ from the vertical (x_3), and a rotation of ξ from north (x_2). Thus,
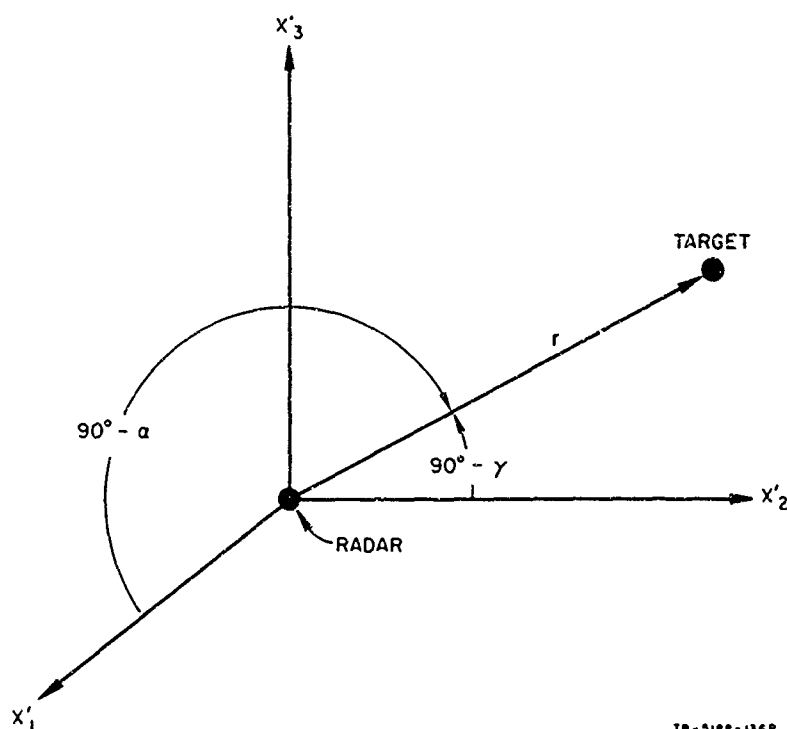
FIG. 1 RADAR MEASUREMENTS

6

$$\begin{bmatrix} x_1 \\ x_2 \\ x_3 \end{bmatrix} = M \begin{bmatrix} x_1' \\ x_2' \\ x_3' \end{bmatrix} \qquad (8)$$

where

$$M = \begin{bmatrix} \cos \xi & \sin \tau \sin \xi & \cos \tau \sin \xi \\ -\sin \xi & \sin \tau \cos \xi & \cos \tau \cos \xi \\ 0 & -\cos \tau & \sin \tau \end{bmatrix} \quad , \qquad (9)$$

and from Fig. 1,

$$x_1' = r \sin \alpha$$
$$x_2' = r \sin \gamma$$
$$x_3' = r \left[1 - \sin^2 \alpha - \sin^2 \gamma \right]^{\frac{1}{2}} \quad . \qquad (10)$$

Hence, the position coordinates x_1, x_2, x_3 are related to the radar coordinates r, α, γ by Eqs. (8), (9), and (10), with τ and ξ being known constants determined by the radar configuration. These non-linear relations can be expressed concisely as

$$\begin{bmatrix} r \\ \alpha \\ \gamma \end{bmatrix} = \underline{h}(x_1, x_2, x_3) = \underline{h}(\underline{x}) \qquad , \qquad (11)$$

where $\underline{h}(\underline{x})$ is a three-dimensional vector function. Thus, the nonlinear measurement equation is given by

$$\underline{z} = \underline{h}(\underline{x}) + \underline{v} \quad , \qquad (12)$$

where $\underline{z}$ is a three-dimensional vector containing the noise-corrupted measurements of r, α, γ and the radar measurement noise $\underline{v}$ is assumed to be a zero-mean, white Gaussian noise process.

7

III   EXTENDED KALMAN FILTER

A.   Estimation Equations

The Kalman filter equations specify an estimate of the state of a
linear, time-varying dynamical system observed sequentially in the
presence of additive white Gaussian noise; the state estimate obtained
at each time is the maximum likelihood estimate conditioned on all
measurements made up to that time.[4] The Kalman theory cannot be applied
directly to estimating the state of a ballistic reentry vehicle on the
basis of noise-corrupted radar measurements, because the equations of
motion (7) governing the missile and the measurement equation (12) are
nonlinear functions of the state $\underline{x}$. However, by first making the ap-
propriate linearizations, the Kalman theory can be applied to the non-
linear case. The linearization equations together with the basic Kalman
filter equations constitute what is referred to as the Extended Kalman
Filter. As shown in Refs. 1 and 2, this approach has been successfully
applied to trajectory estimation problems in the NIKE-X system. Justi-
fication for this approach and a derivation of the extended Kalman filter
is presented in Ref. 5.

Since the extended Kalman filter is to be implemented on a digital
computer, it will be described in its discrete-time form in this
memorandum. The discrete time k will refer to the actual time $k\,\Delta t$,
where Δt is the sampling interval (data processing interval). Through-
out this report, $\underline{\hat{x}}(i/j)$ will denote the estimate of the state $\underline{x}$ at
time i, conditioned on the measurements through time j, and $P(i/j)$
will denote the covariance of the error in this estimate; i.e.,

$$\hat{x}(i/j) = E[\underline{x}(i)/\underline{z}(j),\underline{z}(j-1),\ldots,\underline{z}(1);\underline{\hat{x}}(0/0),\ P(0/0)]$$

$$P(i/j) = E[\{\underline{x}(i)-\underline{\hat{x}}(i/j)\}\{\underline{x}(i)-\underline{\hat{x}}(i/j)\}^{T}/\underline{z}(j),\underline{z}(j-1),\ldots,\underline{z}(1);\underline{\hat{x}}(0/0),P(0/0)],$$

$$(13)$$

where $\underline{\hat{x}}(0/0)$ is the a priori state estimate and $P(0/0)$ is its error
covariance.

The measurement noise $\underline{v}$ given in Eq. (12) is a white Gaussian
random variable with

$$E[\underline{v}(k)] = 0$$

$$E[\underline{v}(k) \ \underline{v}(k)^T] = R(k) \quad . \tag{14}$$

The continuous random disturbance $\underline{w}'$ given in Eq. (7) will be replaced
by an equivalent discrete random disturbance $\underline{w}$, which is a white
Gaussian noise process with

$$E[\underline{w}(k)] = 0$$

$$E[\underline{w}(k) \ \underline{w}^T(k)] = Q(k) \quad . \tag{15a}$$

The value of $Q(k)$ is a function not only of the time k, but also of
the sampling interval Δt. If the continuous noise $\underline{w}'$ has a covariance
given by $E[\underline{w}'(t) \ \underline{w}'^T(\sigma)] = Q'(t) \ \delta(t - \sigma)$, where $\delta(\cdot)$ is the Dirac
delta function, then in the discrete-time form of the missile's dynamical
model, the discrete noise $\underline{w}$ will have (if this model is linear) a co-
variance given by

$$Q(k) = Q'(k) \ \Delta t \quad . \tag{15b}$$

The initial state $\underline{x}(0)$ is assumed to be a Gaussian random variable
with

$$E[\underline{x}(0)] = \underline{\hat{x}}(0/0)$$

$$E[\{\underline{x}(0) - \underline{\hat{x}}(0/0)\}\{\underline{x}(0) - \underline{\hat{x}}(0/0)\}^T] = P(0/0) \quad . \tag{16}$$

Furthermore, it is assumed that $\underline{v}(k)$, $\underline{w}(k)$, and $\underline{x}(0)$ are mutually
uncorrelated.

The resulting estimation equations, which are given by the extended
Kalman filter, can be considered as consisting of two parts: prediction
and correction.

1. Prediction

Given $\underline{\hat{x}}(k/k)$, the estimate of the state at time k, and the
assumption that $E[w(k)] = 0$, the predicted state can be obtained from
the nonlinear equations of motion (7):[*]

$$\underline{\hat{x}}(k+1/k) = \underline{\hat{x}}(k/k) + \underline{f}[\underline{\hat{x}}(k/k)]\Delta t \quad , \tag{17}$$

with the covariance of the error in the state prediction $\underline{\hat{x}}(k+1/k)$ given by

---

[*] More accurate integration formulas can be used if necessary.

9

$$P(k+1/k) = \phi(k+1,k) \, P(k/k) \, \phi^T(k+1,k) + Q'(k) \, \Delta t, \qquad (18)$$

where $\phi(k+1,k)$ is obtained by linearization of Eq. (7) about the state estimate $\hat{\underline{x}}(k/k)$--i.e.,

$$\phi(k+1,k) = I + F[\hat{\underline{x}}(k/k)]\Delta t \quad , \qquad (19)$$

in which F is the 7×7 matrix with components

$$F_{ij}(\underline{x}) = \frac{\partial f_i(\underline{x})}{\partial x_j} \quad . \qquad (20)$$

From Eq. (6),

$$F = \left[\frac{\partial f_i}{\partial x_j}\right] = \begin{bmatrix} 0 & 0 & 0 & 1 & 0 & 0 & 0 \\ 0 & 0 & 0 & 0 & 1 & 0 & 0 \\ 0 & 0 & 0 & 0 & 0 & 1 & 0 \\ F_{41} & F_{42} & F_{43} & F_{44} & F_{45} & F_{46} & F_{47} \\ F_{51} & F_{52} & F_{53} & F_{54} & F_{55} & F_{56} & F_{57} \\ F_{61} & F_{62} & F_{63} & F_{64} & F_{65} & F_{66} & F_{67} \\ F_{71} & F_{72} & F_{73} & F_{74} & F_{75} & F_{76} & F_{77} \end{bmatrix} , \qquad (21)$$

where

$$F_{41} = \omega^2 - g \, r_1^{-1} + 3 \, g \, x_1^2 \, r_1^{-3}$$

$$F_{42} = 3 \, g \, x_1 \, x_2 \, r_1^{-3}$$

$$F_{43} = 3 \, g \, x_1(x_3 + r_o)r_1^{-3}$$

$$F_{44} = -\tfrac{1}{2} \, x_7 \, g_o V - \tfrac{1}{2} \, x_7 \, g_o \, x_4^2 \, V^{-1}$$

$$F_{45} = 2\omega \sin \ell - \tfrac{1}{2} \, x_7 \, g_o \, x_4 \, x_5 \, V^{-1}$$

$$F_{46} = -2\omega \cos \ell - \tfrac{1}{2} \, x_7 \, g_o \, x_4 \, x_6 \, V^{-1}$$

$$F_{47} = -\tfrac{1}{2} \, V \, x_4 \, g_o$$

10

$$F_{51} = 3\ g\ x_1\ x_2\ r_1^{-3}$$

$$F_{52} = \omega^2 \sin^2 \ell + 3\ g\ x_2^2\ r_1^{-3} - g\ r_1^{-1}$$

$$F_{53} = -\ \omega^2 \sin \ell \cos \ell + 3g\ x_2(x_3 + r_o)r_1^{-3}$$

$$F_{54} = -\ 2\omega \sin \ell - \tfrac{1}{2}\ x_7\ g_o\ x_4\ x_5\ V^{-1}$$

$$F_{55} = -\ \tfrac{1}{2}\ x_7\ g_o\ x_5^2\ V^{-1} - \tfrac{1}{2}\ x_7\ V\ g_o$$

$$F_{56} = -\ \tfrac{1}{2}\ x_7\ x_5\ x_6\ V^{-1}\ g_o$$

$$F_{57} = -\ \tfrac{1}{2}\ V\ x_5\ g_o$$

$$F_{61} = 3\ g\ x_1(x_3 + r_o)r_1^{-3}$$

$$F_{62} = -\ \omega^2 \sin \ell \cos \ell + 3\ g\ x_2(x_3 + r_o)r_1^{-3}$$

$$F_{63} = \omega^2 \cos^2 \ell + 3g(x_3 + r_o)^2\ r_1^{-3} - g\ r_1^{-1}$$

$$F_{64} = 2\omega \cos \ell - \tfrac{1}{2}\ x_7\ x_4\ x_6\ V^{-1}$$

$$F_{65} = -\ \tfrac{1}{2}\ x_7\ x_5\ x_6\ V^{-1}\ g_o$$

$$F_{66} = -\ \tfrac{1}{2}\ x_7\ x_6^2\ V^{-1}\ g_o - \tfrac{1}{2}\ x_7\ V\ g_o$$

$$F_{67} = -\ \tfrac{1}{2}\ V\ x_6\ g_o$$

$$F_{71} = -\ x_7\ K\ r_1^{-1}\ x_4 + x_7[x_1\ x_4 + x_2\ x_5 + (x_3+r_o)x_6]\ K\ r_1^{-3}\ x_1$$

$$F_{72} = -\ x_7\ K\ r_1^{-1}\ x_5 + x_7[x_1\ x_4 + x_2\ x_5 + (x_3+r_o)x_6]\ K\ r_1^{-3}\ x_2$$

$$F_{73} = -\ x_7\ K\ r_1^{-1}\ x_6 + x_7[x_1\ x_4 + x_2\ x_5 + (x_3+r_o)x_6]\ K\ r_1^{-3}(x_3 + r_o)$$

$$F_{74} = -\ x_7\ K\ r_1^{-1}\ x_1$$

$$F_{75} = -\ x_7\ K\ r_1^{-1}\ x_2$$

11

$$F_{76} = - x_7 K r_1^{-1} (x_3 + r_o)$$

$$F_{77} = - K r_1^{-1} [x_1 x_4 + x_2 x_5 + (x_3 + r_o)x_6] \quad .$$

2. Correction

The state prediction $\hat{\underline{x}}(k+1/k)$ is then corrected by using $\underline{z}(k+1)$, the actual measurement at time $k+1$, and $\hat{\underline{z}}(k+1/k)$, the predicted measurement for time $k+1$, which is obtained from the nonlinear measurement equation (12) by using the assumption that $E[\underline{v}(k+1)] = 0$:

$$\hat{\underline{z}}(k+1/k) = \underline{h}[\hat{\underline{x}}(k+1/k)] \quad . \tag{22}$$

Hence, the estimate of the state at time $k+1$ is given by

$$\hat{\underline{x}}(k+1/k+1) = \hat{\underline{x}}(k+1/k) + W(k+1)[\underline{z}(k+1) - \hat{\underline{z}}(k+1/k)] \quad , \tag{23}$$

where the weighting matrix is

$$W(k+1) = P(k+1/k)H^T(k+1)[R(k+1) + H(k+1)P(k+1/k)H^T(k+1)]^{-1} \tag{24}$$

and $H(k+1)$ is obtained by linearization of Eq. (12) about the state prediction $\hat{\underline{x}}(k+1/k)$ -- i.e.,

$$H(k+1) = H[\hat{\underline{x}}(k+1/k)] \quad , \tag{25}$$

in which H is the 3×7 matrix with components

$$H_{ij}(\underline{x}) = \frac{\partial h_i(\underline{x})}{\partial x_j} \quad . \tag{26}$$

From Eqs. (8) through (11),

$$H = \left[\frac{\partial h_i}{\partial x_j} \right] = \begin{bmatrix} H_{11} & H_{12} & H_{13} & 0 & 0 & 0 & 0 \\ H_{21} & H_{22} & H_{23} & 0 & 0 & 0 & 0 \\ H_{31} & H_{32} & H_{33} & 0 & 0 & 0 & 0 \end{bmatrix} \quad , \tag{27}$$

where the H_{ij} are most conveniently written in terms of the radar face coordinates x_1', x_2', x_3':

$$H_{11} = \frac{x_1'}{r} \cos \xi + \frac{x_2'}{r} \sin \tau \sin \xi$$

$$+ \frac{x_3'}{r} \cos \tau \sin \xi$$

$$H_{12} = \left[(x_2')^2 + (x_3')^2 \right]^{\frac{1}{2}} \cos \xi$$

$$- \frac{x_1'}{x_3'} \left[(x_2')^2 + (x_3')^2 \right]^{\frac{1}{2}} \cos \tau \sin \xi$$

$$H_{13} = \left[(x_1')^2 + (x_3')^2 \right]^{\frac{1}{2}} \sin \tau \sin \xi$$

$$- \frac{x_2'}{x_3'} \left[(x_1')^2 + (x_3')^2 \right]^{\frac{1}{2}} \cos \tau \sin \xi$$

$$H_{21} = - \frac{x_1'}{r} \sin \xi + \frac{x_2'}{r} \sin \tau \cos \xi + \frac{x_3'}{r} \cos \tau \cos \xi$$

$$H_{22} = - \left[(x_2')^2 + (x_3')^2 \right]^{\frac{1}{2}} \sin \xi$$

$$- \frac{x_1'}{r} \left[(x_2')^2 + (x_3')^2 \right]^{\frac{1}{2}} \cos \tau \sin \xi$$

$$H_{23} = \left[(x_1')^2 + (x_3')^2 \right]^{\frac{1}{2}} \cos \xi \sin \tau$$

$$- \frac{x_2'}{x_3'} \left[(x_1')^2 + (x_3')^2 \right]^{\frac{1}{2}} \cos \tau \cos \xi$$

$$H_{31} = - \frac{x_2'}{r} \cos \tau + \frac{x_3'}{r} \sin \tau$$

$$H_{32} = - \frac{x_1'}{x_3'} \left[(x_2')^2 + (x_3')^2 \right]^{\frac{1}{2}} \sin \tau$$

$$H_{33} = - \left[(x_1')^2 + (x_3')^2 \right]^{\frac{1}{2}} \cos \tau$$

$$- \frac{x_2'}{x_3'} \left[(x_1')^2 + (x_3')^2 \right]^{\frac{1}{2}} \sin \tau$$

and

$$r = \left[(x_1')^2 + (x_2')^2 + (x_3')^2 \right]^{\frac{1}{2}} \quad .$$

13

For use in Eq. (27), the values of x_1', x_2', x_3' are determined from the state prediction $\hat{\underline{x}}(k+1/k)$ by the linear transformation M^{-1}, where M is given in Eq. (9):

$$\begin{bmatrix} x_1' \\ x_2' \\ x_3' \end{bmatrix} = M^{-1} \begin{bmatrix} \hat{x}_1(k/k-1) \\ \hat{x}_2(k/k-1) \\ \hat{x}_3(k/k-1) \end{bmatrix} . \qquad (28)$$

The covariance of the error in the estimate $\hat{\underline{x}}(k+1/k+1)$ is

$$P(k+1/k+1) = [I - W(k+1)H(k+1)]P(k+1/k)$$

$$= P(k+1/k) - P(k+1/k)H^T(k+1)[R(k+1)+H(k+1)P(k+1/k)H^T(k+1)]^{-1}$$

$$\cdot H(k+1)P(k+1/k) . \qquad (29)$$

Equations (17), (18), (23), (24), and (29), together with the matrices defined in Eqs. (19) and (25), comprise the extended Kalman filter. The a priori state estimate $\hat{\underline{x}}(0/0)$ and its error covariance $P(0/0)$ are used to initialize these recursive equations. The measurement noise covariance R is specified by the characteristics of the phased-array radar model. The random disturbance covariance Q is determined in order to compensate for inaccuracies in the model of the equations of motion (see Secs. V and VI).

It should be noted that in the extended Kalman filter, the nonlinear equations (7) and (12) are used to obtain the state prediction [Eq. (17)] and the predicted measurement [Eq. (22)], respectively. The linearization of Eqs. (7) and (12), used to obtain $\tilde{\phi}$ and H, is only employed to calculate the covariances and the weighting matrix in Eqs. (18), (24), and (29).

B.   Basic Flow Diagram

The basic equations of the extended Kalman filter (see Sec. III A) can be displayed in the form of a flow diagram, which is a simplified pictorial representation of the digital computer program that has been developed. This is shown in Fig. 2, where k_{max} is the maximum number of times that the filter processes the measurements. Thus, there are seven major computations involved in each filtering iteration--as indicated by the seven numbered blocks in Fig. 2 (these will be referred

14

INITIALIZE FILTER:
AT k = 0, INPUT
$\hat{\underline{x}}(0/0)$ and P (0/0)

① CALCULATE LINEARIZED DIFFERENTIAL – EQUATION MATRIX, EQ. (21):

$$F = \left[F_{i_j}\{\hat{\underline{x}}(k/k)\}\right] = \left[\frac{\partial f_i\{\hat{\underline{x}}(k/k)\}}{\partial x_i}\right]$$

② CALCULATE TRANSITION MATRIX, EQ. (19):

$$\Phi(k+1, k) = I + F\Delta t$$

③ CALCULATE PREDICTED STATE, EQ. (17):

$$\hat{\underline{x}}(k+1/k) = \hat{\underline{x}}(k/k) + \underline{f}\{\hat{\underline{x}}(k/k)\}\Delta t$$

NEXT ITERATION:

$k \leftarrow k + 1$

④ CALCULATE ERROR COVARIANCE IN PREDICTED STATE, EQ. (18):

$$P(k+1/k) = \Phi(k+1,k)P(k/k)\Phi^T(k+1,k) + Q(k)$$

RANDOM DISTURBANCE COVARIANCE:

$Q(k)$

⑤ CALCULATE WEIGHTING MATRIX, EQS. (24) AND (27):

$$W(k+1) = P(k+1/k)H^T(k+1)[R(k+1) + H(k+1)P(k+1/k)H^T(k+1)]^{-1}$$

MEASUREMENT NOISE COVARIANCE:

$R(k+1)$

⑥ CALCULATE STATE ESTIMATE, EQ. (23):

$$\hat{\underline{x}}(k+1/k+1) = \hat{\underline{x}}(k+1/k) + W(k+1)[\underline{z}(k+1) - \hat{\underline{z}}(k+1/k)]$$

MEASUREMENT:

$\underline{z}(k+1)$

⑦ CALCULATE ERROR COVARIANCE IN STATE ESTIMATE, EQ. (29):

$$P(k+1/k+1) = [I - W(k+1)H(k+1)]P(k+1/k)$$

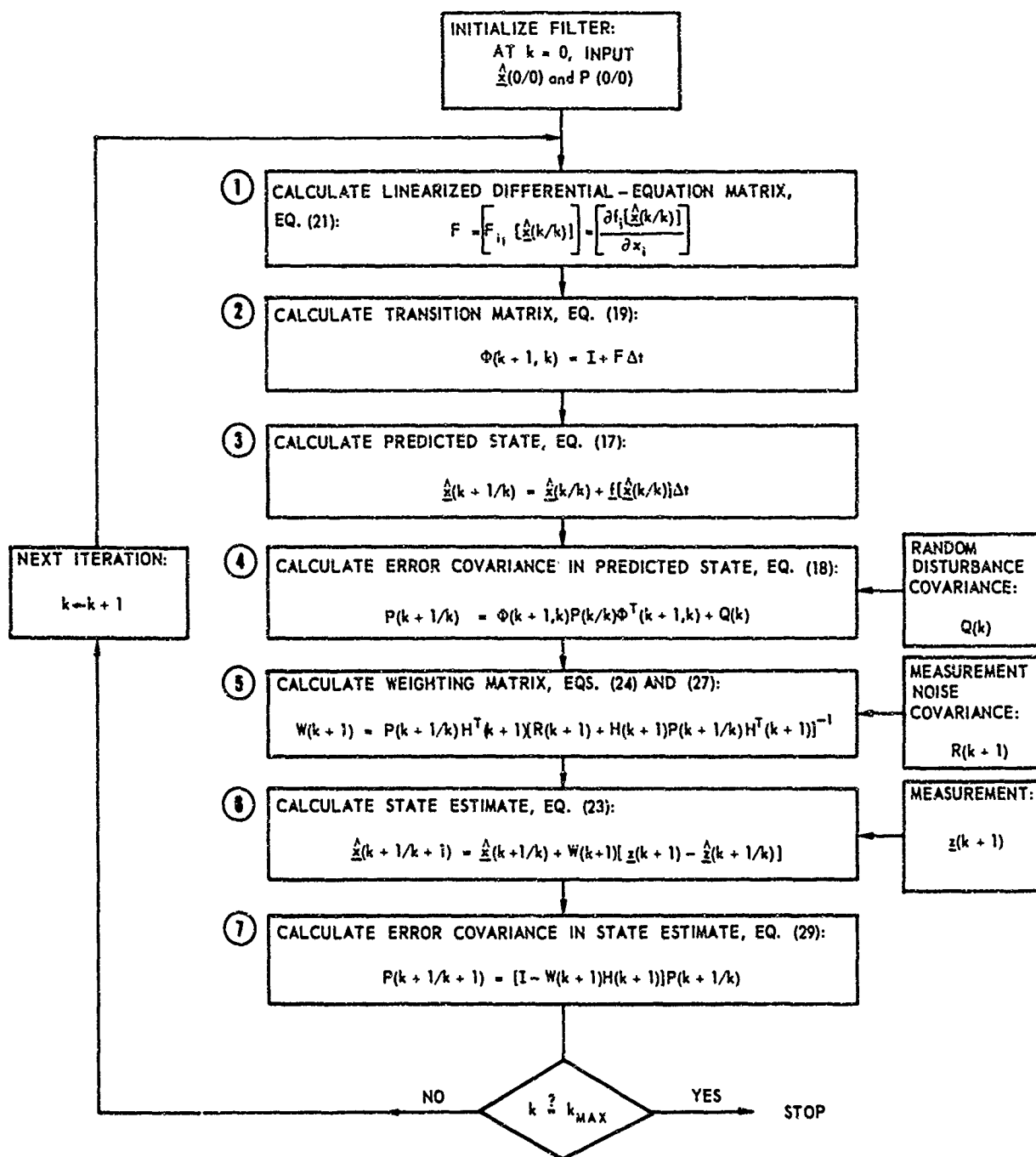NO ◄— $k \stackrel{?}{=} k_{MAX}$ —► YES ——► STOP

FIG. 2 FLOW DIAGRAM FOR EXTENDED KALMAN FILTER

15

to as Steps 1 through 7). Since the state vector of the ballistic
missile has seven components, some of the calculations shown in Fig. 2
require considerable computation time.

In the next section, the contribution made by each of the seven
basic calculations to the total computational time for one filtering
iteration will be found. These timing estimates provide the basis for
making modifications in the filter design to decrease the average computation
tation time per iteration.

C. Computation Time Considerations

In a previous study,[1] when the extended Kalman filter equations
were implemented on the IBM 7090 for endoatmospheric trajectory estimation,
tion, the filter ran approximately 6 times slower than real time with a
data rate of 20 measurements per second (for a single target); i.e., it
took 6 seconds of computer time to process the measurements obtained in
1 second. Since the speed of the Kalman filter is computer-dependent,
one can improve the speed with a faster computer. In fact, with the same
data rate of 20 measurements per second, the Univac 1108 runs approximately
mately 5 times faster than real time (for a single target) for endo-
atmospheric estimation. Even at five times faster than real time (for
a single target), the speed of the extended Kalman filter may still be
inadequate for some situations. For instance, if n missiles must be
tracked and if the speed of the Kalman filter is 5 times real time,
then for n > 5, the filter cannot compute state estimates for all of
the n missiles in real time (at a data rate of 20 measurements per
second).

For exoatmospheric trajectory estimation (for which the filter has
six states instead of seven and is programmed in double precision--see
Sec. VI), the Univac 1108 runs approximately 100 times faster than real
time (for a single target) with a data rate of one measurement per
second.

Thus, particularly in a multi-threat situation for endoatmospheric
estimation, it is essential to improve the computational efficiency of
the extended Kalman filter. This should be done with a minimal amount
of degradation in filter performance. For ballistic-trajectory

16

estimation, where the dynamical description is given by Eqs. (6), (7), and (12), we know the particular structure of the linearized differential-equation matrix F, the transition matrix ϕ, the linearized measurement matrix H, the random disturbance covariance Q, and the measurement-noise covariance R. Therefore, we can take advantage of this knowledge by writing a computer program, which reproduces the flow diagram (Fig. 2) in a computationally efficient manner.

In the extended Kalman filter program, which has been developed, the seven major computations per iteration given in Fig. 2 involve various numerical operations as listed in Table I.[*]

Table I

ARITHMETIC OPERATIONS FOR THE EXTENDED KALMAN FILTER
(ENDOATMOSPHERIC CASES)

	COMPUTATIONAL OPERATION (see Fig. 2)	NUMBER OF MULTIPLICATIONS OR DIVISIONS	NUMBER OF ADDITIONS OR SUBTRACTIONS	NUMBER OF SQUARE ROOTS
(1)	CALCULATE LINEARIZED DIFFERENTIAL-EQUATION MATRIX, EQ. (21)	89	31	2
(2)	CALCULATE TRANSITION MATRIX, EQ. (19)	28	7	0
(3)	CALCULATE PREDICTED STATE, EQ.(17)	30	17	0
(4)	CALCULATE ERROR COVARIANCE IN PREDICTED STATE, EQ. (18)	693	693	0
(5)	CALCULATE WEIGHTING MATRIX, EQS. (24) AND (27)	102	65	0
(6)	CALCULATE STATE ESTIMATE, EQ. (23)	21	42	0
(7)	CALCULATE ERROR COVARIANCE IN STATE ESTIMATE, EQ. (29)	147	147	0
	TOTALS	1110	1002	2

---

[*]Table I applies to endoatmospheric estimation; for exoatmospheric estimation, a comparable table could be obtained.

17

The enumeration of arithmetic operations in Table I gives an indication of the distribution of the total computation time per iteration among the seven basic calculations. For instance, if it can be assumed that the operation of multiplication (or division) requires a computation time of an order of magnitude larger than that for an addition (or subtraction), then the calculation of the predicted error covariance (Step 4) takes about 63% of the total computation time. Clearly, the error covariance matrix calculations of Steps 4 and 7 are the most involved.

The next section discusses various approaches that may be used to modify the Kalman filtering algorithm in order to reduce the computational requirements. Particular emphasis is placed upon simplifying and modifying the two error covariance calculations, since they are the most time-consuming calculations in the Kalman filter.

D. Approaches to Reducing the Computational Requirements

One approach to reducing the computational requirements of the Kalman filter was discussed in detail in Ref. 1. There an approximation to the weighting matrix $W(k)$ was precomputed off-line, rather than calculated recursively on-line. The weighting matrix values for representative trajectories are then stored in the computer memory. The precomputed weighting matrix technique has some disadvantages. First, the weighting matrix $W(k)$ not only is a function of the iteration time k, but it also is altitude-dependent. Second, $W(k)$, even for the same altitude, is dependent to some degree upon the geometry of the trajectory and the ballistic coefficient (at lower altitudes). Consequently, for accurate estimation, many representative weighting-matrix histories should be stored in memory and employed accordingly. The computational advantages of the Kalman filter using a precomputed weighting matrix are impressive, however. In fact, for endoatmospheric estimation, the speed of this filter is approximately 15 times that of the fully implemented Kalman filter.

Another approach for improving the real-time capability of the Kalman filter is to decrease the data rate until it falls within the filter's real-time capability. One disadvantage of this approach is that

18

the estimation is based upon less data and, thus, is inherently less
accurate. As Δt, the time between measurements, is increased, the
calculations yielding $\phi(k+1,k)$ and $\hat{\underline{x}}(k+1/k)$ should be refined so
that their accuracy is not impaired; these refinements consume some of
the computational speed gained by decreasing the data rate. Additionally,
the linearization assumptions for the extended Kalman filter may no
longer be valid for large values of Δt. Clearly the speed of the Kal-
men filter relative to real time is proportional to Δt, so that if the
filter is 6 times slower than real time for a data rate of 20 measure-
ments per second ($\Delta t = 0.05$ sec), then it will be faster than real time
only for data rates less than 3.33 measurements per second. In Ref. 1,
it was shown that the performance of the extended Kalman filter for
endoatmospheric estimation was not markedly affected when the data rate
was decreased by up to a factor of 5 from a basic data rate of 20
measurements per second. Some further results on this approach will be
presented in Secs. V and VI.

IV   PIECEWISE-RECURSIVE KALMAN FILTER

In this study we have combined the advantages of both of the
approaches discussed in Sec. III D. The filter algorithm considered
here calculates the weighting matrix $W(k+1)$ every $\Delta\tau$ seconds, and
uses this weighting matrix for calculating the state estimate $\hat{\underline{x}}(i/i)$
at intervals of Δt sec for $i = k+1$, $k+2$, ... $k+N$, where $\frac{\Delta\tau}{\Delta t} = N \geq 1$.
This is equivalent to calculating $W(k+1)$ at time $k+1$ and retaining
this value of the weighting matrix (to be used in computing the state
estimate) for the times $k+1$, $k+2$, ..., $k+N$, and then calculating
$W[k+(N+1)]$ anew. The design parameters of the filter are then Δt, the
sample interval (data processing interval), and $\Delta\tau$, the interval between
weighting-matrix calculations. This filter has a "piecewise-precomputed"
weighting matrix and its data rate may also be varied. Thus, the computa-
tional advantages of both precomputation and data-rate reduction can be
achieved. This algorithm also avoids the off-line nature of a Kalman filter
that uses a precomputed approximation to the weighting matrix; in this
approach, the weighting-matrix calculations are performed recursively at
intervals of $\Delta\tau$ seconds. This computational algorithm, which will be
referred to as the Piecewise-Recursive (Extended) Kalman Filter, will be
described more completely below.

19

The modified Kalman filter algorithm described above operates as follows: In the first cycle, the equations for the state prediction and estimate are computed just as they are for the fully implemented Kalman filter [see Sec. III A, Eqs. (17), (22), and (23)],

$$\underline{\hat{x}}(k+1/k) = \underline{\hat{x}}(k/k) + \underline{f}[\underline{\hat{x}}(k/k)]\Delta t \tag{30}$$

$$\underline{\hat{x}}(k+1/k+1) = \underline{\hat{x}}(k+1/k) + W(1)[\underline{z}(k+1) - \underline{\hat{z}}(k+1/k)] \tag{31}$$

$$k = 0, 1, \ldots, N-1 \quad .$$

The weighting matrix $W(1)$ for these N iterations is obtained from Eqs. (18) and (24),

$$W(1) = P(1/0)H^T(1)[R(1) + H(1) \ P(1/0)H^T(1)]^{-1} \quad , \tag{32}$$

where

$$P(1/0) = \phi(1,0) \ P(0/0) \ \phi^T(1,0) + Q'(0)\Delta t \tag{33}$$

and

$$\phi(1,0) = I + F[\underline{\hat{x}}(0/0)]\Delta t \quad .$$

The calculations in Steps 1, 2, 3, 4, 5, and 7 of Fig. 2 are not done for $k = 1, 2, \ldots, N-1$.

Before proceeding to the next cycle, this algorithm requires that $P(N/N)$, the covariance of the error in the state estimate $\underline{\hat{x}}(N/N)$ at the end of the previous cycle, be computed. As shown in Ref. 6, this covariance can be obtained by solving the recursive relations:[*]

$$P(k+1/k+1) = [I - W(1)H(k+1)] \ P(k+1/k) \ [I - W(1)H(k+1)]$$
$$+ W(1)R(k+1)W^T(1) \tag{34}$$

$$P(k+1/k) = \phi(k+1,k)P(k/k)\phi^T(k+1,k) + Q'(k)\Delta t \tag{35}$$

$$k = 0, 1, \ldots, N-1 \quad .$$

However, this calculation of $P(N/N)$ defeats the very purpose of the piecewise-recursive Kalman filter--namely, to reduce the computation

---

[*] These relations exactly define the propagation of the covariance for either optimal or sub-optimal values of the weighting matrix.

time. Therefore, simplifications for or approximations to Eqs. (34) and (35) are essential.

The approximation made here is that we can consider the filtering done at the times $k = 1, 2, \ldots, N$ as constituting a presmoothing of measured data. In effect, it can be assumed that at the end of the time interval $[0, \Delta\tau]$, where $k = N$, one measurement (with an appropriately reduced noise covariance) is processed. It can be shown that for the most optimistic conditions this reduced measurement noise covariance is given by

$$R^*(N) = \frac{\overline{R}(N)}{N} \quad , \tag{36}$$

where $\overline{R}(N)$ is the average value of the measurement-noise covariances for the times $k = 1, 2, \ldots, N$ $(\Delta\tau = N\Delta t)$; for practical purposes, $\overline{R}(N)$ is taken to be equal to $R(N)$. It is asserted that $R^*(N)$ represents (approximately) the effective measurement noise over the interval $[0, \Delta\tau]$, if all N measurements are processed by the Kalman filter.

Using this reduced measurement-noise covariance, $P(N/N)$ is then determined [see Sec. III A, Eqs. (18) and (29)] from the equations

$$P(N/N) = P(N/0) - P(N/0) \ H^T(N) \ [\ \frac{R(N)}{N} + H(N) \ P(N/0) \ H^T(N)]^{-1}$$
$$\cdot \ H(N) \ P(N/0) \quad , \tag{37}$$

where

$$P(N/0) = \phi(N,0) \ P(0/0) \ \phi^T(N,0) + Q'(0) \ N\Delta t \tag{38}$$

and

$$\phi(N,0) = I + F[\hat{\underline{x}}(0/0)]N\Delta t \quad .$$

This approach avoids the recursive solution of $P(N/N)$ and has been found to yield satisfactory filter performance as shown in Secs. V and VI.

At $k = N$, the cycle is repeated; i.e., the state prediction and estimate are given by

$$\hat{\underline{x}}(k+1/k) = \hat{\underline{x}}(k/k) + \underline{f}[\hat{\underline{x}}(k/k)]\Delta t \tag{39}$$

21

$$\hat{\underline{x}}(k+1/k+1) = \hat{\underline{x}}(k+1/k) + W(N+1)\left[\underline{z}(k+1) - \hat{\underline{z}}(k+1/k)\right] \qquad (40)$$

$$k = N, \ N+1, \ \ldots, \ 2N-1 \quad .$$

The weighting matrix $W(N+1)$ for these N iterations is obtained as

$$W(N+1) = P(N+1/N) \ H^T(N+1)\left[R(N+1) + H(N+1) \ P(N+1/N) \ H^T(N+1)\right]^{-1}, \qquad (41)$$

where

$$P(N+1/N) = \phi(N+1,N) \ P(N/N) \ \phi^T(N+1,N) + Q'(N)\Delta t \qquad (42)$$

and

$$\phi(N+1,N) = I + F[\hat{\underline{x}}(N/N)]\Delta t \quad .$$

Again, the computations in Steps 1, 2, 4, 5, and 7 in Fig. 2 are omitted for $k = N+1, \ N+2, \ \ldots, \ 2N-1$. Next, $P(2N/2N)$, the covariance of the error in the state estimate $\hat{\underline{x}}(2N/2N)$ at the end of this cycle, is calculated from

$$P(2N/2N) = P(2N/N) - P(2N/N)H^T(2N) \ \left[\frac{R(2N)}{N} + H(2N)P(2N/N)H^T(2N)\right]^{-1}$$

$$\cdot \ H(2N) \ P(2N/N) \quad , \qquad (43)$$

where

$$P(2N/N) = \phi(2N,N) \ P(N/N)\phi^T(2N,N) + Q'(N)N\Delta t \qquad (44)$$

and

$$\phi(2N,N) = I + F[\hat{\underline{x}}(N/N)]N\Delta t \quad .$$

Whenever k is a multiple of N, this cycle is repeated in the manner outlined above.

The use of the piecewise-recursive Kalman filter results in a reduction of computational requirements whenever $N \geq 2$ (i.e., $\Delta\tau \geq 2 \ \Delta t$). The reason for this is that the modified algorithm nearly doubles the number of numerical calculations, with respect to the basic Kalman filter presented in Fig. 2, whenever k is a multiple of N; but for the next $N-1$ sample points, the filter's weighting matrix is fixed so that the number of numerical calculations is very small for these iterations. Thus, there is no computational advantage of this algorithm unless $N \geq 2$.

22

The expected decrease in the computational time for the piecewise-recursive Kalman filter is a function of the size of $\Delta\tau$ relative to Δt, as well as the value of Δt. Let S_o be the ratio of the computational speed of a Kalman filter using a precomputed weighting matrix to the computational speed of the fully implemented Kalman filter at the same data rate (S_o is independent of the sample interval Δt). Since the piecewise-recursive Kalman filter described above is equivalent to using a precomputed weighting matrix for $N-1$ iterations (where $N = \Delta\tau/\Delta t$) before a new weighting matrix is computed, this filter is S_o times faster than the fully implemented Kalman filter for these $N-1$ iterations. As shown above, for the first iteration of each cycle of N iterations, the piecewise-recursive Kalman filter is approximately twice as slow as the fully implemented Kalman filter. Thus, if Δt_K is the computational time consumed by the fully implemented Kalman filter for one iteration, then the time consumed by the piecewise-recursive Kalman filter is approximately $2\Delta t_K$ if the iteration is the first in the cycle of N iterations, and $\Delta t_K/S_o$ if the iteration is one of the remaining $N-1$ iterations before a new weighting matrix is calculated.

Since the total computational time for N data points with the fully implemented Kalman filter is $N\Delta t_K$, and with the piecewise-recursive Kalman filter it is $2\Delta t_K + (N-1)\Delta t_K/S_o$, it follows that the ratio of their average iteration times is approximately

$$\frac{2\Delta t_K + (N-1)\ \Delta t_K/S_o}{N\ \Delta t_K} \quad . \tag{45}$$

Thus, the speed of the piecewise-recursive Kalman filter, relative to the fully implemented Kalman filter, is approximately

$$S_N = \frac{N\ S_o}{2S_o + (N-1)} \quad . \tag{46}$$

If the speed of the fully implemented Kalman filter relative to real time (when the sample interval is Δt_o) is S_R, then its speed relative to real time when the sample interval is Δt will be

23

$$S_R \frac{\Delta t}{\Delta t_o} \quad . \tag{47}$$

Consequently, the speed of the piecewise-recursive Kalman filter with respect to real time will be approximately

$$S_{N,\Delta t} = S_R \left(\frac{\Delta t}{\Delta t_o} \right) \frac{N S_o}{2S_o + (N-1)} \quad . \tag{48}$$

As an illustration of the expected computational advantages in endoatmospheric estimation of such a filter design using the Univac 1108 at a sampling interval of $\Delta t_o = 0.05$ sec, the fully implemented Kalman filter is about 5 times faster than real time (i.e., $S_R = 5$); Table I indicates that the speed of a Kalman filter using a precomputed weighting matrix relative to the fully implemented Kalman filter is about 15 (i.e., $S_o = 15$). Incidentally, it should be noted that S_R is computer-dependent, whereas S_o is not. Thus, for the endoatmospheric estimation on the Univac 1108, $S_{N,\Delta t}$ is given by

$$S_{N,\Delta t} = 5 \left(\frac{\Delta t}{\Delta t_o} \right) \left[\frac{15N}{30 + (N-1)} \right] \quad . \tag{49}$$

Note that $S_{N,\Delta t}$, the speed of the piecewise-recursive Kalman filter relative to real time, increases linearly with Δt; for fixed Δt it is bounded by the speed of a Kalman filter with a precomputed weighting matrix.

To obtain some measure of the improvement in the computational speed for the endoatmospheric cases, let us calculate, using Eq. (49), the iteration times for various values of $N = \frac{\Delta \tau}{\Delta t}$. The average time for one iteration on the Univac 1108 is given by $\Delta t/S_{N,\Delta t}$; thus, for $N = 5$, 10, 20, and 30, we obtain the average iteration times of 0.0045, 0.0026, 0.0016, and 0.0013 sec, respectively. (Recall that the iteration time for the fully implemented Kalman filter is 0.0100 sec.) These estimates of the average iteration time for the piecewise-recursive Kalman filter are in very close agreement with the actual values found experimentally as will be shown in Sec. V. For exoatmospheric estimation, the average iteration times of the piecewise-recursive Kalman filter (for various values of $N = \frac{\Delta \tau}{\Delta t}$) are given in Sec. VI.

24

In Secs. V and VI, we will verify the expected computational advantages of the piecewise-recursive Kalman filter and investigate the performance of this filter for endoatmospheric and exoatmospheric estimation.

Since the piecewise-recursive Kalman filter algorithm essentially employs a weighting matrix whose elements are piecewise-constant functions of the time k, one could theoretically determine the optimal values of the weighting matrix elements, subject to this piecewise-constant constraint. This appears to be a difficult problem to solve analytically. The piecewise-recursive Kalman filter described here can be considered as an approximate solution to this problem.

V   N   RICAL RESULTS FOR ENDOATMOSPHERIC TRAJECTORY ESTIMATION

A.   Description of the Test Cases and Filter Design Parameters

Data from two representative endoatmospheric trajectories generated by simulation using an accurate model of reentry dynamics[6] was used to evaluate the performance of the piecewise-recursive Kalman filter described in Sec. IV. The computer program used in generating these trajectories was developed by M.I.T. Lincoln Laboratory.

The reentry angle for both trajectories is approximately 22°. Case 1 is a trajectory of a high-β missile, which is tracked starting at an altitude of about 205,000 ft. This trajectory impacts approximately at the radar site. Case 2 is a trajectory of a low-β missile, which is tracked from an altitude of about 153,000 ft. This trajectory impacts about 80,000 ft east and 30,000 ft north of the radar site. Cases 1 and 2 are essentially the same as Cases 1 and 4, respectively, of Ref. 1.

The filtering computations start with an initial state estimate $\hat{x}(0/0)$ and its error covariance matrix $P(0/0)$. The initial state estimates for the endoatmospheric cases, generated as in Ref. 7, are given in Table II.

Based on the work presented in Ref. 1, the initial error covariance (for the endoatmospheric trajectories) is chosen to be the 7×7 diagonal matrix

25

$$P(0/0) = \begin{bmatrix} 10^6 & & & & & & \\ & 10^6 & & & & & \\ & & 10^6 & & & & \\ & & & 10^6 & & & \\ & & & & 10^6 & & \\ & & & & & 10^6 & \\ & & & & & & 5 \times 10^{-21} \end{bmatrix} . \qquad (50)$$

The measurement-noise covariance $R(k)$ is obtained from a model of actual radar noise characteristics of the MSR based on work by Bell Telephone Laboratories.[8] The expressions for the elements of this covariance are found in Ref. 9. This radar model is used to generate the measurement noise of Eq. (12) in the simulation. Observations may be taken as often as every 0.05 sec for the endoatmospheric cases, but the filter may process fewer measurements than are taken (i.e., $\Delta t \geq 0.05$ sec).

Table II

INITIAL CONDITIONS FOR ENDOATMOSPHERIC TRAJECTORIES

	x_1 (ft)	x_2 (ft)	x_3 (ft)	x_4 (ft/sec)	x_5 (ft/sec)	x_6 (ft. sec)	x_7 (lb. ft^2)
CASE 1							
ACTUAL $\underline{x}(0)$	338110	338110	199910	15297	15297	8653	4.395×10^{-10}
ESTIMATE. $\hat{\underline{x}}(0/0)$	290952	292135	199911	16046	14466	12751	6.118×10^{-10}
ERROR	47158	45975	1	749	831	4098	
CASE 2							
ACTUAL $\underline{x}(0)$	80000	360440	149910	0	21633	8653	7.950×10^{-9}
ESTIMATE $\hat{\underline{x}}(0 \, 0)$	80093	318857	149842	1187	20891	11592	2.376×10^{-9}
ERROR	93	41583	68	1187	742	2939	

26

The random disturbance covariance $Q(k)$ [see Eqs. (15a) and (15b)], compensates for the model inaccuracies as described in Sec. II A. Based on studies described in Ref. 1, this covariance (for the endoatmospheric trajectories) is chosen to be the 7×7 diagonal matrix

$$\frac{Q(k)}{\Delta t} = Q'(k) = \begin{bmatrix} 0 & & & & & & \\ & 0 & & & & & \\ & & 0 & & & & \\ & & & 50 & & & \\ & & & & 50 & & \\ & & & & & 50 & \\ & & & & & & Q_{77}(k) \end{bmatrix} \quad , \tag{51}$$

where

$$Q_{77}(k) = \begin{cases} 3.2 \times 10^{-19} & , & \hat{x}_3 \geq 160000 \\ 1.0 \times 10^{-18} & , 95000 \leq \hat{x}_3 < 160000 \\ 2.2 \times 10^{-15} \exp(-5 \times 10^{-5} \hat{x}_3) & , 25000 \leq \hat{x}_3 < 95000 \\ 2.2 \times 10^{-15} [1 + 1.5 \times 10^{-3} (2.7 \times 10^4 - \hat{x}_3)] \exp(-5 \times 10^{-5} \hat{x}_3) & , 14700 \leq \hat{x}_3 < 25000 \\ 3.6 \times 10^{-14} [1 + 1.5 \times 10^{-3} (2.7 \times 10^4 - \hat{x}_3)] \exp(-5 \times 10^{-5} \hat{x}_3) & , & \hat{x}_3 < 14700 \end{cases}$$

and $\hat{x}_3$ is the present vertical distance estimate.

B. Performance of the Fully Implemented Extended Kalman Filter

For the endoatmospheric trajectories, the standard which is used to evaluate the performance of the piecewise-recursive Kalman filter is the fully implemented (extended) Kalman filter with a sample interval of $\Delta t = 0.05$ sec. The recursive equations for the extended Kalman filter are given in Sec. III A. This filter was used to estimate the ballistic trajectories for Cases 1 and 2 using simulated trajectories and measurement noise. The filter yields state estimates $\hat{\underline{x}}(k/k)$ at sample intervals of $\Delta t = 0.05$ sec.

The magnitudes of the measurement errors in position are shown in Figs. 3a and b for Cases 1 and 2. In order to relate altitude and time, these magnitudes are plotted as a function of both variables; in all other figures, the plots are a function of time only. Figures 4a, b, and d show the magnitudes of the estimation errors for position, velocity,

27
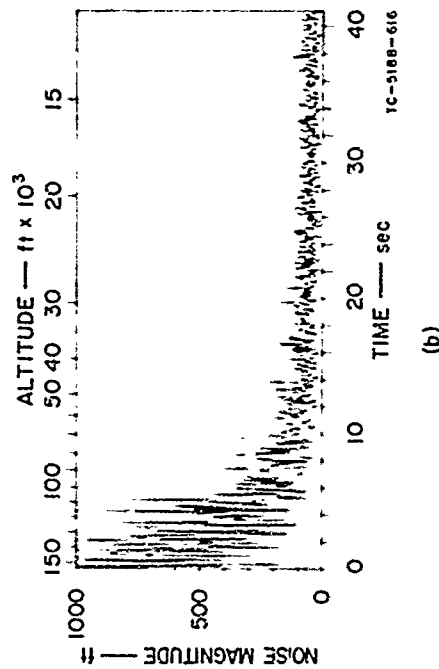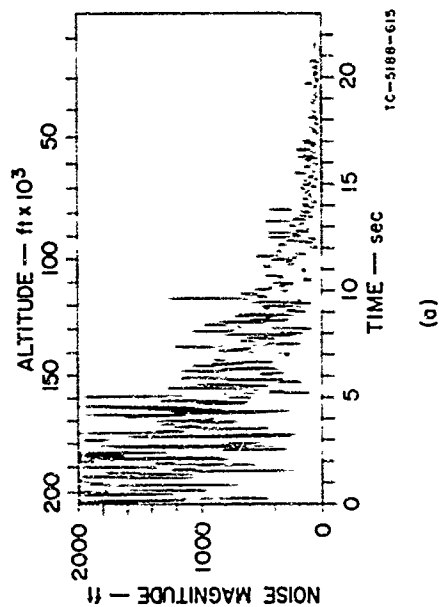
FIG. 3 MEASUREMENT NOISE — CASES 1 AND 2

28
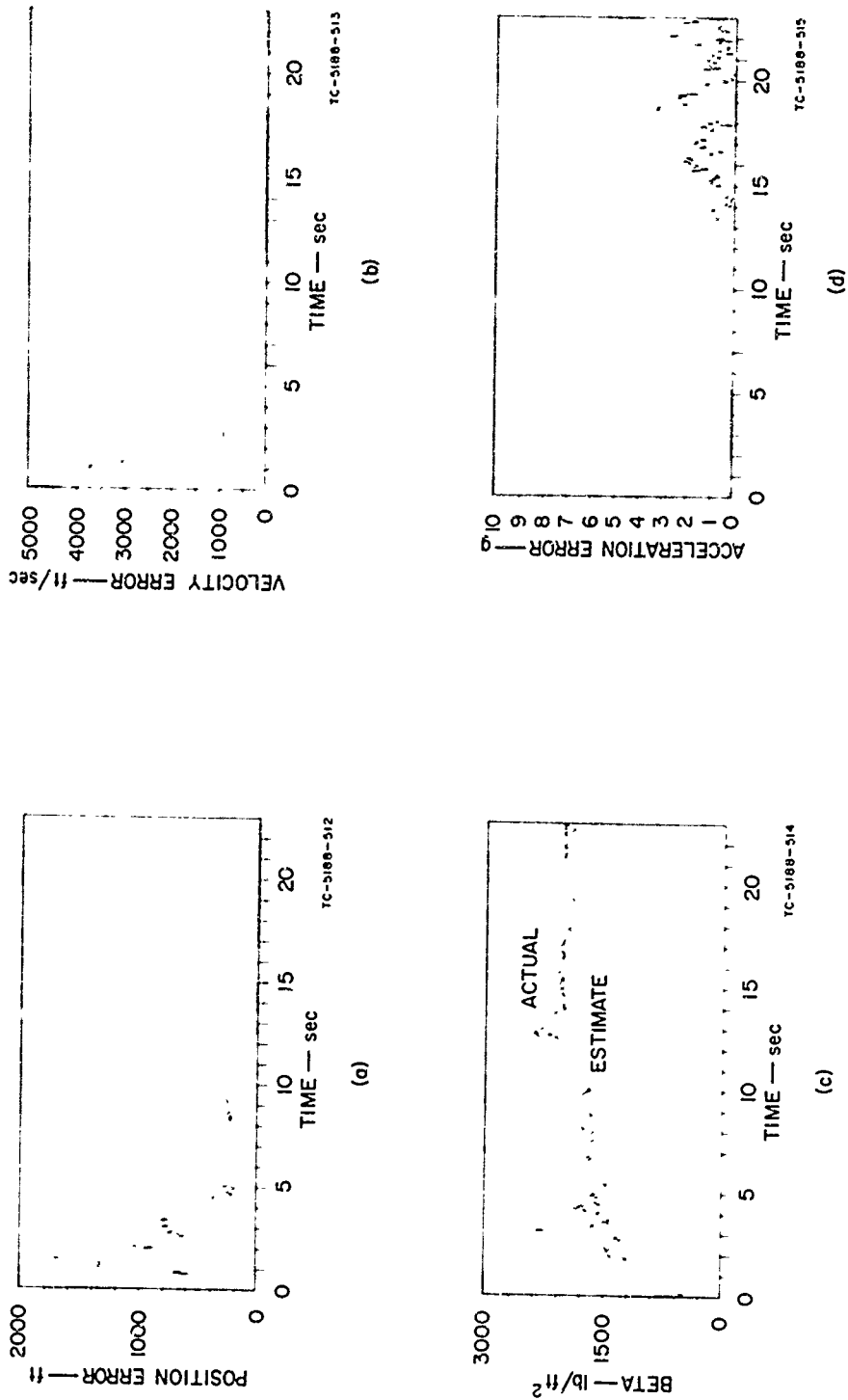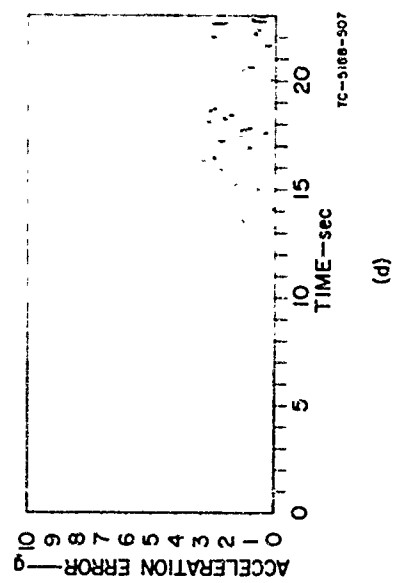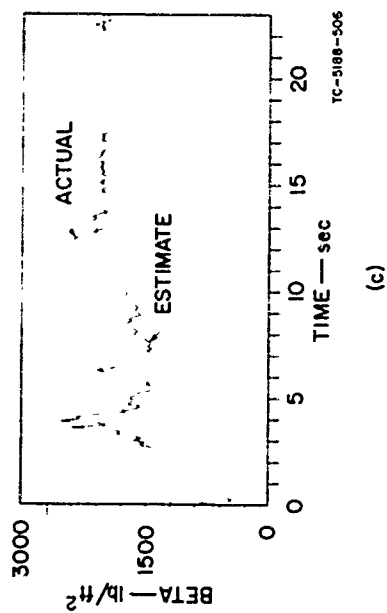
FIG. 4 ESTIMATION ERRORS FOR FULLY-IMPLEMENTED KALMAN FILTER — CASE 1, $\Delta t = 0.05$ sec

and acceleration, respectively, for Case 1. Figure 4c shows both
actual and estimated β, where the estimated β is obtained by assuming
$\hat{\beta}(k/k) = \rho[\hat{h}(k/k)]/\hat{x}_7(k/k)$ in which $\hat{h}(k/k)$ is the estimated altitude
obtained from Eq. (2). It should be noted that acceleration is not
computed directly by the filter but is calculated from the state esti-
mate using Eqs. (1) of Sec. II A. Figures 5a, b, c, and d show the
corresponding estimation errors for Case 2.

Note that after 3.5 sec of filtering, the magnitude of the errors
in estimated position in both cases is never any worse than 830 ft (and
in Case 1, the initial position error is approximately 65,000 ft).
After 3.5 sec, the magnitude of error in estimated velocity in both
cases is never any worse than 285 ft/sec. The magnitude of error in
estimated β for Case 1 is never more than 665 lb/ft^2, and for Case 2
it is never more than 105 lb/ft^2 after 3.5 sec of filtering.

C. Performance of the Fully Implemented Extended Kalman Filter with Different Data Rates

The simplest scheme for improving the real-time capability of the
Kalman filter is simply to decrease the data rate. If the sample
intervals are lengthened and the additional time between samples is not
used to presmooth the measurements (i.e., the intermediate measurements
are discarded), then obviously the filter performance will deteriorate
to some extent. Reference 1 discusses the performance of the extended
Kalman filter for four representative endoatmospheric cases. However,
no attempt was made in Ref. 1 to investigate the effect of both decreasing
the data rate and presmoothing the intermediate measurements. The present
study considers the situation where the presmoothing is done by fitting
the data to a curve that approximates the trajectory of the ballistic
missile. Of course, in practice, data is presmoothed by curve-fitting
with polynomials that are not precise representations of missile tra-
jectories.

The assumption of data presmoothing implies that in the filter
equations the measurement-noise covariance should be reduced accordingly.
If the measurement-noise covariance at a particular time is $R^0(k)$ for
a sample interval of Δt_o, then one approximation to its reduced value,

30

VELOCITY ERROR — ft/sec

2500

1250

0

POSITION ERROR — ft

1000

500

0

ACCELERATION ERROR — g

10
8
6
4
2
0

BETA — lb/ft²

3000

1500

0

TIME — sec
(a)

TIME — sec
(b)

TIME — sec
(c)

TIME — sec
(d)

ESTIMATE

ACTUAL
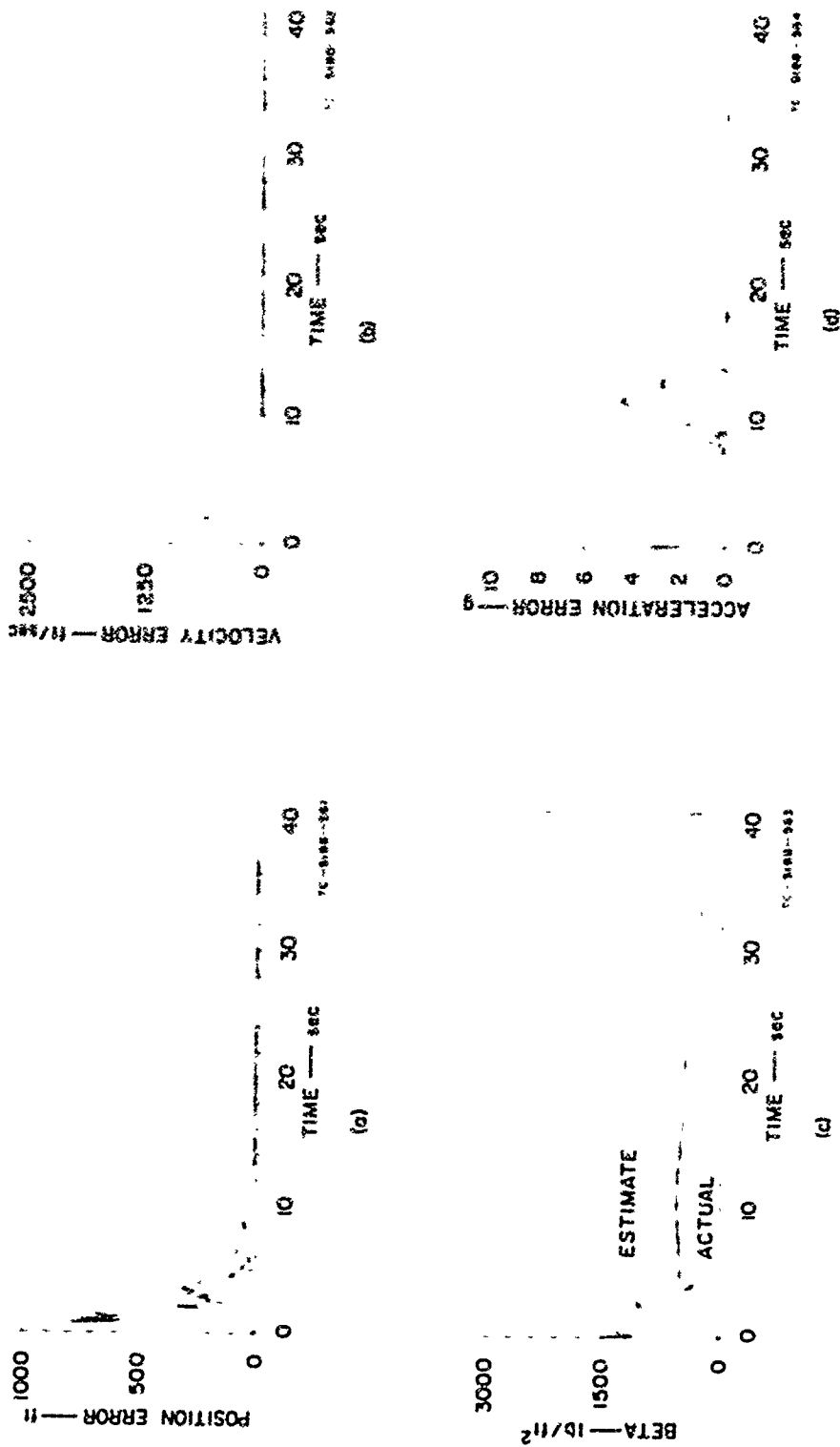
FIG 5 ESTIMATION ERRORS FOR FULLY-IMPLEMENTED KALMAN FILTER — CASE 2, γ_t 0.05 sec

with a larger sample interval Δt and with presmoothing, is
$R(k) = R^O(k) \dfrac{\Delta t_o}{\Delta t}$. To see how this is derived, suppose that the measure-
ment vector is a linear function of time t_i in the interval $[t_k,$
$t_k + \Delta t]$ with additive noise v_i (i.e., $z_i = p + st_i + v_i$), and its
rate of change, s, at $t = t_k$ is known (equivalently, our estimate
of the velocity s equals its actual value). Now, we estimate the
unknown parameter p by subtracting st_i from the measurements at the
times $t_i = t_k$, $t_k + \Delta t_o$, $t_k + 2\Delta t_o$, ..., $t_k + \Delta t$ (where $\Delta t = n \Delta t_o$)
and average the resulting quantities. Let $\bar{p}$ designate the computed
average and $\bar{z}(t_k + \Delta t) = \bar{p} + s(t_k + \Delta t)$ be the presmoothed version of
the measurement $z(t_k + t)$, where v_i is zero mean.

Noting that $E[\bar{p}] = p$, the covariance of $\bar{z}$ is seen to be given by

$$
\begin{aligned}
E\{(\bar{z} - E[\bar{z}])(\bar{z} - E[\bar{z}])^T\} &= E\{(\bar{p} - E[\bar{p}])(\bar{p} - E[\bar{p}]^T\} \\
&= E\{(\bar{p} - p)(\bar{p} - p)^T\} \\
&= E\{[\frac{1}{n} \sum_i^n (p + v_i) - p][\frac{1}{n} \sum_{i=1}^n (p + v_i) - p]^T\} \\
&= E\{\frac{1}{n^2} \left(\sum_{i=1}^n v_i\right)\left(\sum_{j=1}^n v_j\right)^T\} \\
&= \frac{1}{n^2} \sum_{i=1}^n E[v_i v_i^T] \quad , \quad \text{since } E[v_i v_j^T] = 0 \text{ for } i \neq j \\
&= \frac{R^O}{n} \\
&= R^O \frac{\Delta t_o}{\Delta t} \quad , \quad\quad\quad\quad (52)
\end{aligned}
$$

where R^O, the covariance of the measurement noise v_i, is assumed
constant over the interval $[t_k, t_k + \Delta t]$.

In the computer simulations done for this report, the presmoothing
of the measurements was simulated by scaling the measurement noise by
the factor $\sqrt{\Delta t_o/\Delta t}$. This corresponds to decreasing the measurement
noise covariance by the factor $\Delta t_o/\Delta t$. It should be noted that this
presmoothing assumption is overly optimistic.

The estimation error plots of Figs. 6 through 11 illustrate the
effects of data presmoothing upon the extended Kalman filter's performance
for Case 1. Figures 6, 8, and 10 show the effects of increasing the

32
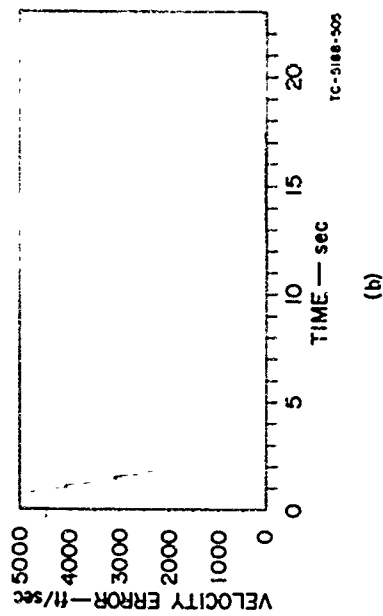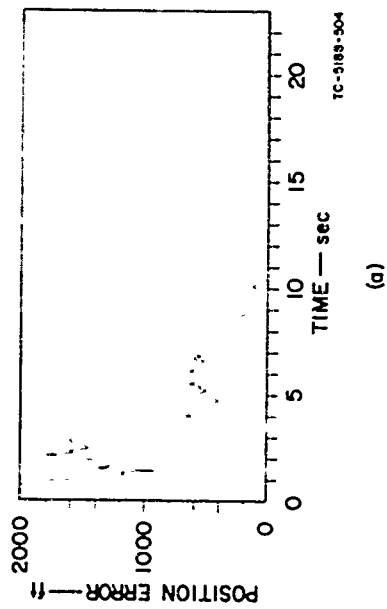
FIG. 6 ESTIMATION ERRORS FOR FULLY-IMPLEMENTED KALMAN FILTER — CASE 1,
Δt = 0.10 sec WITHOUT PRESMOOTHING

FIG. 7 ESTIMATION ERRORS FOR FULLY-IMPLEMENTED KALMAN FILTER — CASE 1,
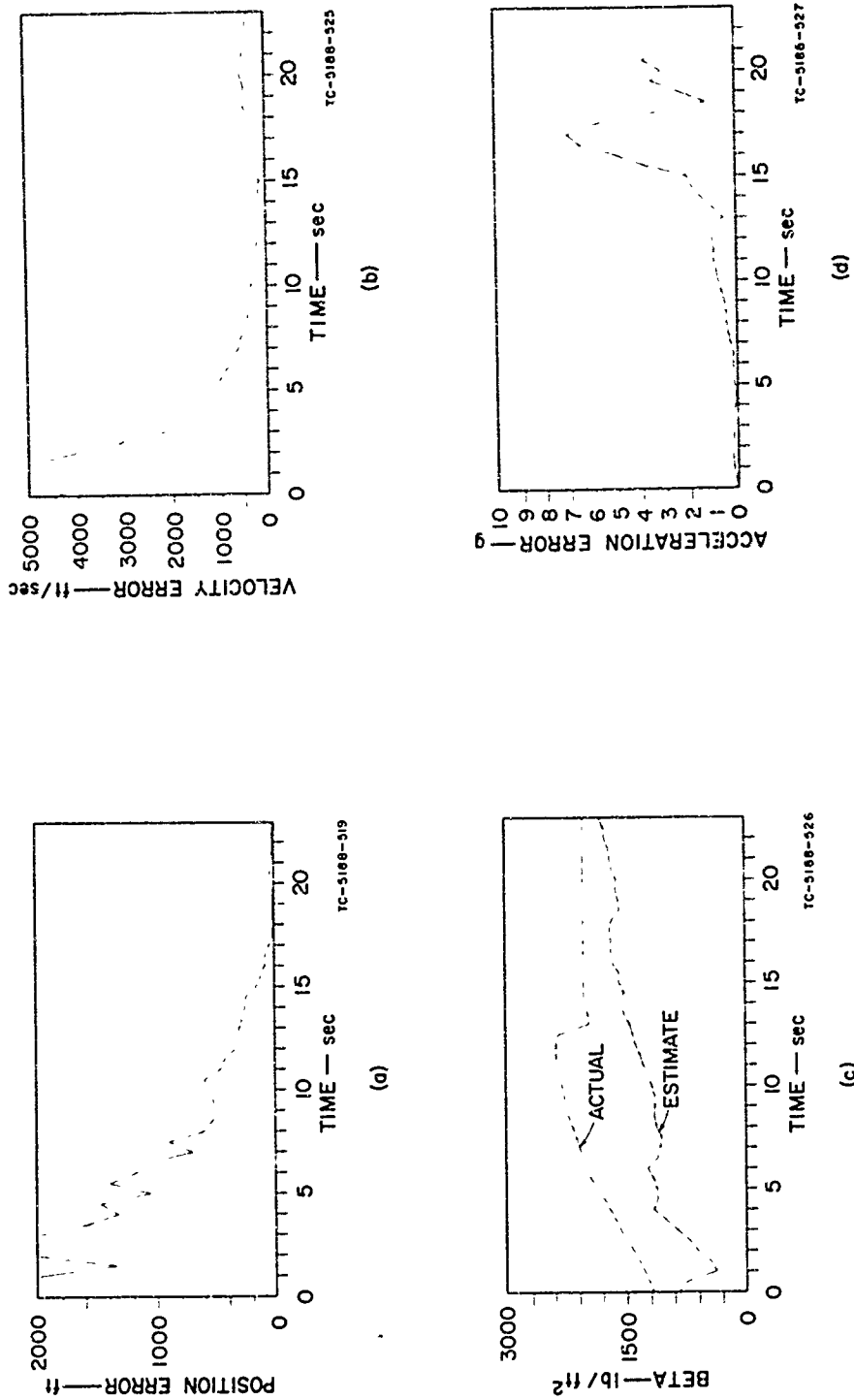Δt = 0.10 sec WITH PRESMOOTHING

34

VELOCITY ERROR—ft/sec

5000
4000
3000
2000
1000
0

TIME — sec

0   5   10   15   20

(b)

TC-5188-509

ACCELERATION ERROR—g

10 9 8 7 6 5 4 3 2 1 0

TIME — sec

0   5   10   15   20

(d)

TC-5188-511

POSITION ERROR—ft

2000
1000
0

TIME — sec

0   5   10   15   20

(a)

TC-5188-508

BETA—lb/ft²

3000
1500
0

ACTUAL

ESTIMATE

TIME — sec

0   5   10   15   20

(c)

TC-5188-510
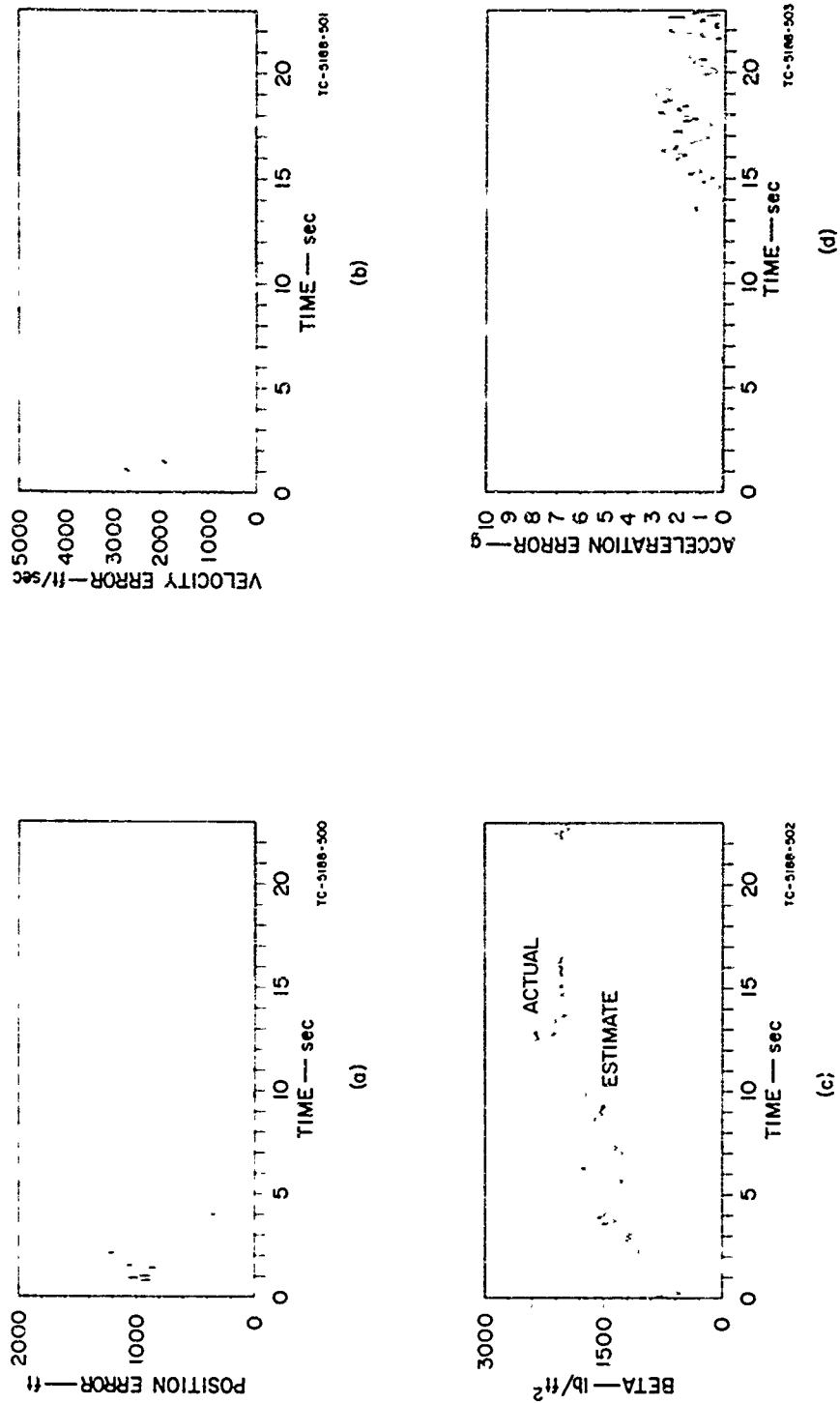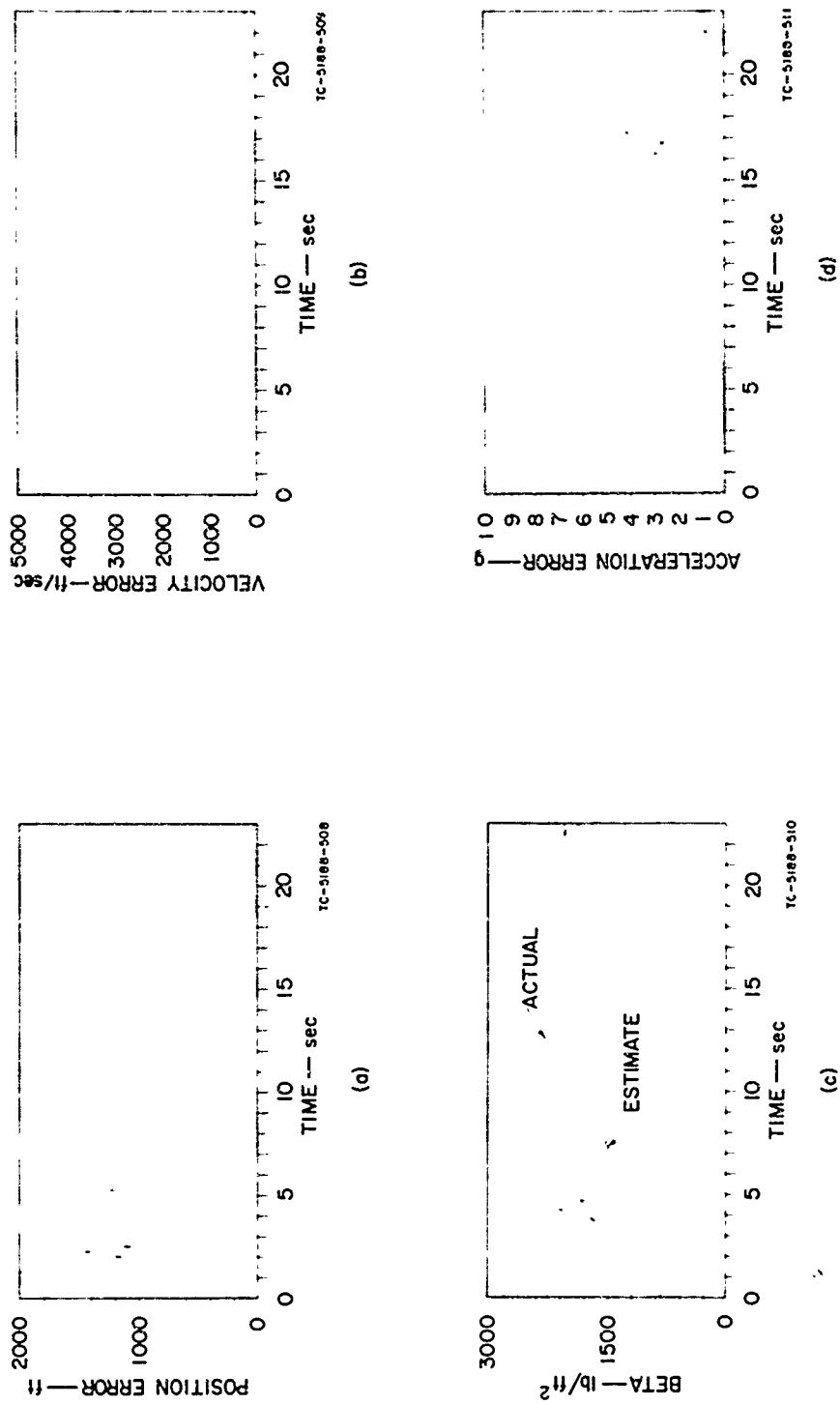
FIG. 8   ESTIMATION ERRORS FOR FULLY-IMPLEMENTED KALMAN FILTER — CASE 1,
Δt 0.25 sec WITHOUT PRESMOOTHING

35
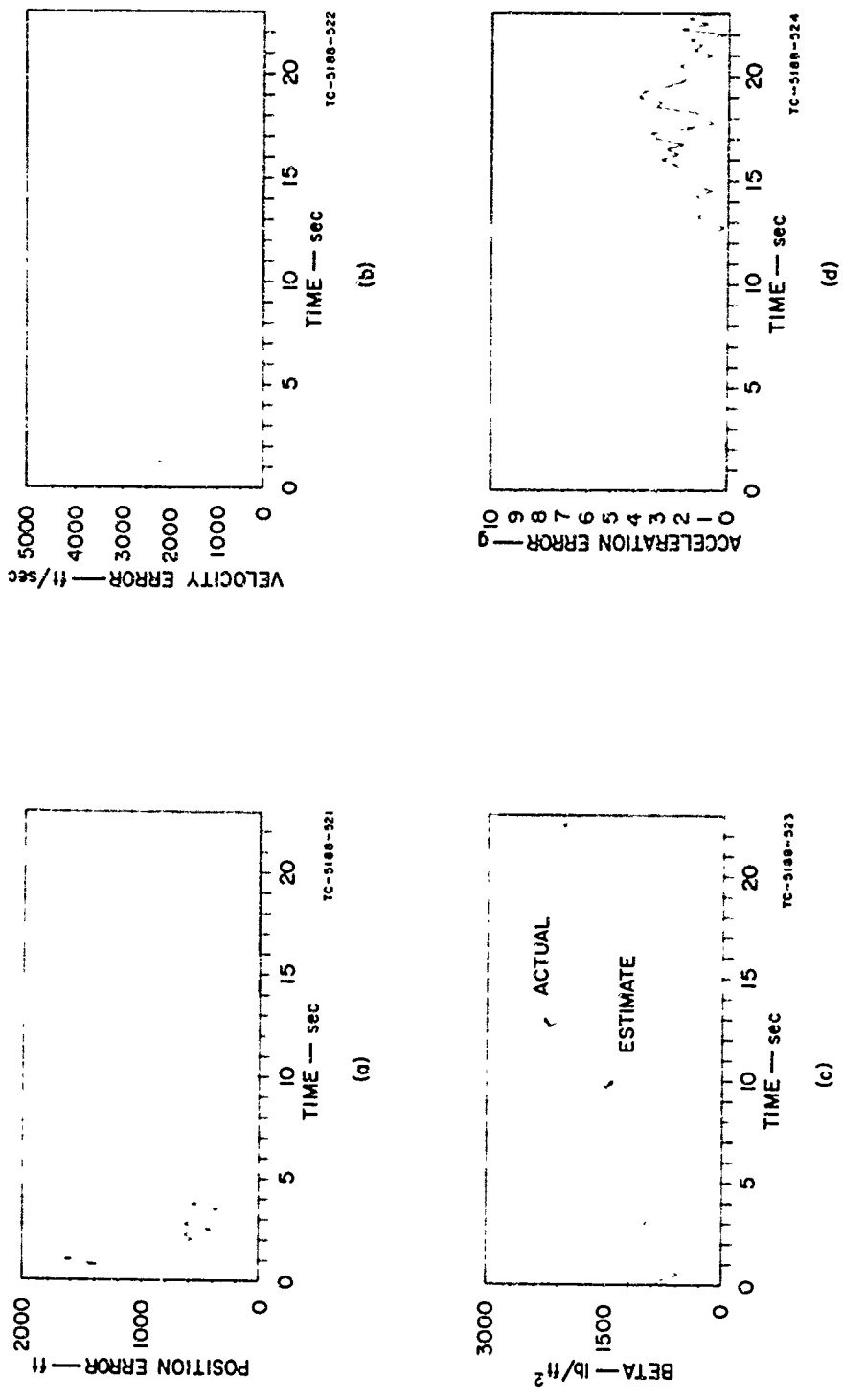
FIG. 9 ESTIMATION ERRORS FOR FULLY-IMPLEMENTED KALMAN FILTER — CASE 1,
Δt = 0.25 sec WITH PRESMOOTHING

36

FIG. 10 ESTIMATION ERRORS FOR FULLY-IMPLEMENTED KALMAN FILTER — CASE 1,
$\Delta t = 0.50$ sec WITHOUT PRESMOOTHING

37
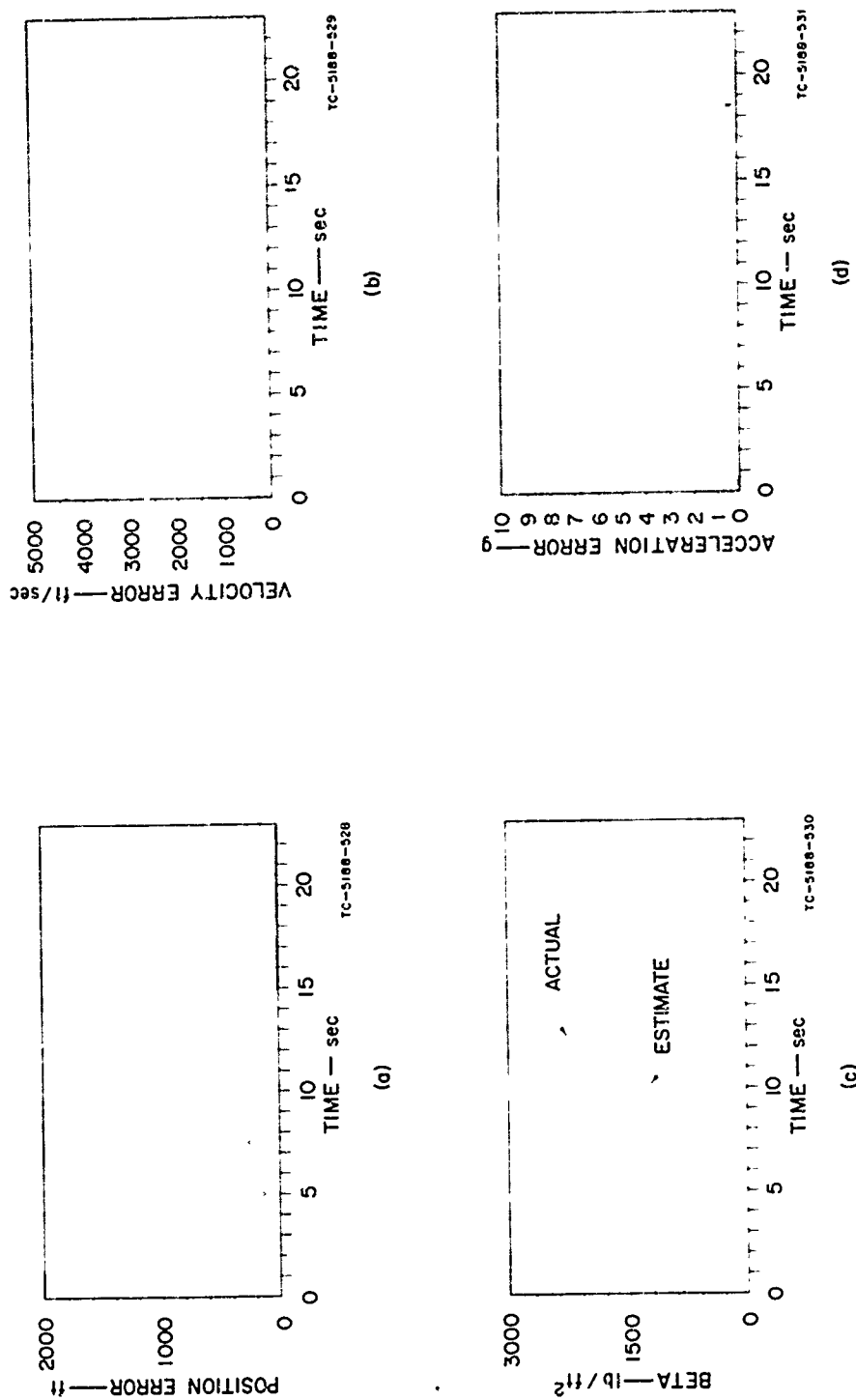
FIG. 11 ESTIMATION ERRORS FOR FULLY-IMPLEMENTED KALMAN FILTER — CASE 1,
Δt = 0.50 sec WITH PRESMOOTHING

sample interval (decreasing the data rate) from $\Delta t = 0.05$ sec to $\Delta t = 0.10$, 0.25, and 0.50 sec, respectively, when no data presmoothing is done. In other words, the filter's data rate is decreased by processing fewer measurements in any given time. Figures 7, 9, and 11 show the effects of increasing the sample interval of the filter from $\Delta t = 0.05$ sec to $\Delta t = 0.10$, 0.25, and 0.50 sec, respectively, while also using the increased time between samples to presmooth the measurement data. The presmoothing assumptions described above are used for the results presented in Figs. 7, 9, and 11.

Figures 6, 8, and 10 indicate that if presmoothing is not done the estimation errors become increasingly larger as the filter's sample interval Δt is increased. However, Figs. 7, 9, and 11 indicate that if the data is presmoothed the position and velocity estimation errors generally decrease with increasing Δt. Thus, the reduction of the measurement noise through presmoothing is beneficial in position and velocity estimation.

The random disturbance covariance $Q(k)$ given by Eq. (51) is seen to increase linearly with increasing Δt. For ballistic coefficient and acceleration estimation, this increase in $Q(k)$ apparently dominates the decrease in the measurement noise covariance $R(k)$ when the data is presmoothed. That is, the errors in the β and acceleration estimates, as shown in Figs. 7, 9, and 11, increase with increasing Δt, even with presmoothing of the data. Hence, increasing the sample interval generally leads to a deterioration in ballistic coefficient and acceleration estimation. This is to be expected since the square root of $Q_{77}(k)$ [see Eq. (51)], which is the standard deviation in the assumed random disturbance noise affecting x_7, is of the same order of magnitude as the actual values of x_7; whereas, the standard deviation of the position disturbance noise is zero, and the standard deviation of the velocity disturbance noise is very small in relation to the actual velocity values [see Eq. (51)]. Since the ballistic coefficient β is derived from x_7 (i.e., $\beta = \rho/x_7$), the random disturbance affecting x_7 is of major importance in estimating β. Consequently, since $Q_{77}(k)$ increases linearly with the sample interval Δt with or without presmoothing, it follows that β estimation errors are expected to increase

39

with increasing Δt. In turn, the errors in ballistic coefficient estimation lead to errors in the estimate of acceleration, since the aerodynamic-drag accelerations are in error.

For Case 1, the pairs of Figs. 6 and 7, 8 and 9, 10 and 11 illustrate the extended Kalman filter performance, with and without data presmoothing, for sample intervals of $\Delta t = 0.10$, 0.25, and 0.50 sec, respectively. As noted above, the presmoothing assumption of Eq. (52) is optimistic; and for a given Δt, the filter estimation errors for actual presmoothing will be somewhere between the errors given in the corresponding pair of figures. Thus, for the particular simulations presented here, we have bounded the filter estimation errors for different values of Δt.

Figures 12 a, b, and c show the standard deviations in the estimates of position, velocity, and β as computed from the diagonal elements of the calculated estimation error covariance [Eq. (29)]. Each of the Figs. 12 a, b, and c shows two curves: Curve (i) is the calculated standard deviation when data is not presmoothed, and Curve (ii) is the calculated standard deviation when presmoothing has been performed; these plots are for Case 1, with a sample interval of $\Delta t = 0.25$ sec. The standard deviation in position error is calculated as the square root of the sum of the first three diagonal elements of the filter covariance matrix, $P(k/k)$. That is, the standard deviation of position error is given by $\sqrt{P_{11} + P_{22} + P_{33}}$. Likewise, the standard deviation of velocity error is calculated as $\sqrt{P_{44} + P_{55} + P_{66}}$. The standard deviation for the error in β estimation is calculated using a rough approximation. The ballistic coefficient β is not estimated directly, but is derived from $\hat{x}_7$. Since x_7 is defined as $x_7 = \rho/\beta$ (with ρ = mass density of the atmosphere), it follows that $\beta = \rho/x_7$. To first order, we have

$$\hat{\beta} - \beta = \frac{-\hat{\rho}}{(\hat{x}_7)^2} (\hat{x}_7 - x_7) \quad ,$$

so that a rough approximation for the standard deviation of $\hat{\beta}$ is

$$\frac{\hat{\rho}}{(\hat{x}_7)^2} \sqrt{P_{77}} \quad ,$$

in which P_{77} is the seventh diagonal element of $P(k/k)$ and $\hat{\rho} = \rho(\hat{h})$.

The standard deviation plots of Fig. 12 a, b, and c provide a valuable measure of the filter's performance. For instance, if the

40
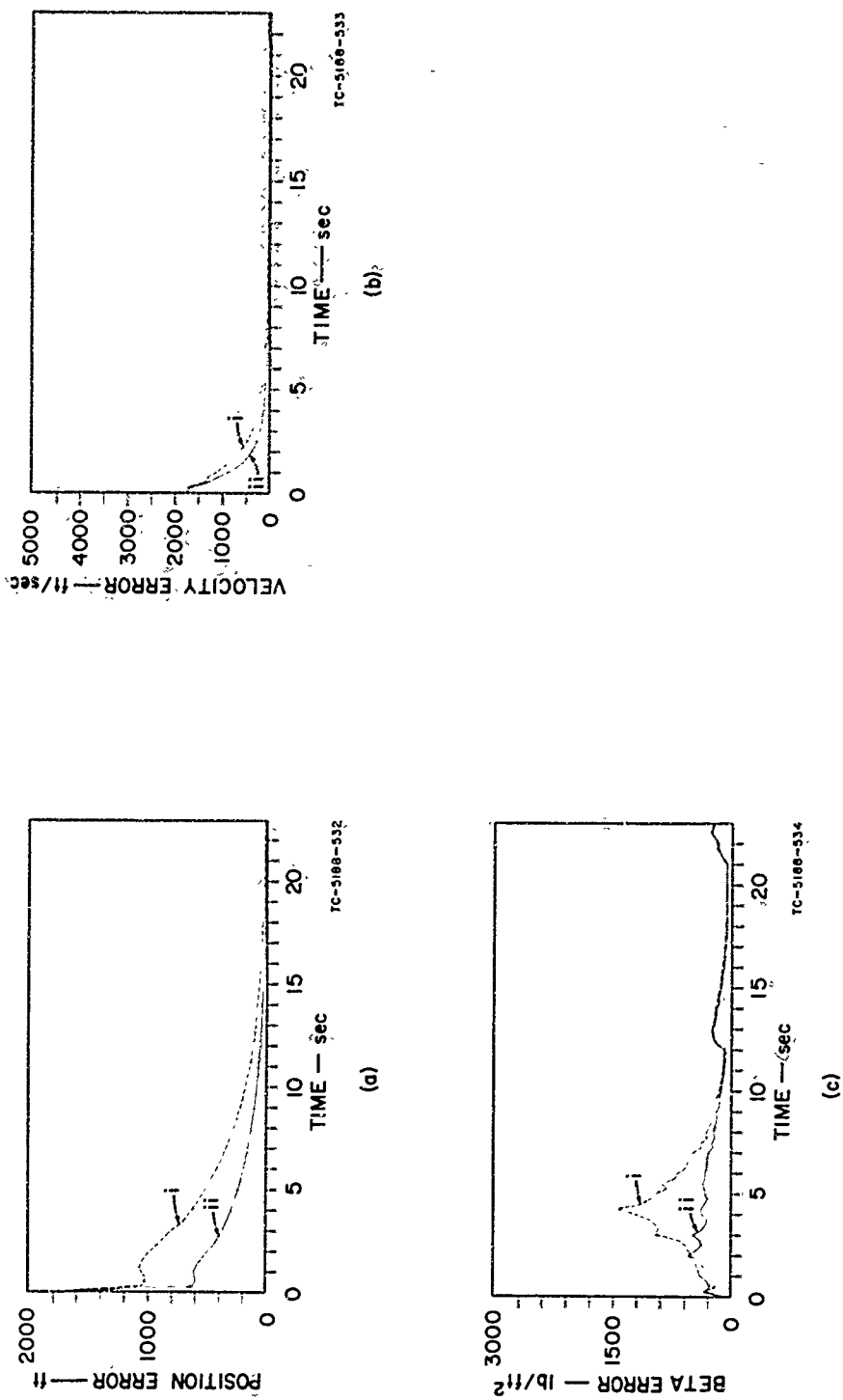
FIG. 12 STANDARD DEVIATIONS FOR FULLY-IMPLEMENTED KALMAN FILTER — CASE 1.
Δt = 0.25 sec: (i) WITHOUT PRESMOOTHING, (ii) WITH PRESMOOTHING.

41

magnitude of the position estimation error differs significantly from the calculated standard deviation of the position error [as computed from $P(k/k)$], then the filter is doing the estimation task poorly-- perhaps because of inaccurate modeling of the missile dynamics or measurement noise in the filter equations. Also, when presmoothing of the measurements leads to a reduction in the magnitude of the estimation errors, the calculated standard deviations should also show a reduction. Figure 12 shows that the calculated standard deviations [derived from $P(k/k)$] are in correspondence with the actual estimation error magnitudes (both with and without presmoothing). Also, the standard deviations in position and velocity estimation errors are reduced (as expected) when data is presmoothed. Comparison of Figs. 8 and 9 with Fig. 12 reveals that the actual estimation errors are less than two standard deviations for almost all of the filtering time.

Figures 13 a, b, and c show the standard deviations in position, velocity, and β estimation errors for (i) a sample interval of 0.05 sec, and (ii) a sample interval of 0.50 sec; Curves (i) and (ii) are for Case 1 with no data presmoothing. Again, the standard deviation plots agree with the actual estimation error magnitudes. For instance, comparison of Figs. 4 and 10 with Fig. 13 shows that the position esti- mation error magnitude increases when Δt is increased from 0.05 sec to 0.50 sec, but this is to be expected since, with no presmoothing, the calculated position standard deviation (Fig. 13 a) also increases.

Figures 14 through 19 show the estimation error magnitudes when the sample interval length is increased from $\Delta t = 0.05$ sec to $\Delta t = 0.10$, 0.25, and 0.50 sec for Case 2. Estimation error magnitudes are pre- sented for the situation where there is presmoothing of measurements and also where there is no presmoothing. The conclusions are similar to those drawn for Case 1 from Figs. 6 through 11.

Figure 20 shows the effect of presmoothing upon the calculated standard deviations of the estimation errors for a sample interval of $\Delta t = 0.25$ sec in Case 2. Again, the conclusions are the same as those drawn for Case 1 from Fig. 12.

42
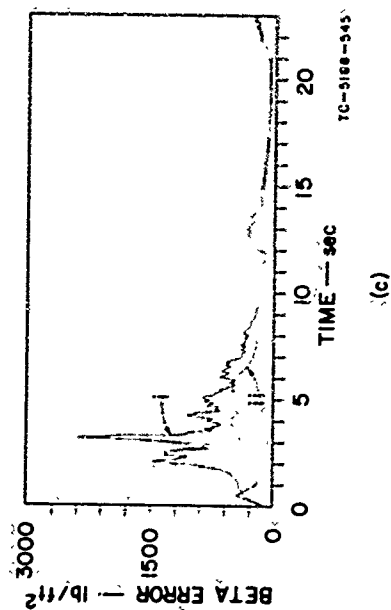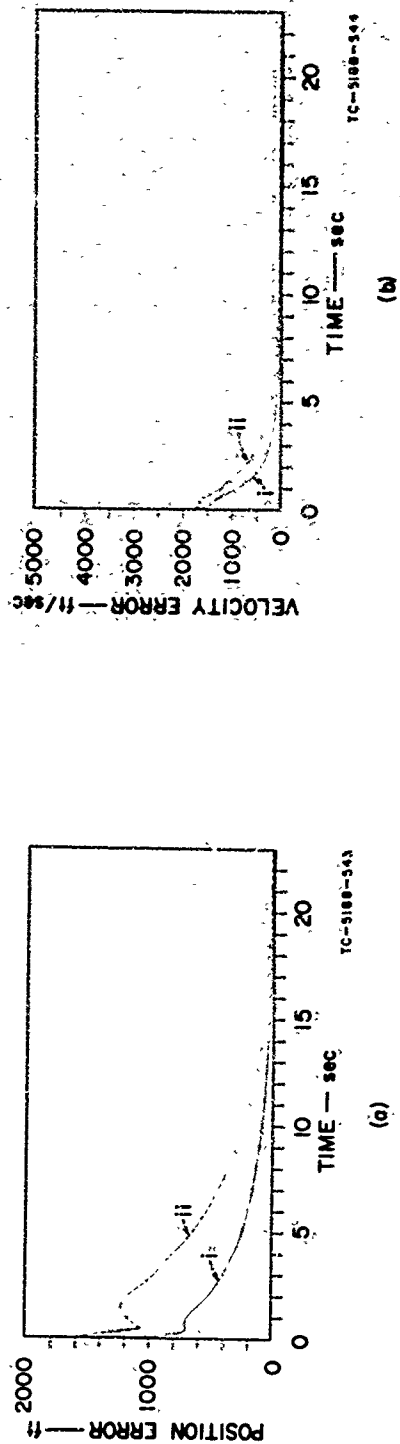
FIG. 13 STANDARD DEVIATIONS FOR FULLY-IMPLEMENTED KALMAN FILTER — CASE 1, WITHOUT PRESMOOTHING: (i) $\Delta t = 0.05$ sec, (ii) $\Delta t = 0.50$ sec

43
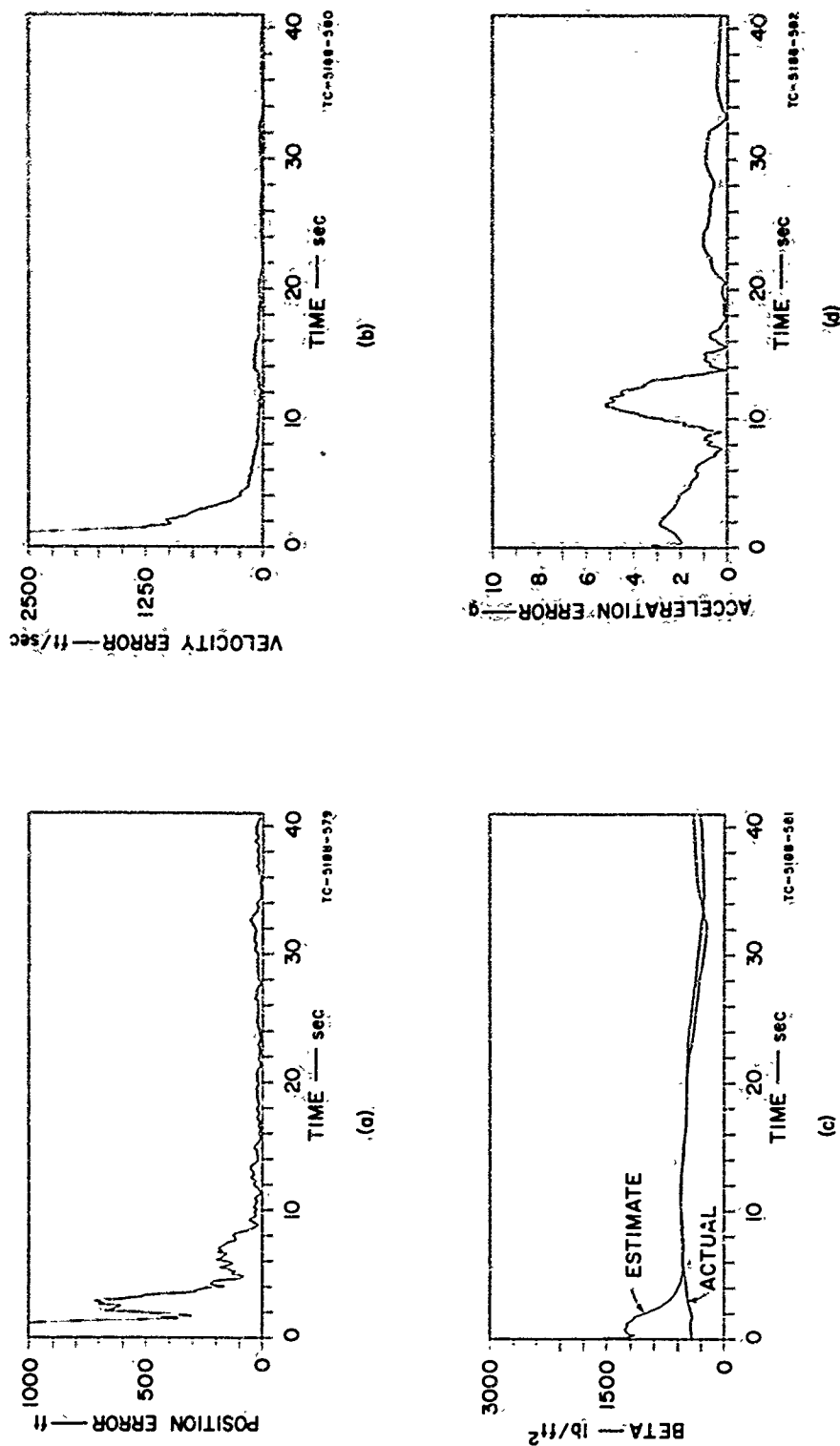
FIG. 14   ESTIMATION ERRORS FOR FULLY-IMPLEMENTED KALMAN FILTER — CASE 2,
$\Delta t = 0.10$ sec WITHOUT PRESMOOTHING

44
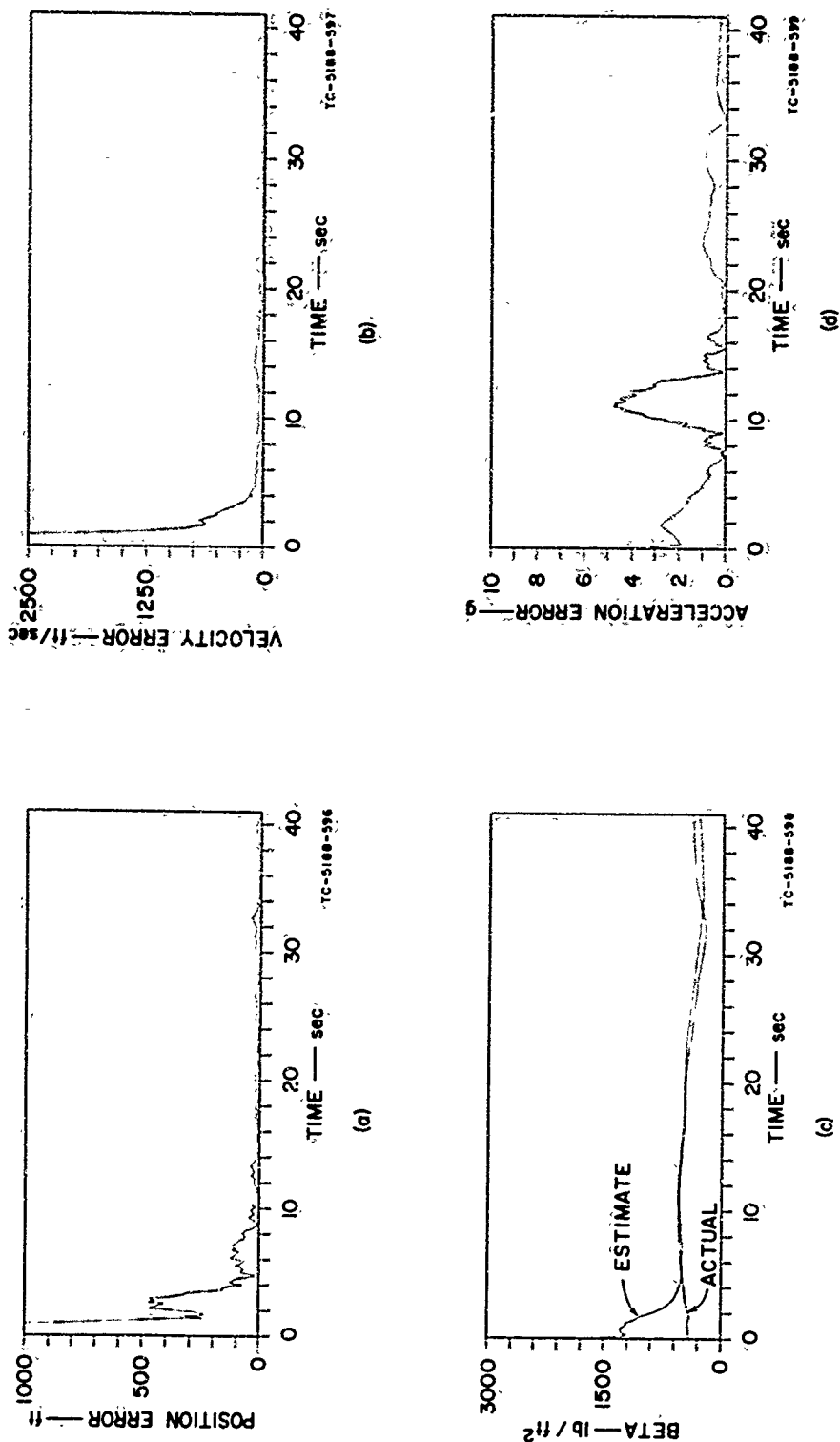
FIG. 15 ESTIMATION ERRORS FOR FULLY-IMPLEMENTED KALMAN FILTER — CASE 2;
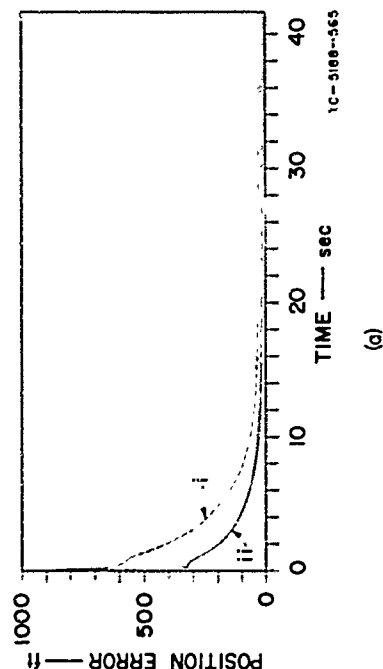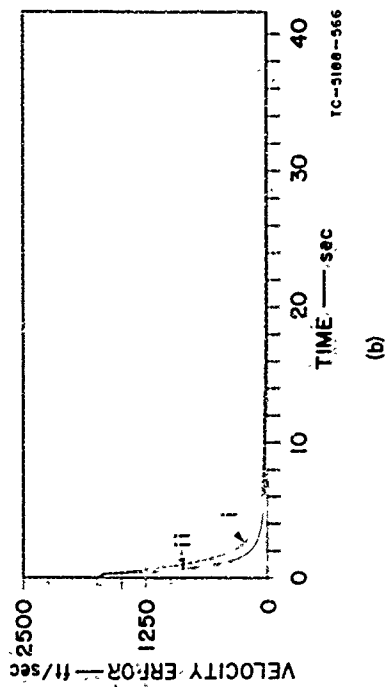Δt = 0.10 sec WITH PRESMOOTHING

45
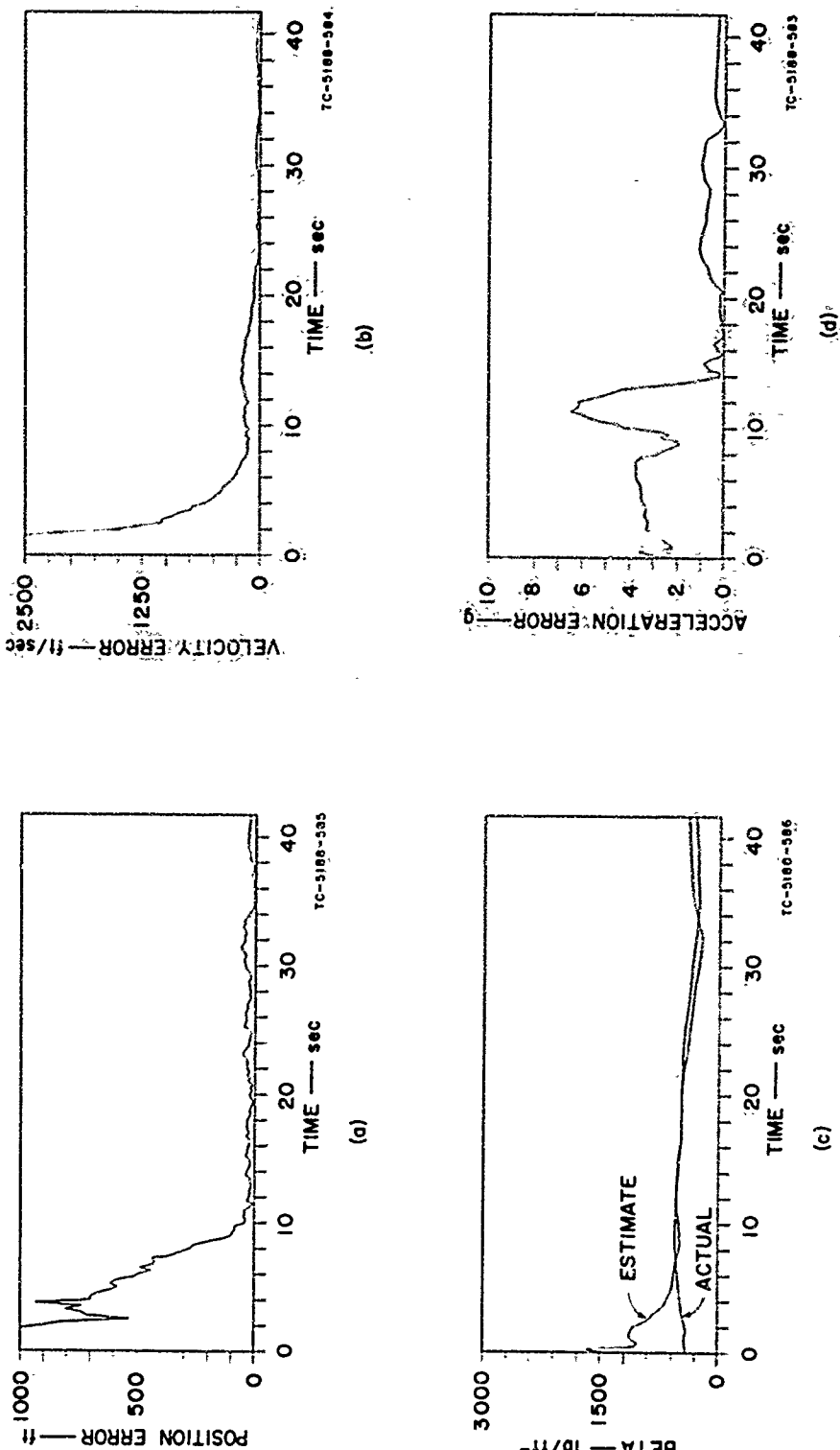
FIG. 16 ESTIMATION ERRORS FOR FULLY-IMPLEMENTED KALMAN FILTER — CASE 2,
Δt = 0.25 sec WITHOUT PRESMOOTHING

46
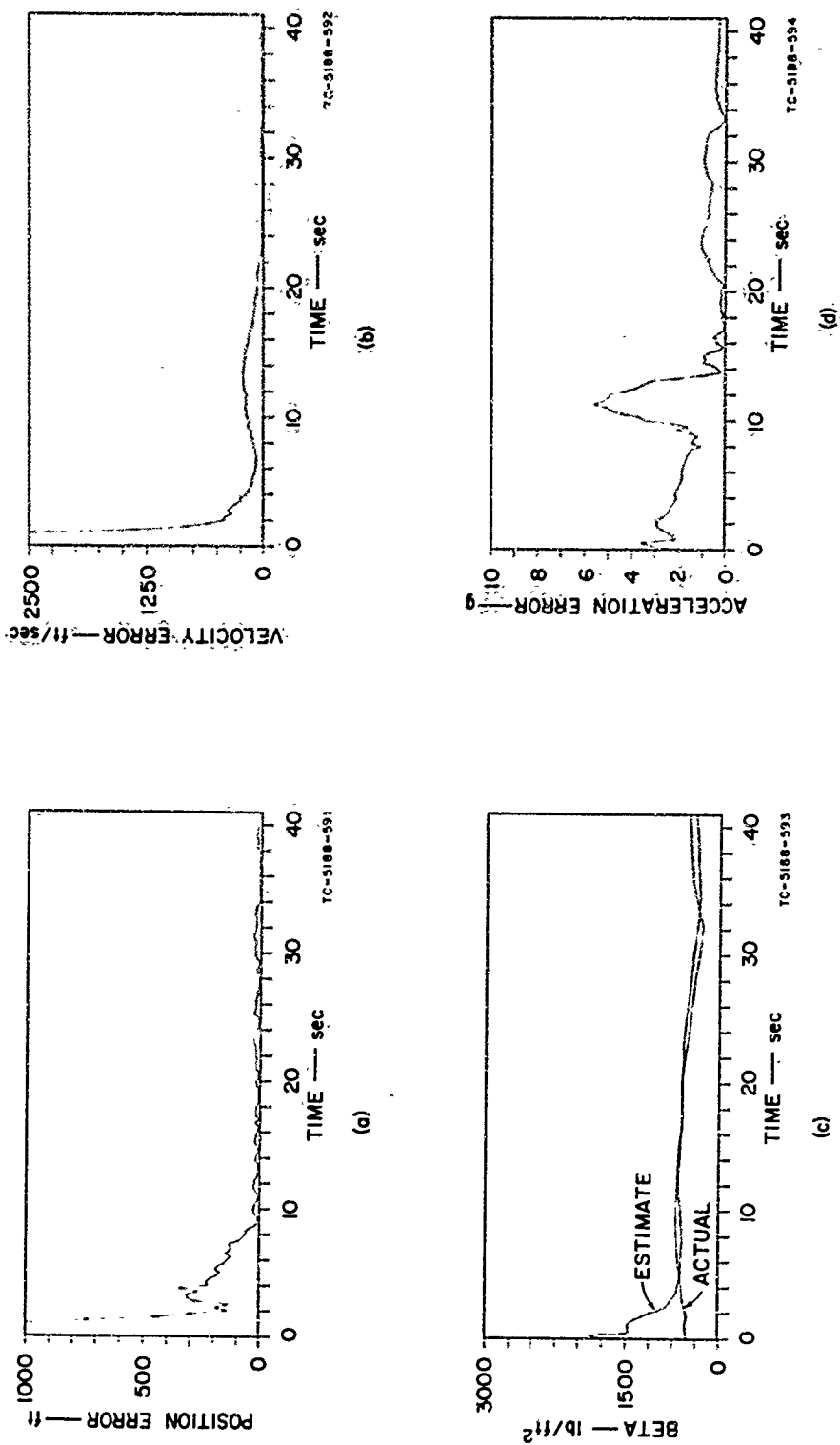
FIG. 17 ESTIMATION ERRORS FOR FULLY-IMPLEMENTED KALMAN FILTER — CASE 2,
Δt = 0.25 sec WITH PRESMOOTHING

47
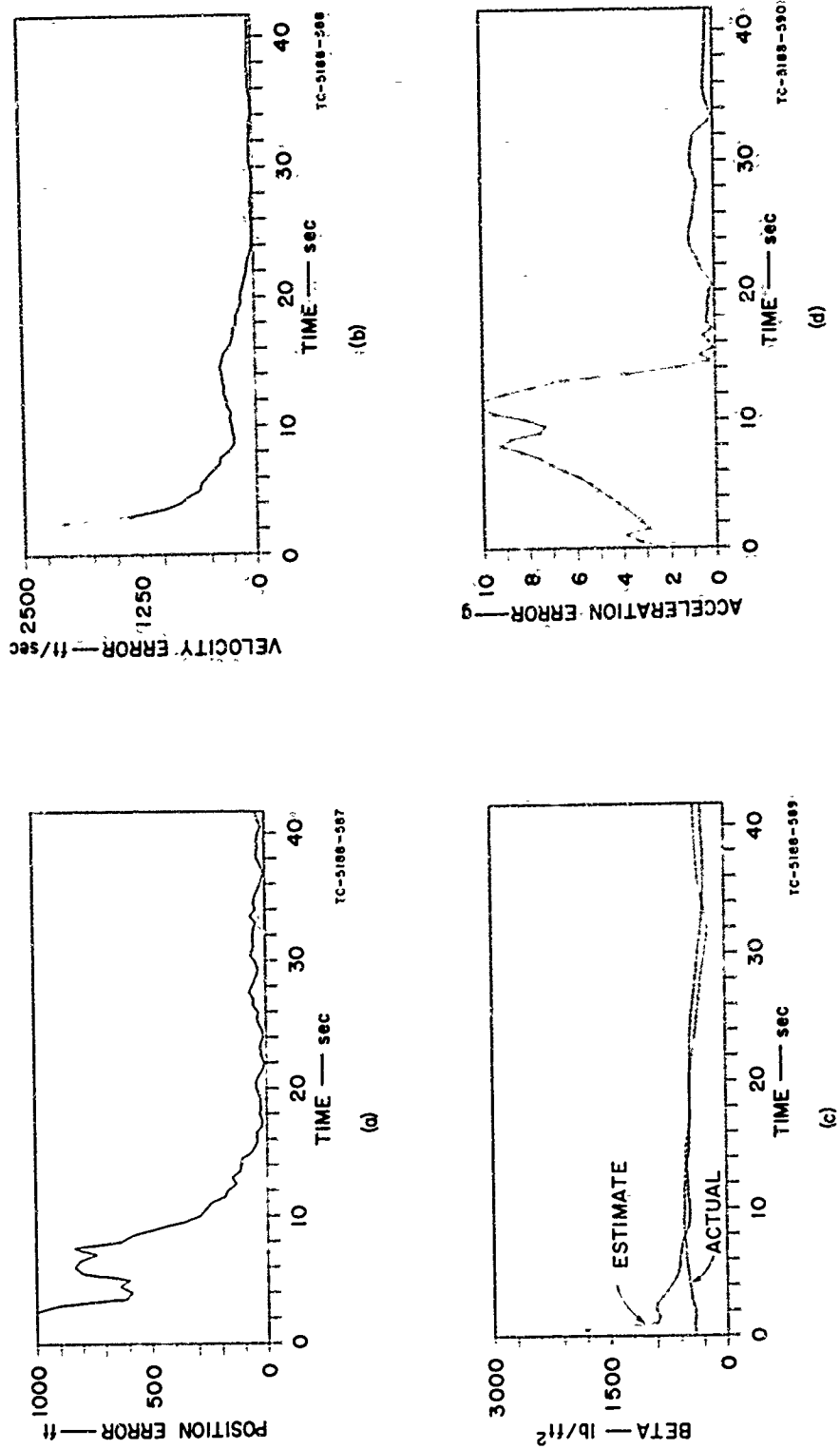
FIG. 18   ESTIMATION ERRORS FOR FULLY-IMPLEMENTED KALMAN FILTER — CASE 2,
$\Delta t = 0.50$ sec WITHOUT PRESMOOTHING

48
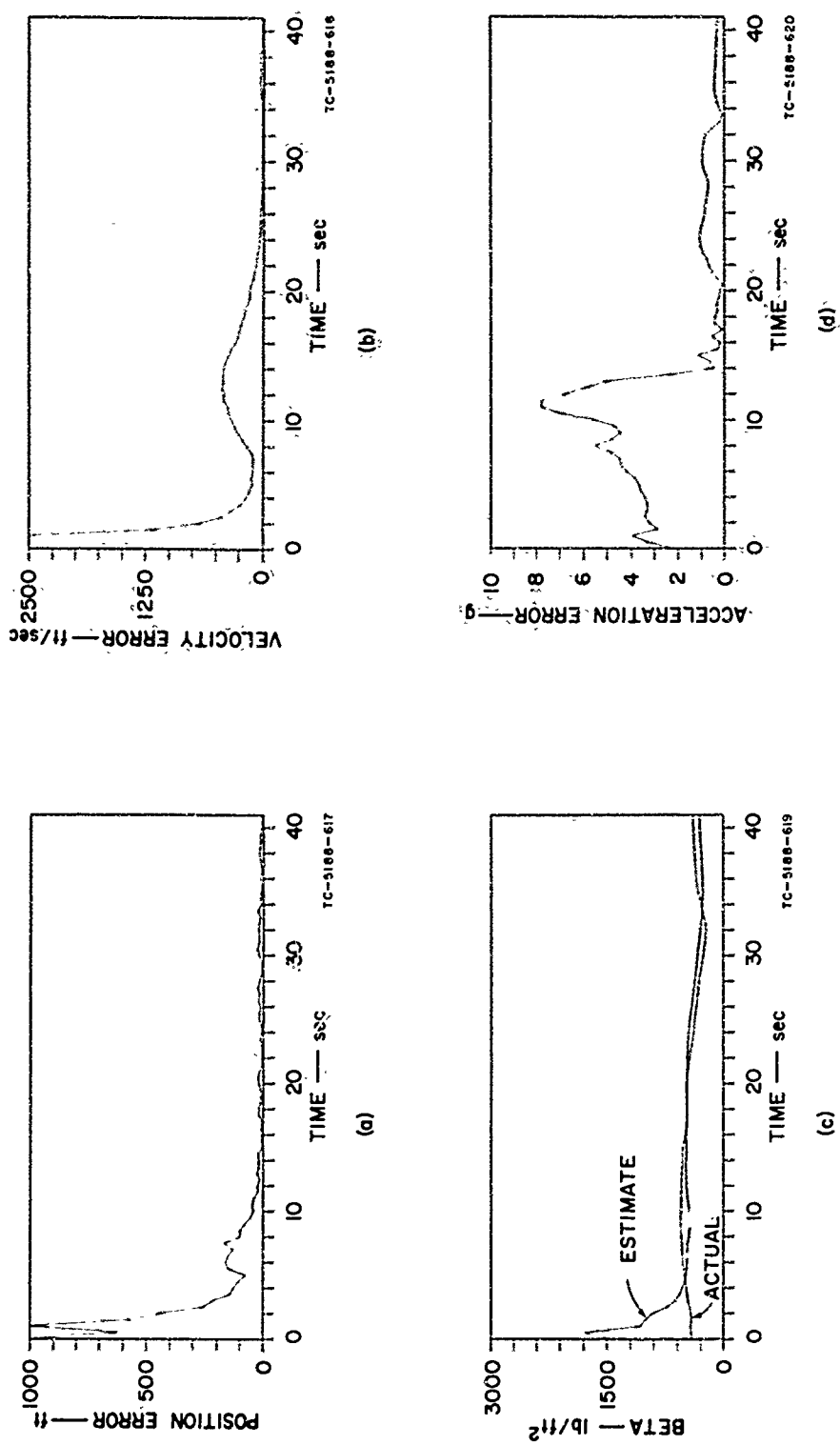
FIG. 19 ESTIMATION ERRORS FOR FULLY-IMPLEMENTED KALMAN FILTER — CASE 2, Δt = 0.50 sec WITH PRESMOOTHING.

49
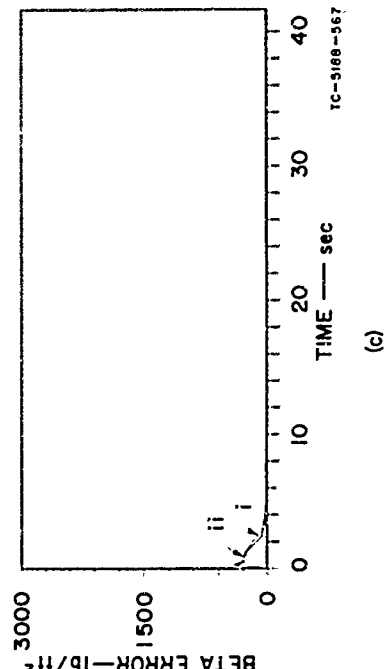
FIG. 20 STANDARD DEVIATIONS FOR FULLY-IMPLEMENTED KALMAN FILTER — CASE 2;
$\Delta t = 0.25$ sec: (i) WITHOUT PRESMOOTHING, (ii) WITH PRESMOOTHING

50

Figure 21 shows the effect (for Case 2) upon the calculated standard deviations in the estimation errors of decreasing the data rate. The plots show the effect of decreasing the data rate from 20 measurements per second to 2 measurements per second--when there is no measurement presmoothing. Again, the conclusions are the same as those drawn for Case 1 from Fig. 13.

A recent study[6] discusses the sensitivity of the Kalman filter performance to changes in the sample interval Δt. In particular, the effects of data presmoothing are discussed there. It was shown that the presmoothing assumed here tends to be overly optimistic; since any change of the noise assumptions tends to cause the filter performance to deteriorate from its performance with the assumed presmoothing [Eq. (52)].

D. Performance of the Piecewise-Recursive Kalman Filter

The figures and timing estimates given below indicate that the piecewise-recursive Kalman filter (described in Sec. IV) is an extremely attractive alternative to the fully implemented (extended) Kalman filter for real-time endoatmospheric estimation. Using this filtering method, it is possible to obtain large reductions in computation time with little sacrifice in estimation accuracy. With the Univac 1108 computer, it is possible (as shown below) to filter measurements at a speed approximately 25 times faster than real time for endoatmospheric estimation, and yet obtain accuracy approaching that of the fully implemented Kalman filter.

Since the fully implemented Kalman filter is approximately five times faster than real-time (see Sec. III C) on the Univac 1108 for endoatmospheric trajectory estimation ($\Delta t = 0.05$ sec), this means that the piecewise-recursive Kalman filter is about five times faster than the fully implemented Kalman filter (the relative speed of the two filters is computer-independent). With the Univac 1108 Computer, a total time of 0.010 sec is needed to process each measurement and compute an estimate of the state of the ballistic missile (as well as the estimation error covariance) using the fully implemented Kalman filter. When the piecewise-recursive Kalman filter is used for the estimation, two timing figures should be noted. This arises from the fact (as discussed in Sec. IV) that there are two different modes of operation for the

51
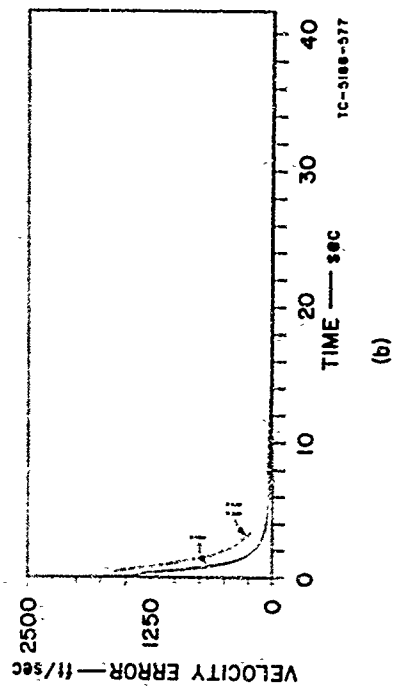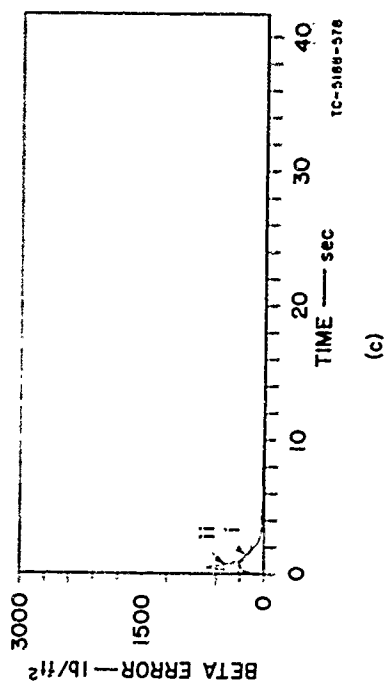
FIG. 21 STANDARD DEVIATIONS FOR FULLY-IMPLEMENTED KALMAN FILTER — CASE 2, WITHOUT PRESMOOTHING: (i) $\Delta t = 0.05$ sec, (ii) $\Delta t = 0.50$ sec

52

piecewise-recursive Kalman filter: in the first mode, the filter calculates a weighting matrix, two error covariance matrices, and a state estimate; in the second mode, the filter only calculates a state estimate without the weighting matrix or error covariance computations being performed.

From the simulations on the Univac 1108 for the endoatmospheric cases, it was found that in the first mode, the piecewise-recursive Kalman filter used an average of 0.0173 sec per iteration, while it used an average of only 0.0007 sec per iteration in the second mode. Since on the Univac 1108 a filter iteration takes 0.0100 sec using the fully implemented (extended) Kalman filter, this means that in the first mode, the piecewise-recursive Kalman filter is approximately 1.7 times slower than the fully implemented Kalman filter; however, in the second mode, the piecewise-recursive Kalman filter is about 14 times faster than the fully implemented Kalman filter. The piecewise-recursive Kalman filter encounters a first-mode calculation once every $\Delta\tau$ seconds; and if $N = \Delta\tau/\Delta t$, it encounters a second-mode calculation $N-1$ times during a time span of $\Delta\tau$ seconds. Thus, for large values of N, the speed of the piecewise-recursive Kalman filter in the second mode predominates over that of the first mode. For the endoatmospheric trajectories, the average iteration time of the piecewise-recursive Kalman filter as a function of N (for the values of N encountered in the computer simulations) is given in Table III.

Using the values in Table III, one can calculate the average speed of the piecewise-recursive Kalman filter relative to real time for different $\Delta\tau$ and Δt. For instance, if $\Delta\tau = 0.5$ sec and $\Delta t = 0.10$ sec, then the speed of the filter is about 25 times faster than real time (on the Univac 1108); if $\Delta\tau = 0.5$ sec and $\Delta t = 0.05$ sec, then the speed of the filter is about 20 times faster than real time (on the Univac 1108). Thus, the piecewise-recursive Kalman filter can, on the average, process incoming measurements 20 to 25 times faster than they are received. Effectively then, one Kalman filter of this type could give state estimates for 20 to 25 endoatmospheric ballistic targets in real time.

53

Table III

ITERATION TIMES FOR PIECEWISE-RECURSIVE KALMAN FILTER
(ENDOATMOSPHERIC CASES)

$N = \dfrac{\Delta\tau}{\Delta t}$	AVERAGE FILTER ITERATION TIME (sec)	ITERATION TIME IN FIRST MODE (sec)	ITERATION TIME IN SECOND MODE (sec)
3	0.0061		
5	0.0040		
6	0.0035		
10	0.0024	0.0173	0.0007
15	0.0019		
20	0.0016		
30	0.0013		

Now, let us discuss the accuracy of the state estimation using the piecewise-recursive Kalman filter. It should be pointed out that in all of the figures of this section (for both Case 1 and Case 2) the filter was allowed to operate as a fully implemented Kalman filter for the first four iterations; this operation serves as an initialization for the piecewise-recursive Kalman filter. The estimation errors obtained through simulation for Case 1 are exhibited in Figs. 22 through 27. Figures 22, 23, and 24 show the estimation errors for $\Delta\tau = 0.5, 1.0,$ and 1.5 sec, respectively, when the sample interval is $\Delta t = 0.05$ sec. Figures 25, 26, and 27 show the estimation errors for $\Delta\tau = 0.5, 1.0,$ and 1.5 sec, respectively, when the sample interval is $\Delta t = 0.10$ sec, and there is no data presmoothing. The estimation errors exhibited in Figs. 22 through 27 indicate that, for Case 1, the piecewise-recursive Kalman filter has acceptable performance for $\Delta\tau$ as large as 1.5 sec, with $\Delta t = 0.05$ or 0.10 sec.

Recall that the error magnitudes plotted in Fig. 4 for the fully implemented (extended) Kalman filter with a sample interval of $\Delta t = 0.05$ sec show that after 3.5 sec of filtering, the error in estimated position

54
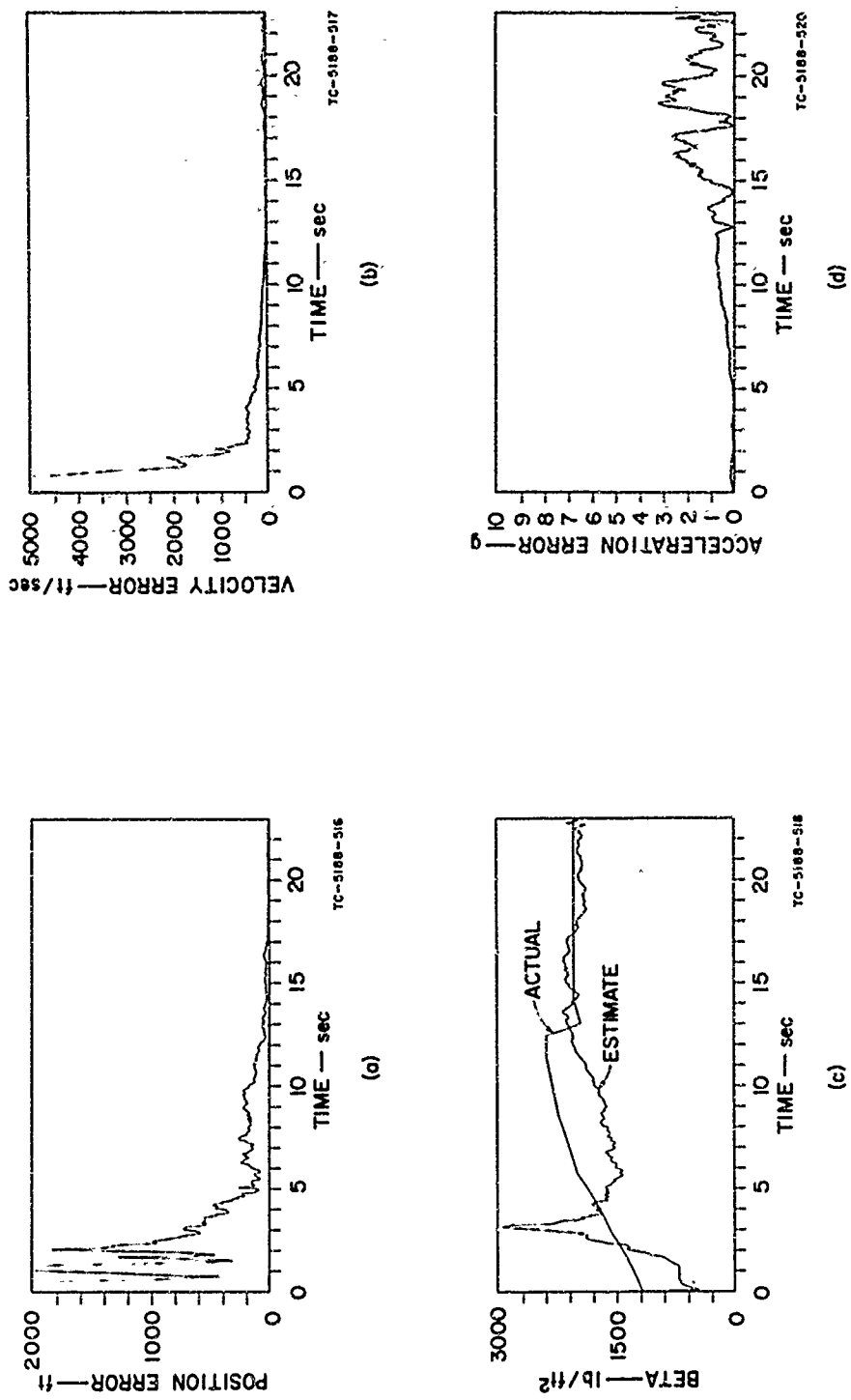
FIG. 22 ESTIMATION ERRORS FOR PIECEWISE–RECURSIVE KALMAN FILTER — CASE 1,
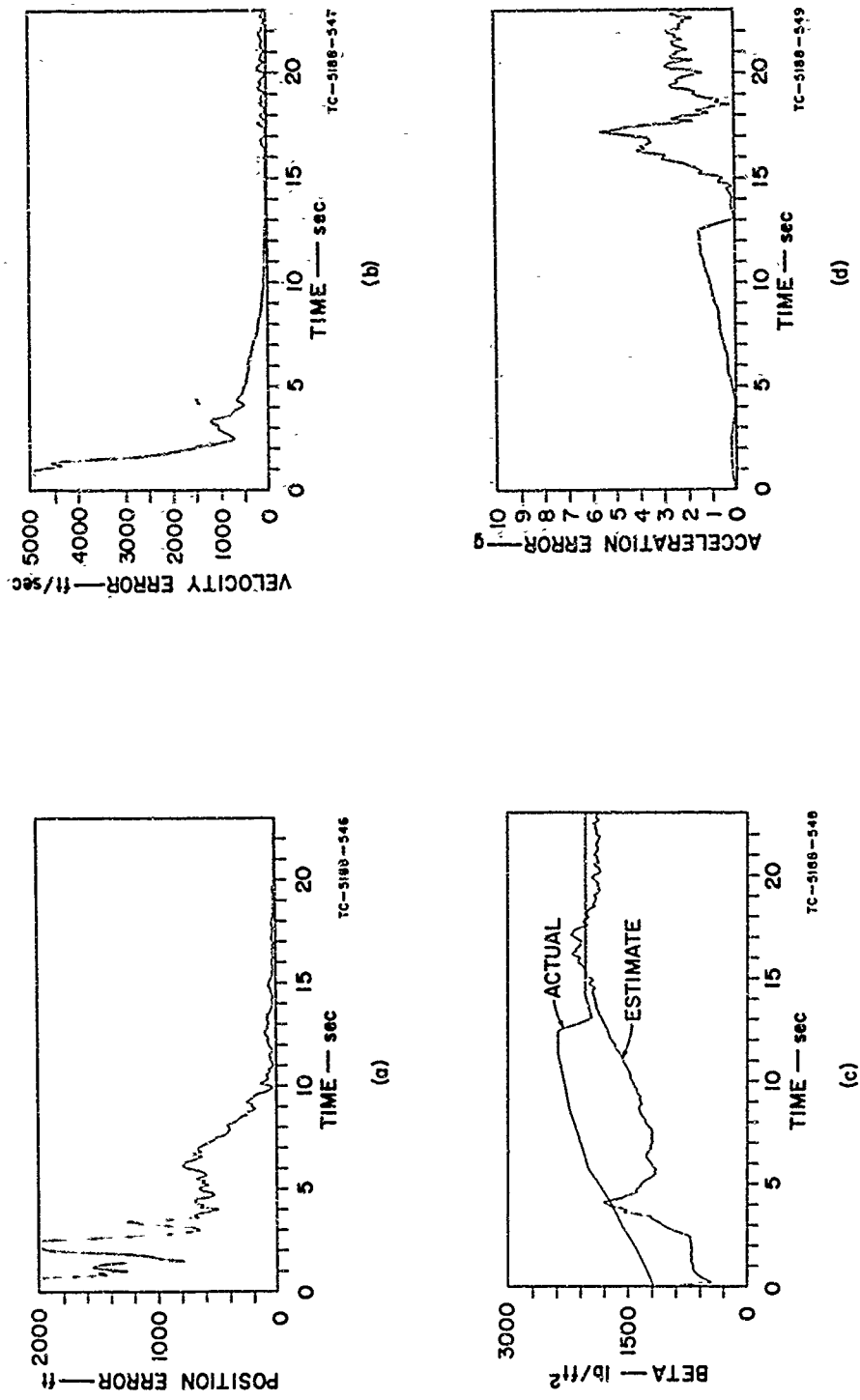Δt = 0.05 sec AND $\Delta \tau$ = 0.5 sec

55
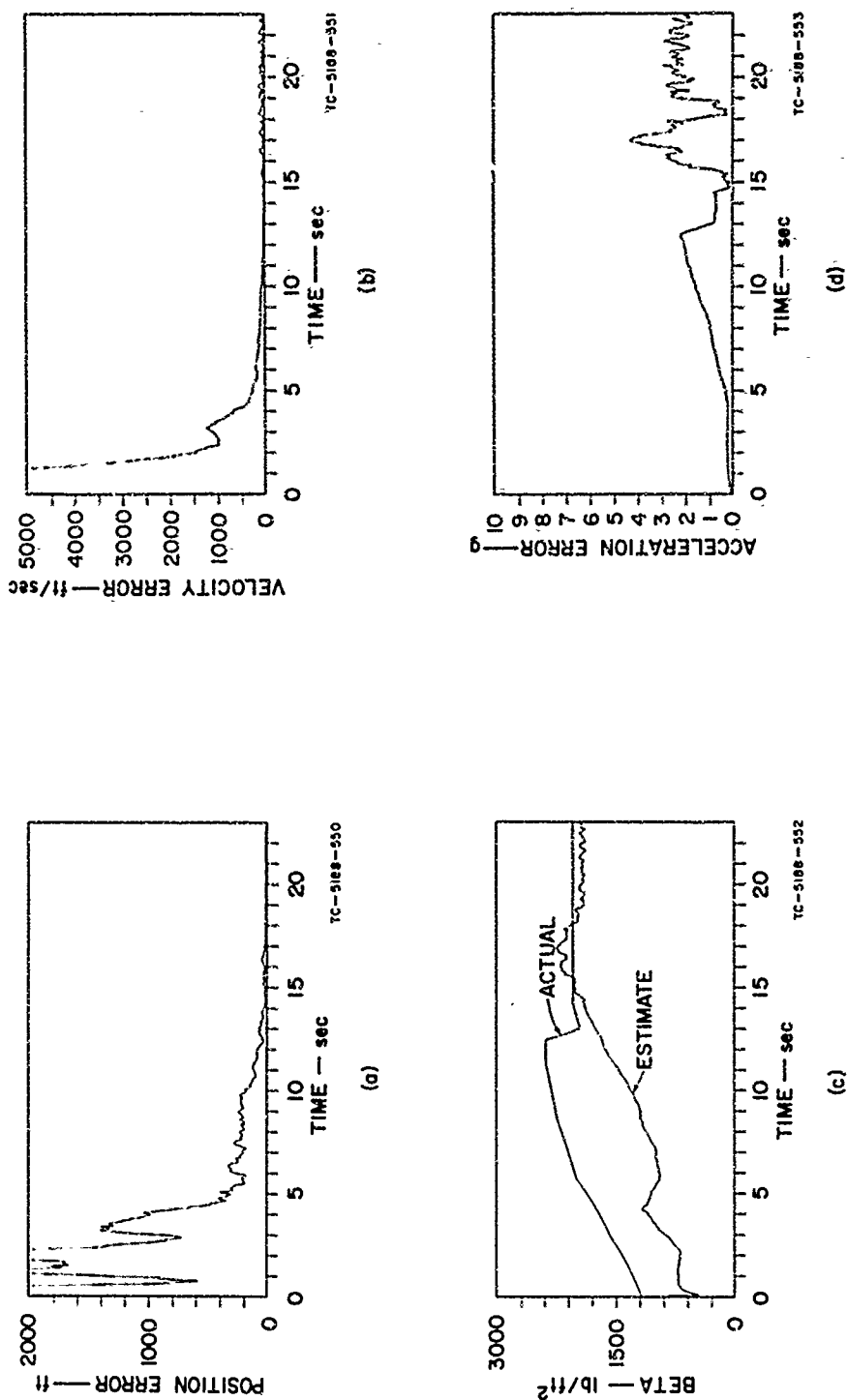
FIG. 23 ESTIMATION ERRORS FOR PIECEWISE-RECURSIVE KALMAN FILTER — CASE 1,
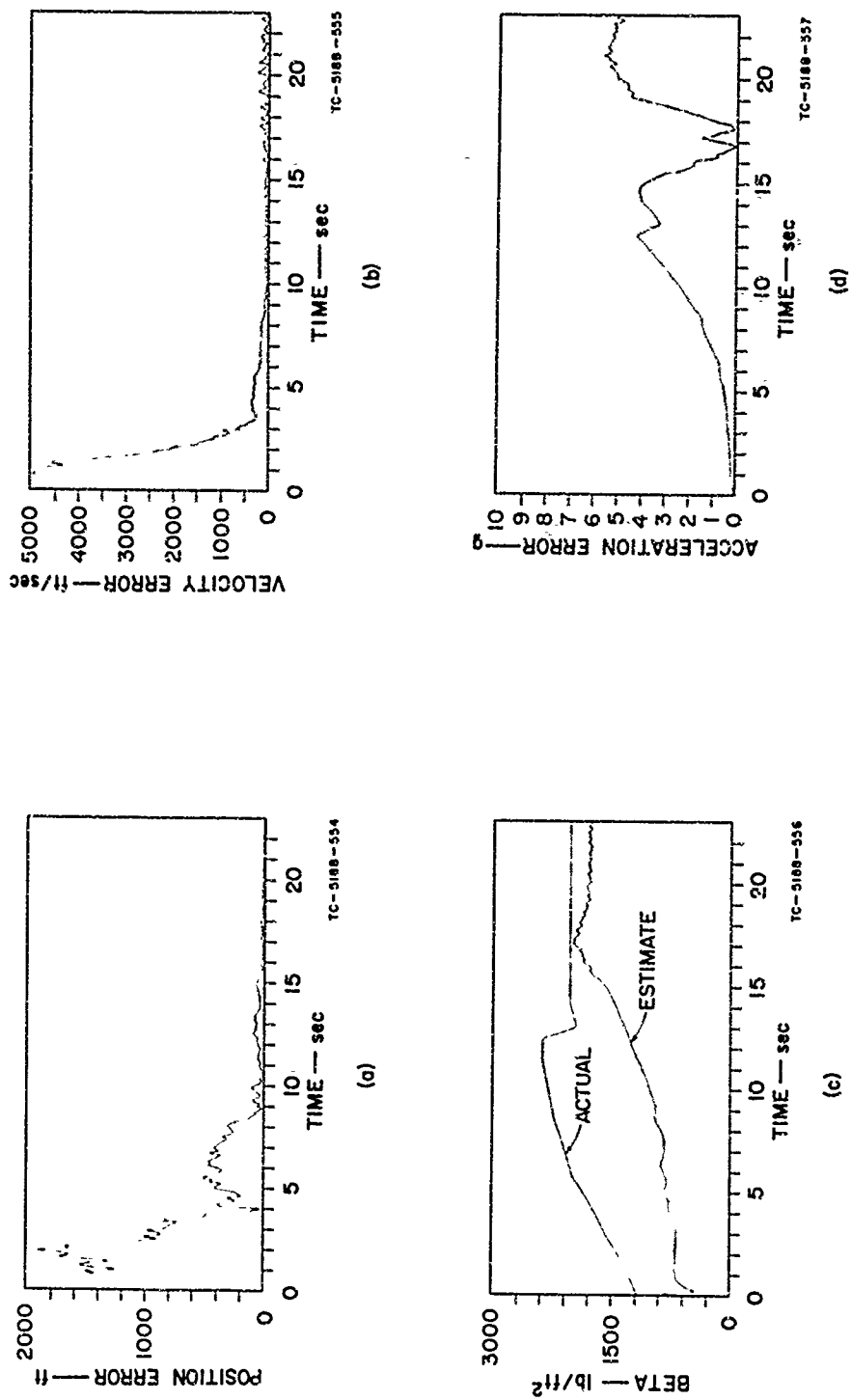$\Delta t = 0.05$ sec AND $\Delta \tau = 1.0$ sec

56
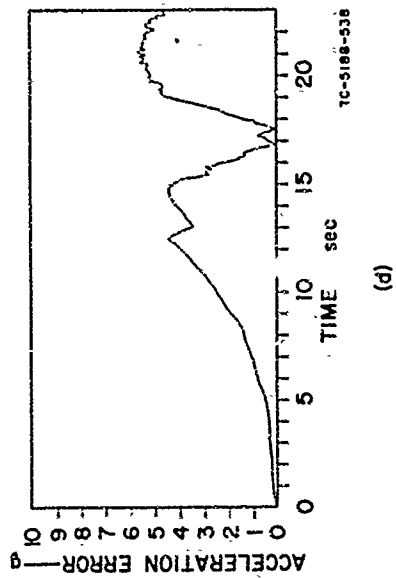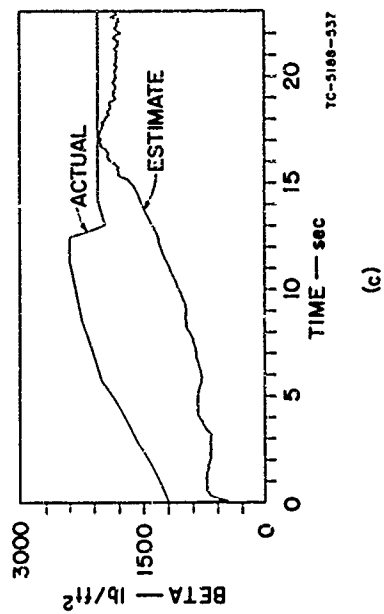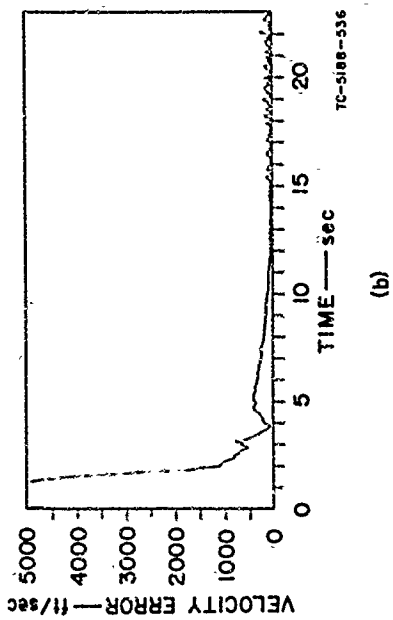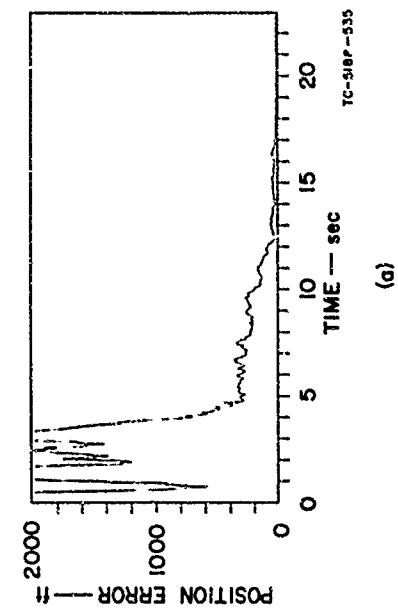
FIG. 24   ESTIMATION ERRORS FOR PIECEWISE-RECURSIVE KALMAN FILTER — CASE 1,
$\Delta t = 0.05$ sec AND $\Delta \tau = 1.5$ sec

57
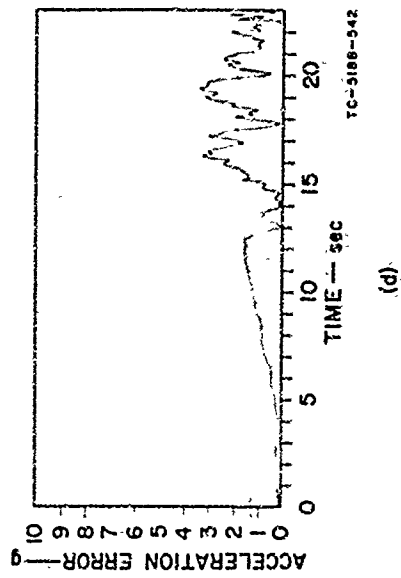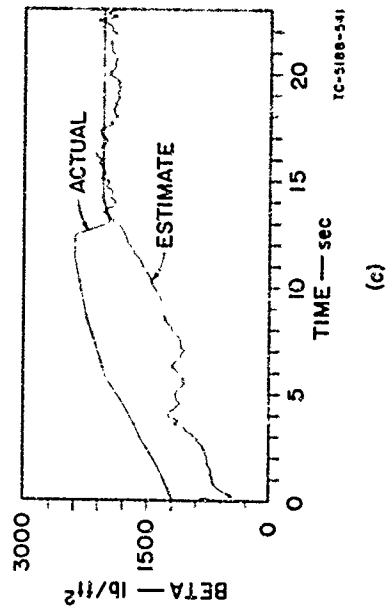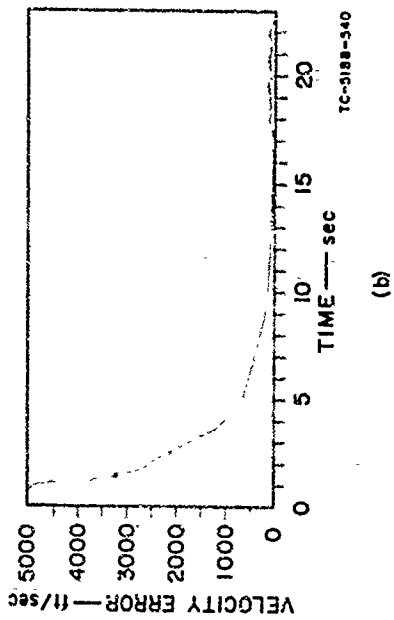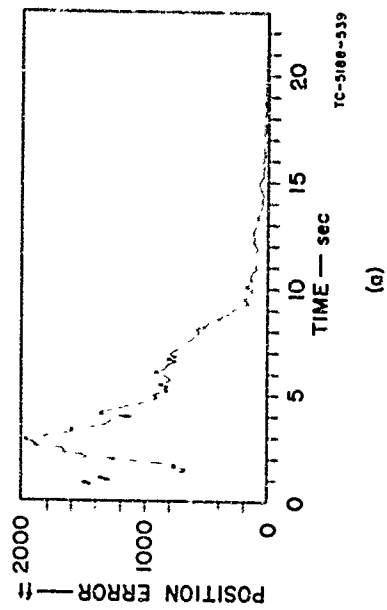
FIG. 25 ESTIMATION ERRORS FOR PIECEWISE-RECURSIVE KALMAN FILTER — CASE 1, $\Delta t = 0.10$ sec AND $\Delta \tau = 0.5$ sec

58

FIG. 26 ESTIMATION ERRORS FOR PIECEWISE-RECURSIVE KALMAN FILTER — CASE 1,
$\Delta t = 0.10$ sec AND $\Delta \tau = 1.0$ sec

59

FIG. 27 ESTIMATION ERRORS FOR PIECEWISE-RECURSIVE KALMAN FILTER — CASE 1,
$\Delta t = 0.10$ sec AND $\Delta \tau = 1.5$ sec

60

is less than 830 ft, the error in estimated velocity is less than
285 ft/sec, and the error in estimated β is less than 665 lb/ft^2.
Figures 22 through 27 indicate that for Case 1 the piecewise-recursive
Kalman filter estimation errors do not converge as rapidly as those of
the fully implemented Kalman filter; however, in the worst case, the
position estimation errors are less than 830 ft after 6.2 sec, the
velocity estimation errors are less than 285 ft/sec after 8.1 sec,
and the β estimation errors are less than 665 lb/ft^2 after 12.0 sec.

Figure 28 shows the standard deviations (for Case 1) of position,
velocity, and β estimation errors [as calculated from $P(k/k)$] for
(i) the fully implemented Kalman filter with a sample interval,
$\Delta t = 0.10$ sec, and (ii) the piecewise-recursive Kalman filter with
$\Delta t = 0.10$ sec and $\Delta\tau = 1.0$ sec. These two curves indicate that the
assumption made in Eqs. (36) and (37) of Sec. IV concerning the approxi-
mation of the filtering done by the piecewise-recursive Kalman filter
is valid. Specifically, we had considered the filtering done with a
fixed weighting matrix as being equivalent to measurement presmoothing,
so that when the estimation error covariance matrix was updated [see
Eq. (37)], the calculation used a measurement-noise covariance reduced
to $R(k)\Delta t/\Delta\tau$. The validity of this assumption is verified in Fig. 28,
since each new calculation of the estimation error covariance at inter-
vals of $\Delta\tau$ seconds gives a decrease to nearly the value of the
covariance matrix obtained with the use of the fully implemented Kalman
filter when it is calculated at intervals of Δt seconds.

Figures 29 through 34 show the estimation error magnitudes obtained
through computer simulation for Case 2. Figures 29, 30, and 31 show the
estimation errors for $\Delta\tau = 0.5$, 1.0, and 1.5 sec, respectively, when
the sample interval $\Delta t = 0.05$ sec. Figures 32, 33, and 34 show the
estimation errors for $\Delta\tau = 0.5$, 1.0, and 1.5 sec, respectively, when
the sample interval is $\Delta t = 0.10$ sec. For Case 2, we see from Figs. 29
through 34 that for either $\Delta t = 0.05$ sec or $\Delta t = 0.10$ sec, the filter
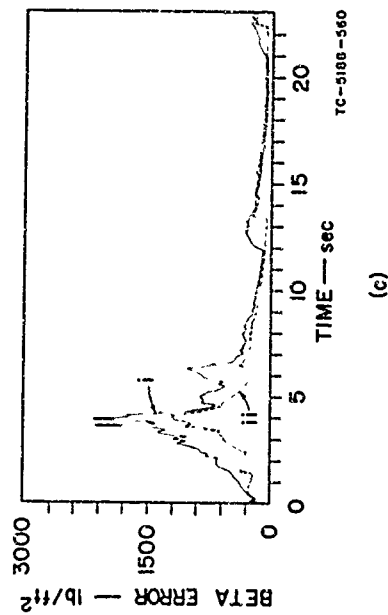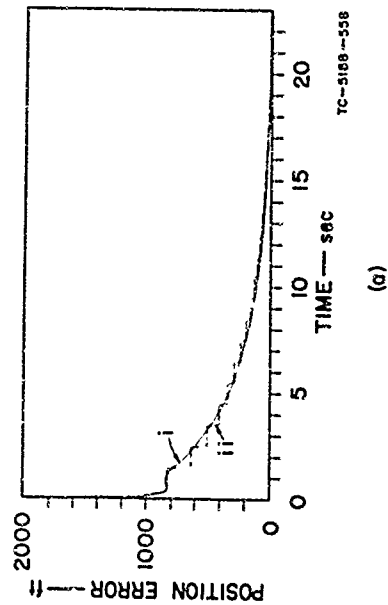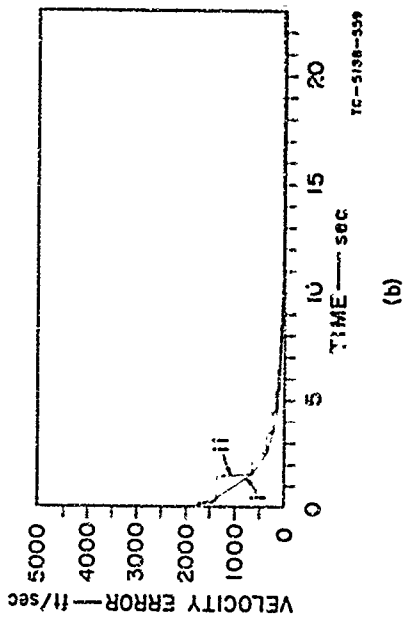performance deteriorates as $\Delta\tau$ increases from 0.5 sec to 1.5 sec.

FIG. 28 STANDARD DEVIATIONS FOR PIECEWISE–RECURSIVE KALMAN FILTER — CASE 1
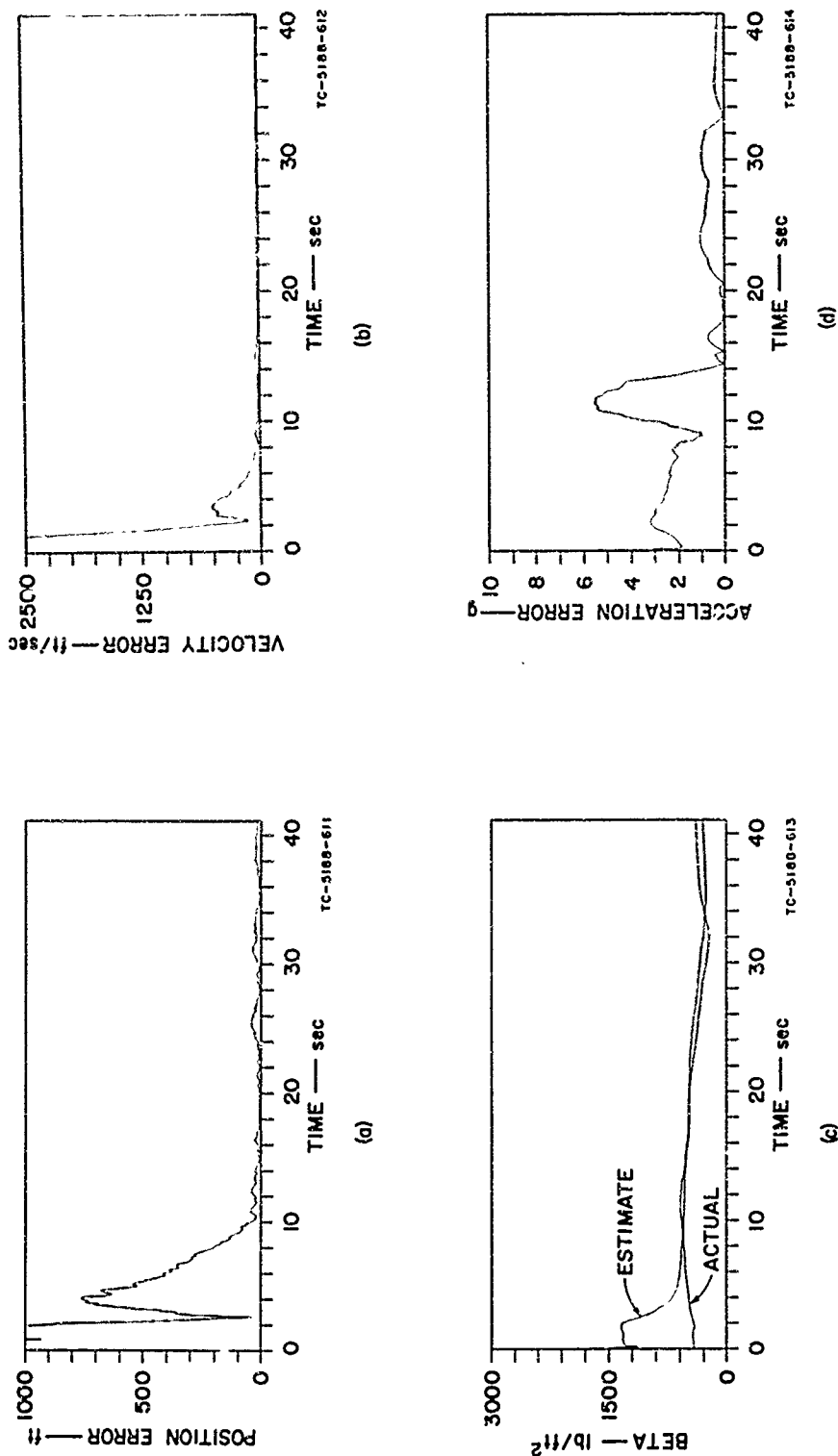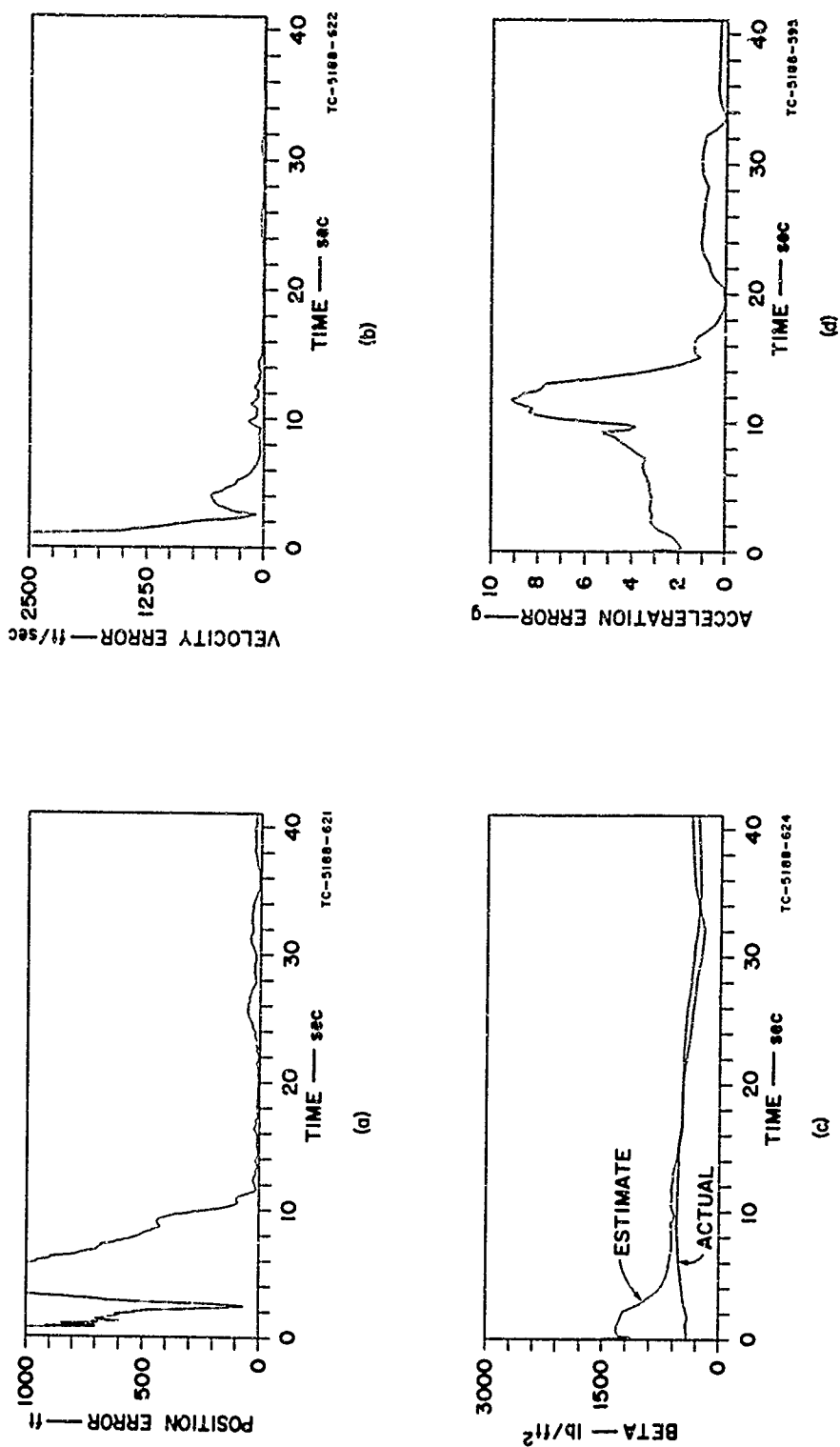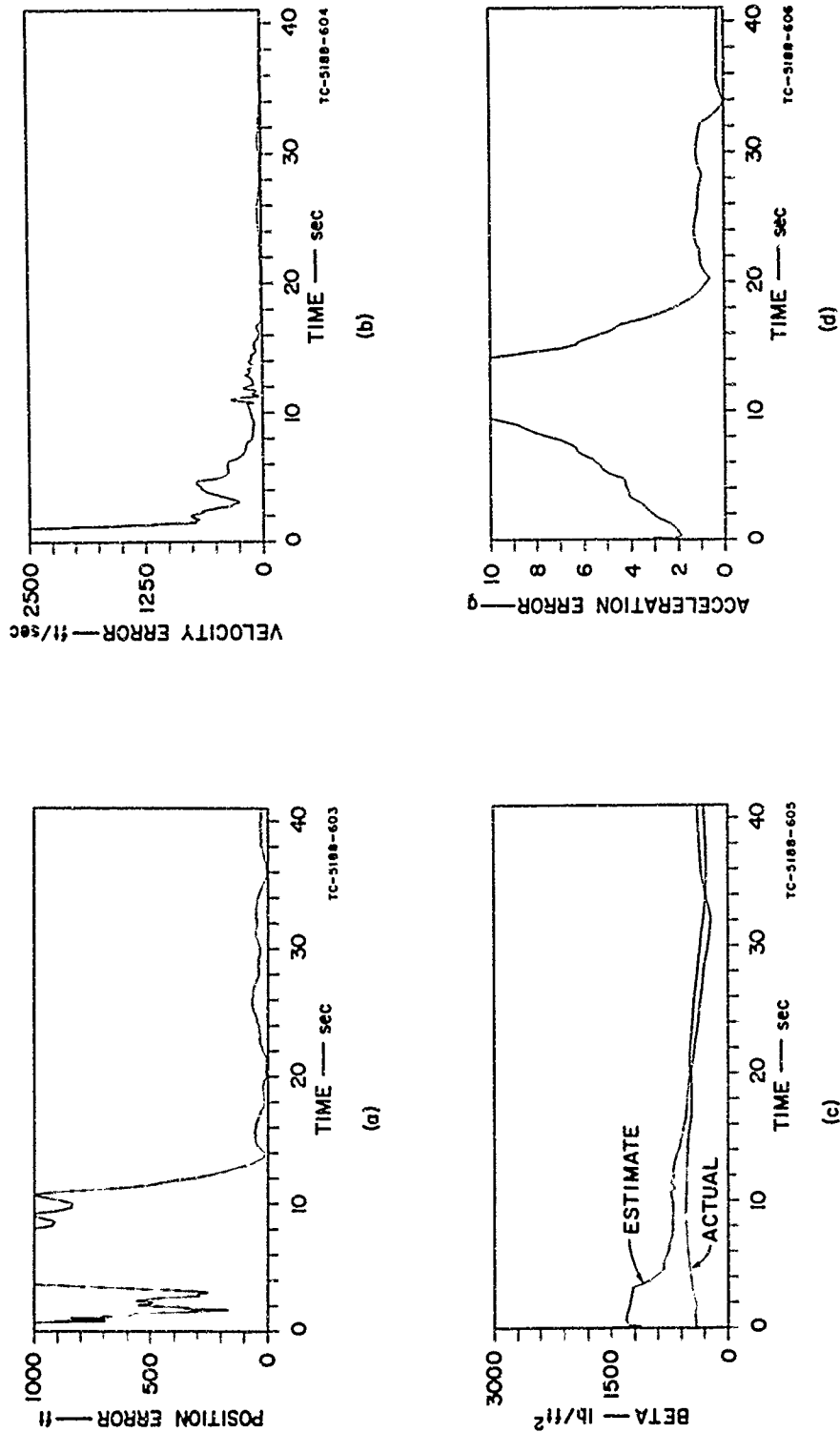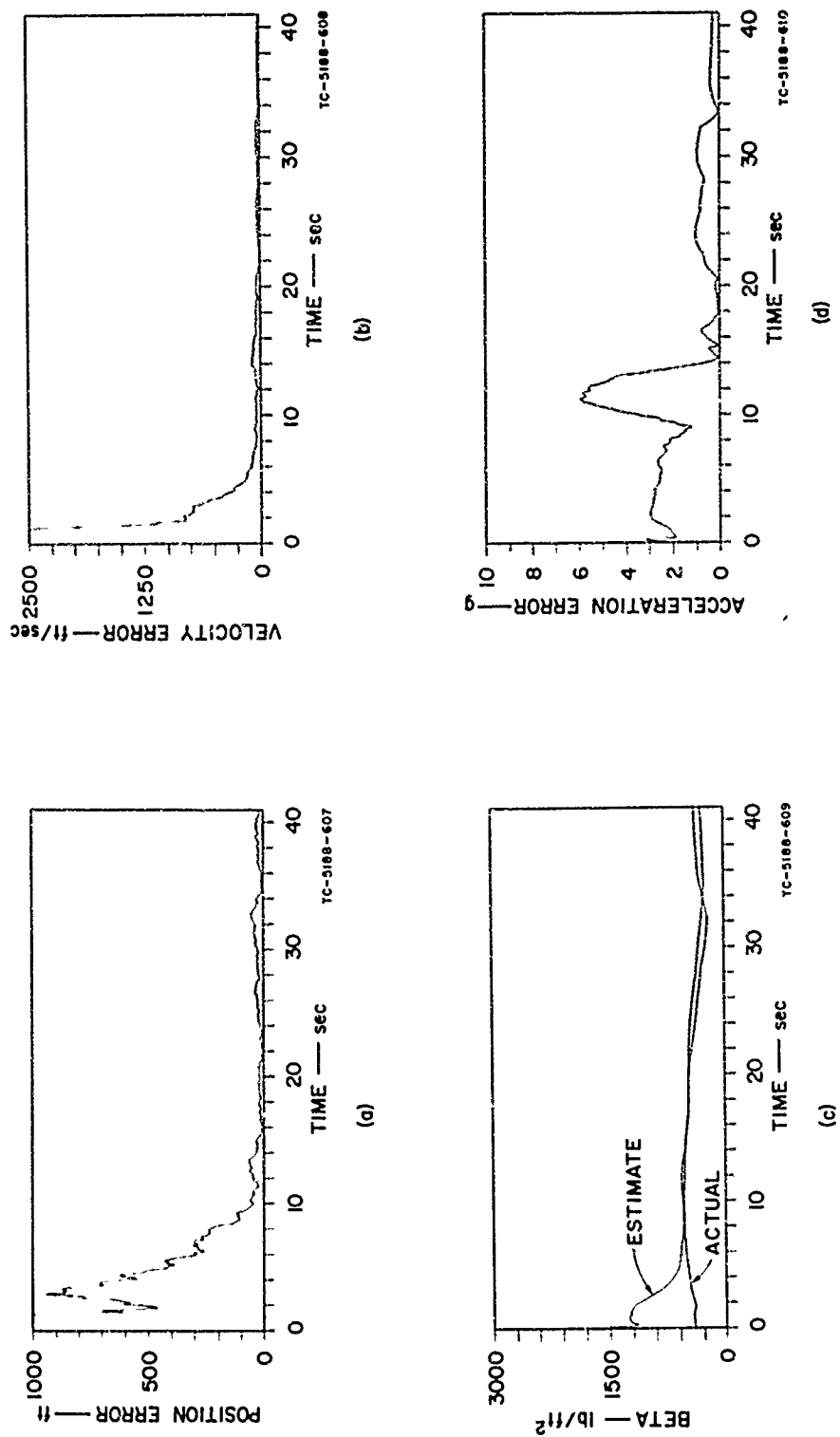$\Delta t = 0.10$ sec: (i) $\Delta \tau = 0.1$ sec, (ii) $\Delta \tau = 1.0$ sec

FIG. 29 ESTIMATION ERRORS FOR PIECEWISE-RECURSIVE KALMAN FILTER — CASE 2,
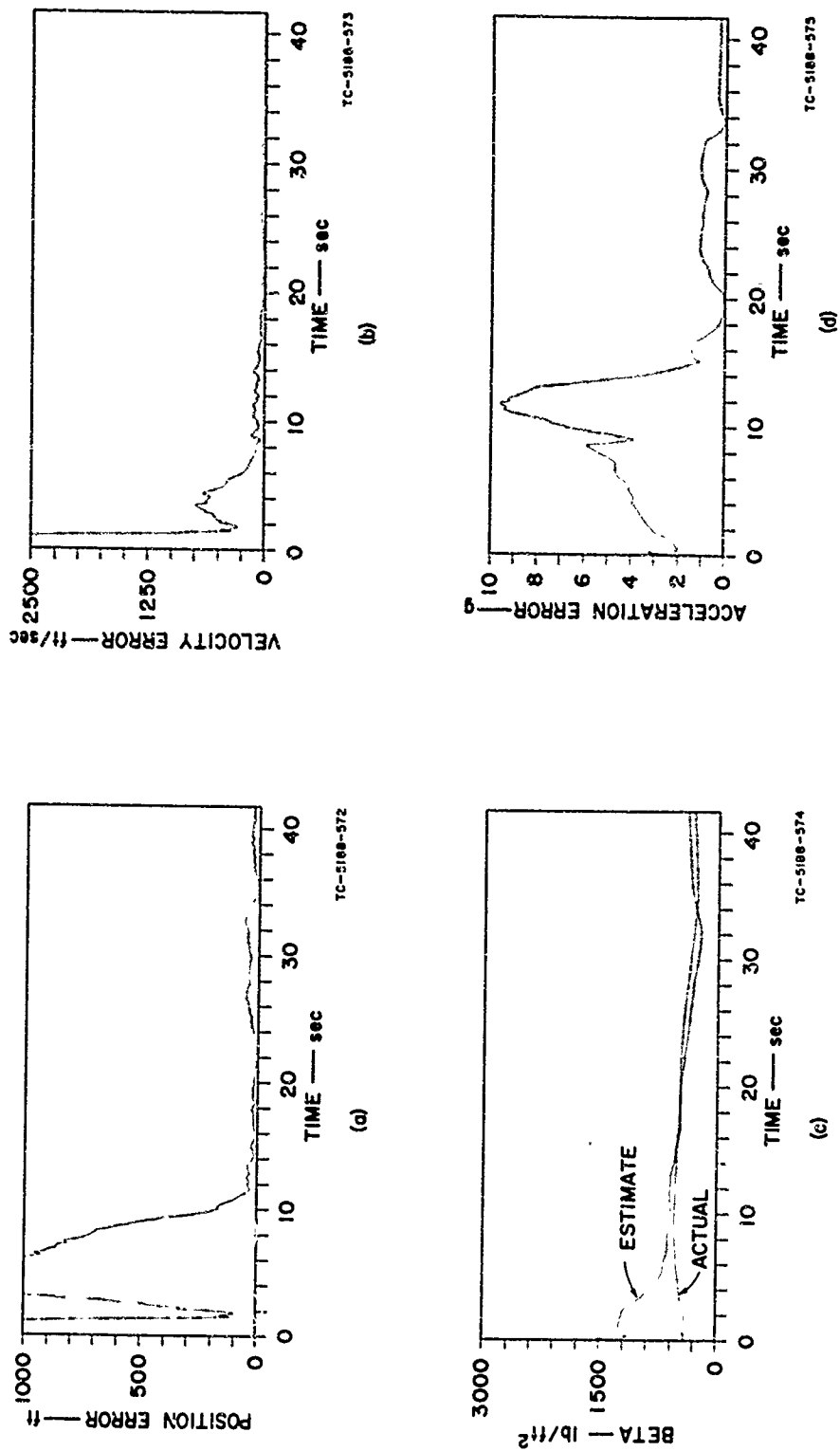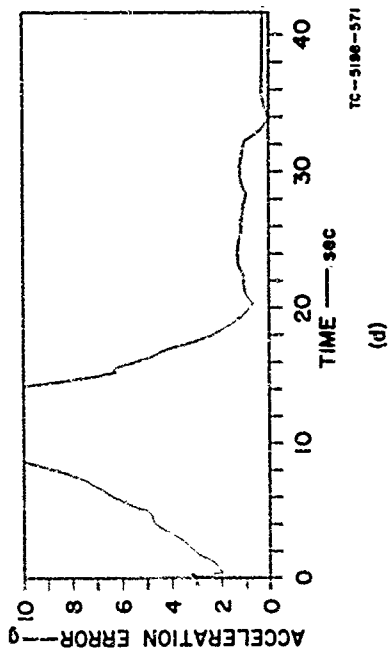$\Delta t = 0.05$ sec AND $\Delta \tau = 0.5$ sec

63

FIG. 30 ESTIMATION ERRORS FOR PIECEWISE-RECURSIVE KALMAN FILTER — CASE 2,
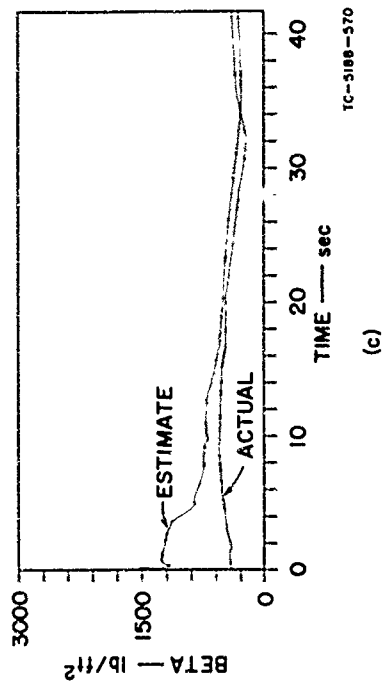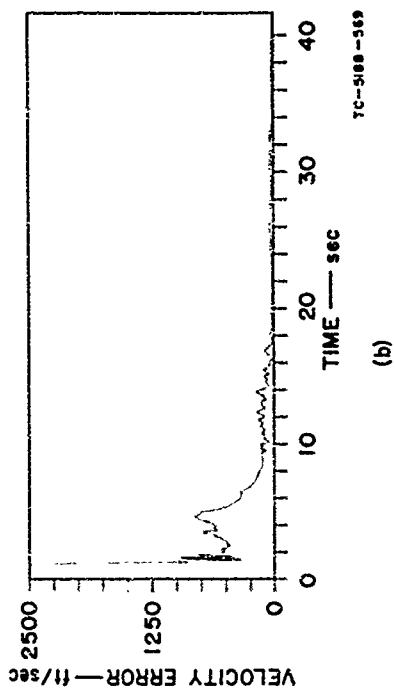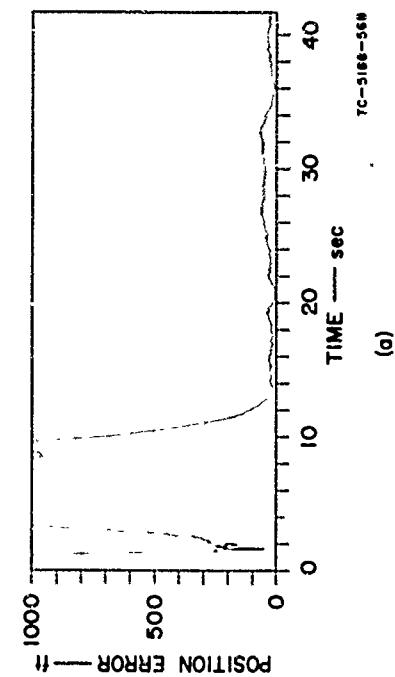$\Delta t = 0.05$ sec AND $\Delta \tau = 1.0$ sec

64

FIG. 31 ESTIMATION ERRORS FOR PIECEWISE-RECURSIVE KALMAN FILTER — CASE 2,
$\Delta t = 0.05$ sec AND $\Delta \tau = 1.5$ sec

65

FIG. 32 ESTIMATION ERRORS FOR PIECEWISE-RECURSIVE KALMAN FILTER — CASE 2,
$\Delta t = 0.10$ sec AND $\Delta \tau = 0.5$ sec

66

FIG. 33 ESTIMATION ERRORS FOR PIECEWISE-RECURSIVE KALMAN FILTER — CASE 2, $\Delta t = 0.10$ sec AND $\Delta \tau = 1.0$ sec

FIG. 34 ESTIMATION ERRORS FOR PIECEWISE-RECURSIVE KALMAN FILTER — CASE 2,
$\Delta t = 0.10$ sec AND $\Delta T = 1.5$ sec

68

Figure 35 shows the standard deviations (for Case 2) of position, velocity, and β estimation errors [as calculated from P(k/k)] for (i) the fully implemented Kalman filter with a sample interval of Δt = 0.10 sec, and (ii) the piecewise-recursive Kalman filter with Δt = 0.10 sec and Δτ = 1.0 sec. As in Case 1, Fig. 35 indicates that the assumption concerning the approximation of the measurement-noise covariance in the estimation error covariance for the piecewise-recursive filter is valid for Case 2.

In summary, the computer simulations indicate that for endoatmospheric estimation the accuracy of the piecewise-recursive Kalman filter is comparable with that of the fully implemented Kalman filter, and that it offers significant savings in computation time.

VI   NUMERICAL RESULTS FOR EXOATMOSPHERIC ESTIMATION

A.   Description of the Test Case and Filter Design Parameters

Data from a representative exoatmospheric trajectory generated by simulation using an accurate model of reentry dynamics was used to evaluate the performance of the piecewise-recursive Kalman filter described in Sec. IV. The computer program used in generating this trajectory was developed by M.I.T. Lincoln Laboratory.

In this report, the exoatmospheric test trajectory will be referred to as Case 3. It is a minimum-energy ellipse having a range of approximately 2.6×10^7 ft (4300 nmi) from launch to impact, with a reentry angle of about $23°$. This trajectory is estimated from a range of 9.4×10^6 ft (1600 nmi) to a range of 0.4×10^6 ft (66 nmi), which corresponds to an altitude of approximately 370,000 ft for the particular geometry of this case.

At altitudes greater than 300,000 ft, the atmospheric drag is negligible; hence, in the filter's model for the equations of the ballistic missile, the drag terms have been dropped [see Eqs. (1) in Sec. II A]. Thus, the state variable x_7, which contains β, can also be eliminated; of course, the dimensions of the system matrices (Φ, H, W,
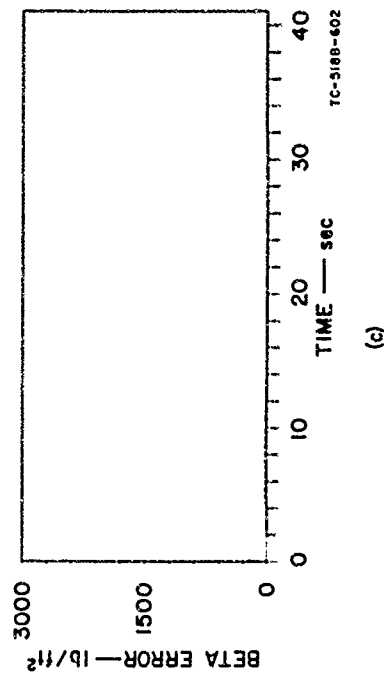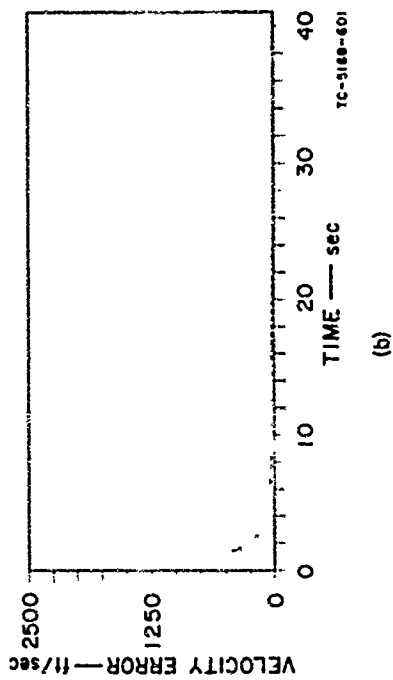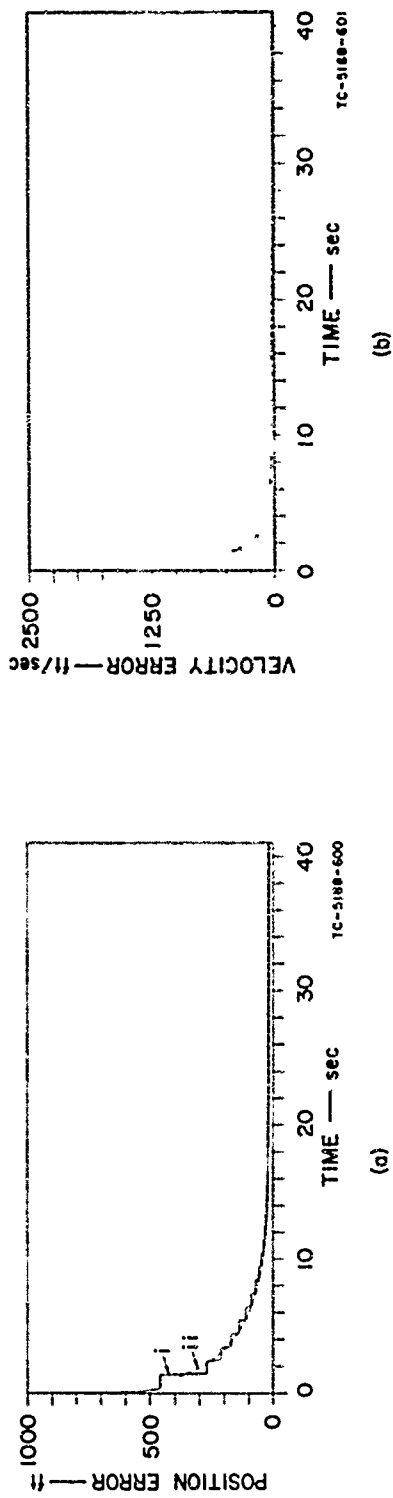
69

FIG. 35 STANDARD DEVIATIONS FOR PIECEWISE–RECURSIVE KALMAN FILTER — CASE 2,
Δt = 0.10 sec: (i) Δτ = 0.1 sec, (ii) Δτ = 1.0 sec

Q, and P) are modified accordingly. Due to numerical difficulties that were encountered in calculating the covariance matrices, the filter was programmed in double precision for exoatmospheric estimation.

The filtering computations start with an initial state estimate $\hat{x}(0/0)$, which is now a six-dimensional vector, and its error covariance $P(0/0)$. The initial state estimates for the exoatmospheric case are given in Table IV.

Table IV

INITIAL CONDITIONS FOR EXOATMOSPHERIC TRAJECTORY

	x_1 (ft $\times 10^6$)	x_2 (ft $\times 10^6$)	x_3 (ft $\times 10^6$)	x_4 (ft/sec)	x_5 (ft/sec)	x_6 (ft/sec)
CASE 3 ACTUAL: x (0)	−6.01	7.04	1.73	11500	−12200	3020
ESTIMATE: $\hat{x}(0/0)$	−6.10	7.14	1.63	12300	−11420	3268
|ERROR|	0.09	0.10	0.10	800	780	248

The initial error covariance (for the exoatmospheric trajectory) was determined experimentally to be the 6 X 6 diagonal matrix

$$P(0/0) = \begin{bmatrix} 10^{12} & & & & & \\ & 10^{12} & & & & \\ & & 10^{12} & & & \\ & & & 10^{6} & & \\ & & & & 10^{6} & \\ & & & & & 10^{6} \end{bmatrix} . \qquad (53)$$

The measurement-noise covariance $R(k)$ is based upon a model of actual radar-noise characteristics of the PAR; the model was obtained by making suitable modifications of the results presented in Ref. 9. This radar model is used to generate the measurement noise of Eq. (12) in the simulation. Observations may be taken as often as every second

71

for the exoatmospheric case, but the filter may process fewer measure-ments than are taken (i.e., $\Delta t \geq 1.0$ sec).

The random disturbance covariance $Q(k)$ [see Eqs. (15a) and (15b)] compensates for model inaccuracies as described in Sec. II A. This covariance was determined experimentally to be the 6×6 diagonal matrix

$$\frac{Q(k)}{\Delta t} = Q'(k) = \begin{bmatrix} 0 & & & & & \\ & 0 & & & & \\ & & 0 & & & \\ & & & 50 & & \\ & & & & 50 & \\ & & & & & 50 \end{bmatrix} \; . \tag{54}$$

B. Performance of the Fully Implemented Extended Kalman Filter

For the exoatmospheric trajectory, the standard used to evaluate the performance of the piecewise-recursive Kalman filter is the fully implemented (extended) Kalman filter with a sample interval of $\Delta t = 1.0$ sec. The recursive equations for the extended Kalman filter are given in Sec. III A, with the system matrices (Φ, H, W, Q, and P) modified appropriately. This filter was used to estimate the ballistic trajectory for Case 3, using the simulated trajectory and measurement noise. The filter yields state estimates $\hat{\underline{x}}(k/k)$ at sample intervals of $\Delta t = 1.0$ sec.
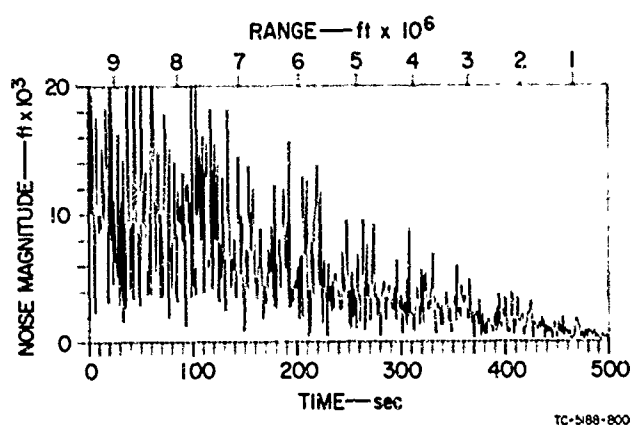

FIG. 36 MEASUREMENT NOISE — CASE 3

The magnitude of the measurement error in position is shown in Fig. 36 for Case 3. In order to relate range and time, the measurement error is plotted as a function of both variables; in all other figures, the plots are a function of time only. Figures 37 a, b, and c show the magnitude of the estimation errors for position, velocity, and acceleration, respectively, for Case 3. It should be noted that acceleration is not computed directly by the filter but is calculated from the state estimate using Eqs. (1) of Sec. II A. Additionally, as noted above, β is not estimated for the exoatmospheric case.

From Fig. 37, it can be seen that after 30 sec of filtering, the magnitude of the error in estimated position is less than 6,000 ft (for Case 3, the initial error in position is 167,000 ft); after 170 sec, the position error is less than 2,000 ft. After 30 sec of filtering the magnitude of the error in estimated velocity is less than 200 ft/sec (for Case 3, the initial error in velocity is almost 1200 ft/sec); after 100 sec, the velocity error is less than 50 ft/sec.

C. Performance of the Fully Implemented Extended Kalman Filter with Different Data Rates

As discussed in Sec. V C, the simplest scheme for improving the real-time capability of the Kalman filter is simply to decrease the data rate. If the sample intervals are lengthened and the additional time between samples is not used to presmooth the measurements (i.e., the intermediate measurements are discarded), then obviously the filter performance will deteriorate to some extent. The present study also considers the situation where there is presmoothing of the measurements. In practice, data is presmoothed by curve-fitting with polynomials that are not precise representations of missile trajectories.

The assumption of data presmoothing implies that in the filter equations the measurement-noise covariance should be reduced accordingly. In the computer simulations done for this report, the presmoothing of the measurements was simulated by scaling the measurement noise by the factor $\sqrt{\Delta t_o/\Delta t}$. This corresponds to decreasing the measurement-noise covariance by the factor $\Delta t_o/\Delta t$. A justification for the approximation is presented in Sec. V C, although it should be noted that this pre-smoothing assumption is overly optimistic.
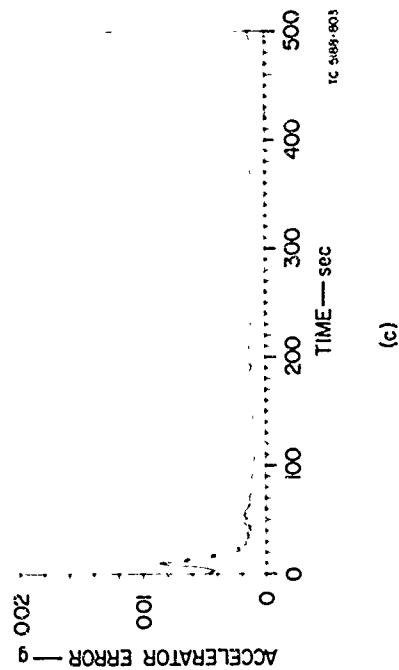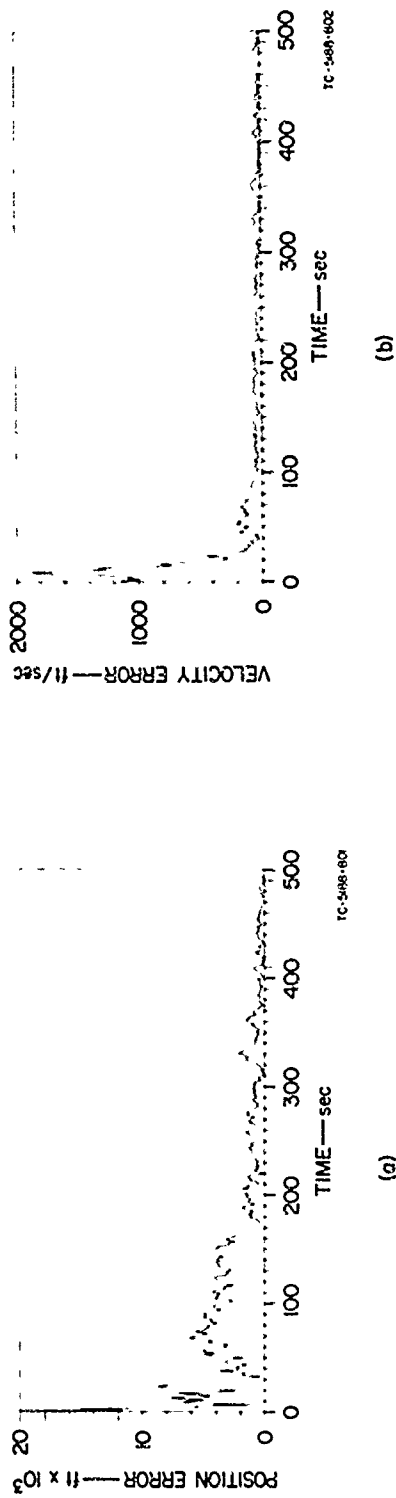
73

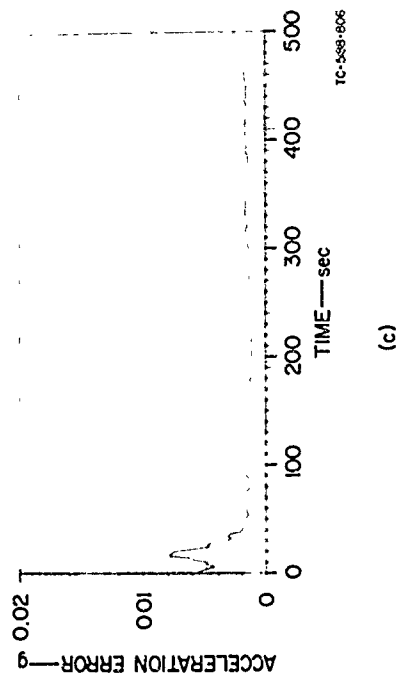FIG. 37 ESTIMATION ERRORS FOR FULLY-IMPLEMENTED KALMAN FILTER — CASE 3, $\Delta t = 1.0$ sec

74

FIG. 38 ESTIMATION ERRORS FOR FULLY-IMPLEMENTED KALMAN FILTER — CASE 3,
Δt = 2.0 sec WITHOUT PRESMOOTHING

75
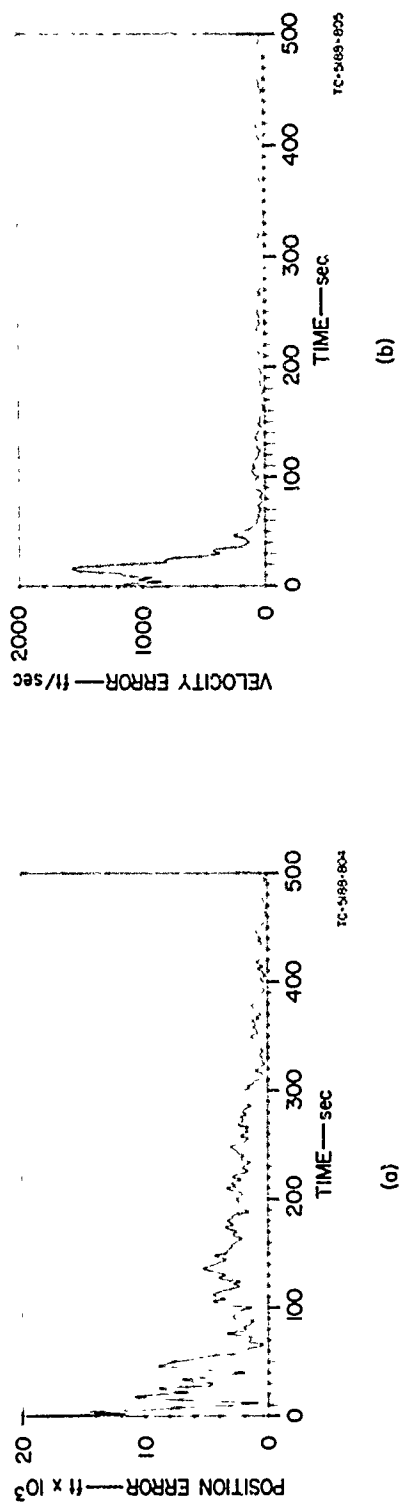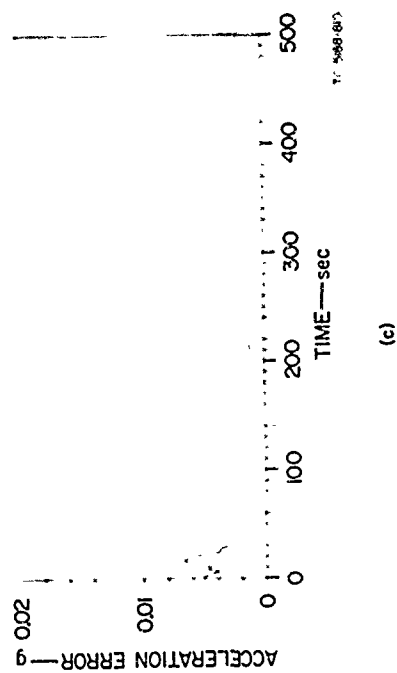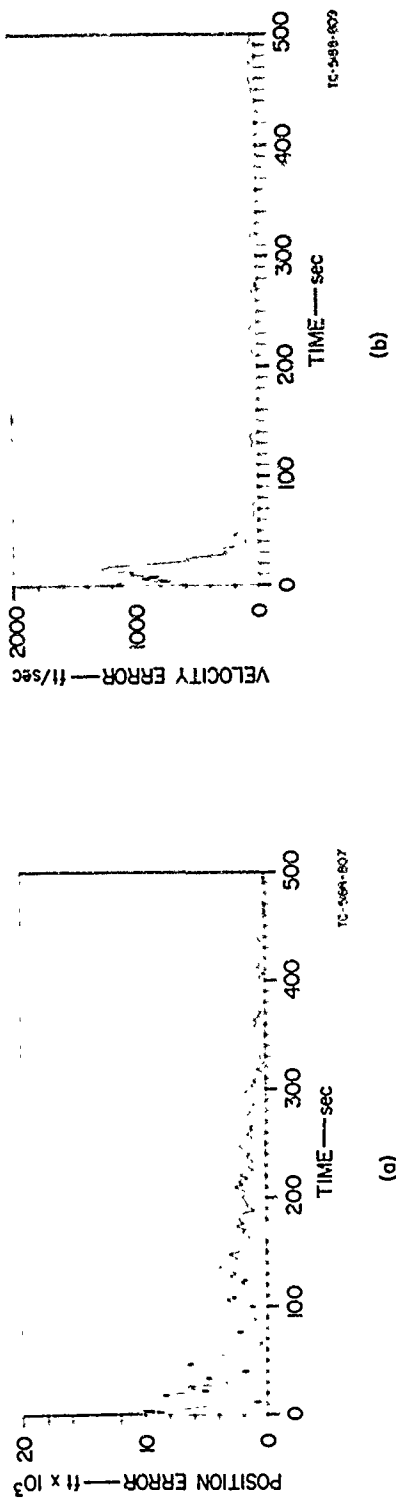
FIG. 39 ESTIMATION ERRORS FOR FULLY-IMPLEMENTED KALMAN FILTER — CASE 3,
$\Delta t = 2.0$ sec WITH PRESMOOTHING

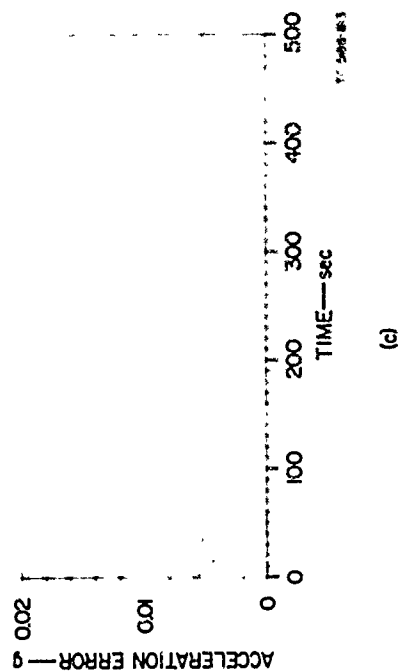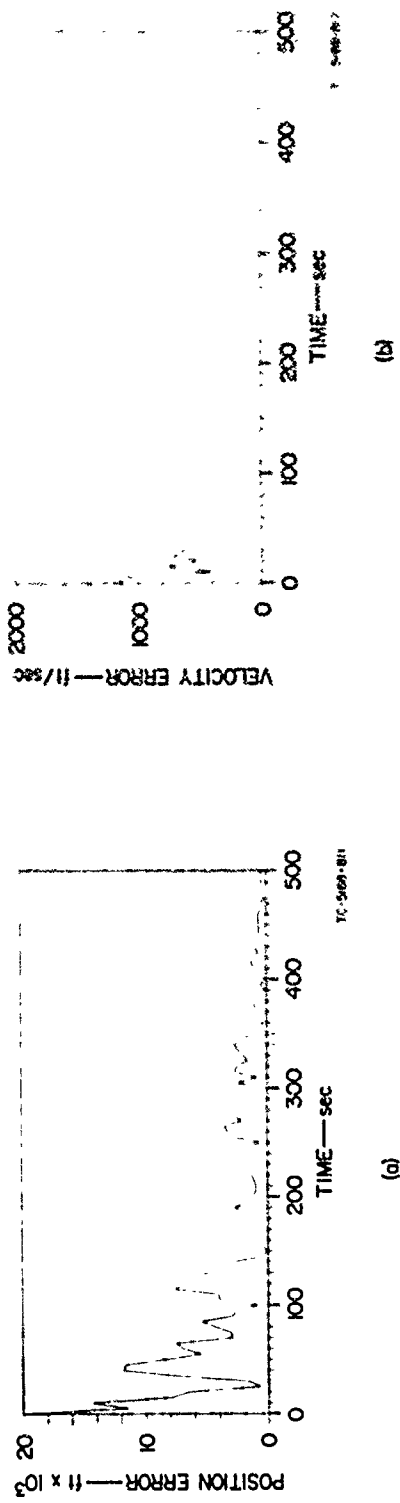76

FIG. 40 ESTIMATION ERRORS FOR FULLY-IMPLEMENTED KALMAN FILTER — CASE 3,
Δt 5.0 sec WITHOUT PRESMOOTHING

77

FIG. 41 ESTIMATION ERRORS FOR FULLY-IMPLEMENTED KALMAN FILTER — CASE 3,
$\Delta t = 5.0$ sec WITH PRESMOOTHING

78

The estimation error plots of Figs. 38 through 41 illustrate the effects of data presmoothing upon the extended Kalman filter's performance for Case 3. Figures 39 and 41 show the effects of increasing the sample interval (decreasing the data rate) from $\Delta t = 1.0$ sec to $\Delta t = 2.0$ and 5.0 sec, respectively, while also using the increased time between samples to presmooth the measurement data. The presmoothing assumptions described above are used for the results presented in Figs. 39 and 41.

Figures 38 and 40 indicate that without presmoothing the estimation errors become increasingly larger as the filter's sample interval Δt is increased. However, Figs. 39 and 41 indicate that if the data is presmoothed the position and velocity estimation errors generally decrease with increasing Δt. Thus, the reduction of the measurement noise through presmoothing is beneficial in position and velocity estimation.

The pairs of Figs. 38 and 39, 40 and 41 illustrate the extended Kalman-filter performance, with and without data presmoothing, for sample intervals of $\Delta t = 2.0$ and 5.0 sec, respectively. As noted above, the presmoothing assumption is optimistic and for a given Δt, the filter estimation errors for actual presmoothing will be somewhere between the errors given in the corresponding pair of figures. Thus, for the particular simulations presented here, we have bounded the filter estimation errors for different values of Δt.

Figures 42 a and b show the standard deviations in the estimates of position and velocity as computed from the diagonal elements of the calculated estimation error covariance [Eq. (29)]. Each of the Figs. 42 a and b shows two curves: Curve (i) is the calculated standard deviation when there is no data presmoothing, and Curve (ii) is the calculated standard deviation when there is presmoothing; these plots are for Case 3, with a sample interval of $\Delta t = 5.0$ sec. The standard deviation in position error is calculated as the square root of the sum of the first three diagonal elements of the filter covariance matrix, $P(k/k)$. That is, the standard deviation of position error is given by

$$\sqrt{P_{11} + P_{12} + P_{33}}$$. Likewise, the standard deviation of velocity error
is calculated as $\sqrt{P_{44} + P_{55} + P_{66}}$.

Figure 42 shows that the calculated standard deviations [derived
from $\hat{P}(k/k)$] are in correspondence with the actual estimation error
magnitudes (both with and without presmoothing). Also, the standard
deviations in position and velocity estimation errors are reduced (as
expected) when there is presmoothing.

Figures 43 a and b show the standard deviations in position and
velocity estimation errors for (i) a sample interval of 1.0 sec, and
(ii) a sample interval of 5.0 sec; Curves (i) and (ii) are for Case 3
with no data presmoothing. Again, the standard deviation plots agree
with the actual estimation error magnitudes. For instance, comparison
of Figs. 37 and 40 with Fig. 43 shows that the position estimation error
magnitude increases when Δt is increased from 1.0 sec to 5.0 sec, but
this is to be expected since, with no presmoothing, the calculated
position standard deviation [Fig. 43 a] also increases.

D. Performance of the Piecewise-Recursive Kalman Filter

The figures and timing estimates given below indicate that the
piecewise-recursive Kalman filter (described in Sec. IV) is an extremely
attractive alternative to the fully implemented (extended) Kalman filter
for real-time exoatmospheric estimation. Using this filtering method,
it is possible to obtain large reductions in computation time with little
sacrifice in estimation accuracy. With the Univac 1108 computer, it is
possible (as shown below) to filter measurements at a speed approximately
500 times faster than real time for exoatmospheric estimation, and yet
obtain accuracy approaching that of the fully implemented Kalman filter.

Since the fully implemented Kalman filter is approximately 100 times
faster than real-time (see Sec. III C) on the Univac 1108 for exoatmos-
pheric trajectory estimation ($\Delta t = 1.0$ sec), this means that the piecewise-
recursive Kalman filter is about 5 times faster than the fully implemented
Kalman filter (the relative speed of the two filters is essentially
computer-independent). With the Univac 1108 Computer, a total time of
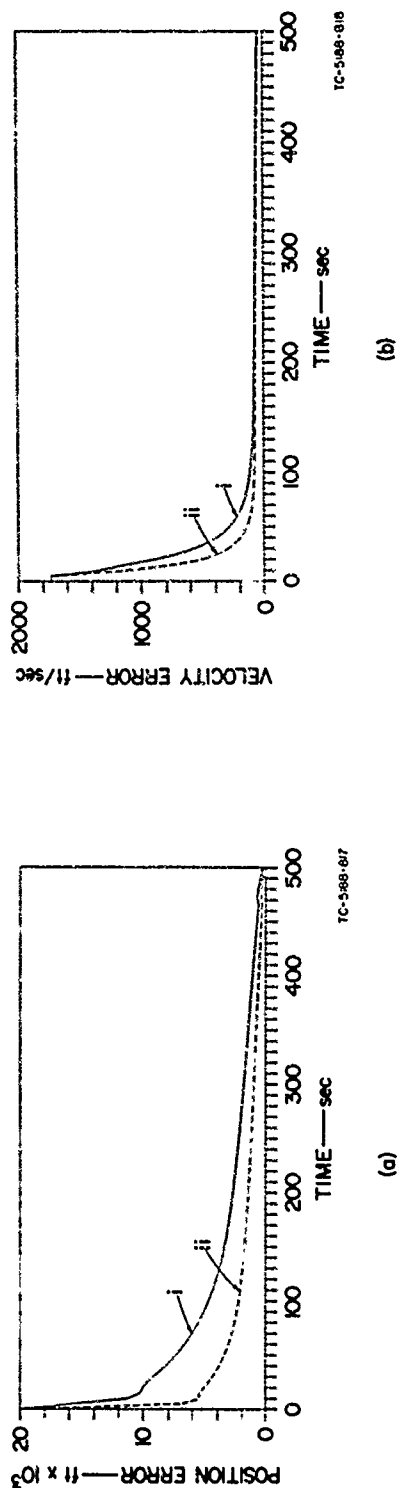0.011 sec is needed to process each measurement and compute an estimate

80

FIG. 42 STANDARD DEVIATIONS FOR FULLY-IMPLEMENTED KALMAN FILTER — CASE 3,
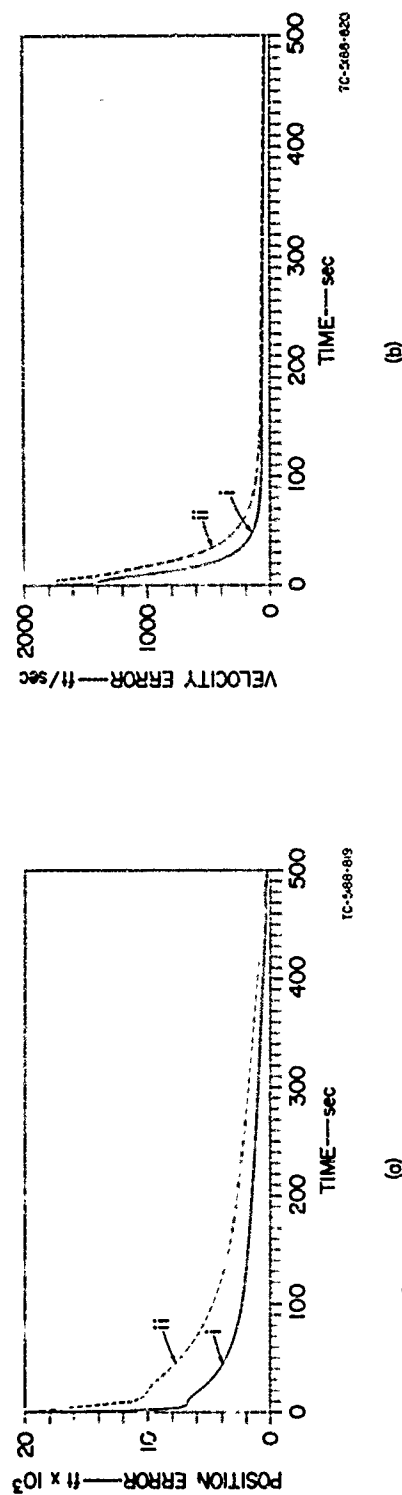Δt = 5.0 sec: (i) WITHOUT PRESMOOTHING, (ii) WITH PRESMOOTHING

FIG. 43 STANDARD DEVIATIONS FOR FULLY-IMPLEMENTED KALMAN FILTER — CASE 3,
WITHOUT PRESMOOTHING: (i) Δt = 1.0 sec, (ii) Δt = 5.0 sec

81

of the state of the ballistic missile (as well as the estimation error covariance) using the fully implemented Kalman filter. When the piecewise-recursive Kalman filter is used for the estimation, two timing figures should be noted. This arises from the fact (as discussed in Sec. IV) that there are two different modes of operation for the piecewise-recursive Kalman filter: in the first mode, the filter calculates a weighting matrix, two error covariance matrices, and state estimate; in the second mode, the filter calculates only the state estimate, without the weighting matrix or error covariance computations being performed.

From the simulations on the Univac 1108 for the exoatmospheric case, it was found that in the first mode, the piecewise-recursive Kalman filter used an average of 0.0200 sec per iteration, while it used an average of only 0.0010 sec per iteration in the second mode. Since a filter iteration on the Univac 1108 takes 0.0110 sec using the fully implemented (extended) Kalman filter, this means that, in the first mode, the piecewise-recursive Kalman filter is approximately 1.8 times slower than the fully-implemented Kalman filter; however, in the second mode, the piecewise-recursive Kalman filter is about 11 times faster than the fully implemented Kalman filter. The piecewise-recursive Kalman filter encounters a first-mode calculation once every $\Delta\tau$ seconds; and if $N = \Delta\tau/\Delta t$, it encounters a second-mode calculation $N-1$ times during a time span of $\Delta\tau$ seconds. Thus, for large values of N, the speed of the piecewise-recursive Kalman filter in the second mode predominates over that of the first mode. For the exoatmospheric trajectory, the average iteration time of the piecewise-recursive Kalman filter as a function of N (for the values of N encountered in the computer simulations) is given in Table V.

Using the values in Table V, one can calculate the average speed of the piecewise-recursive Kalman filter relative to real time for different $\Delta\tau$ and Δt. For instance, if $\Delta\tau = 20$ sec, and $\Delta t = 1.0$ sec, then the speed of the filter is about 500 times faster than real time (on the Univac 1108). Thus, with $\Delta\tau = 20$ sec and $\Delta t = 1.0$ sec, the piecewise-recursive Kalman filter can, on the average, process incoming measurements

82

Table V

ITERATION TIMES FOR PIECEWISE-RECURSIVE KALMAN FILTER
(EXOATMOSPHERIC CASES)

$N = \dfrac{\Delta \tau}{\Delta t}$	AVERAGE FILTER ITERATION TIME (sec)	ITERATION TIME IN FIRST MODE (sec)	ITERATION TIME IN SECOND MODE (sec)
5	0.0048		
10	0.0029		
20	0.0020	0.0200	0.0010
50	0.0014		
100	0.0012		

500 times faster than they are received. Effectively then, one Kalman filter of this type could give state estimates for 500 exoatmospheric ballistic targets in real time.

Now, let us discuss the accuracy of the state estimation using the piecewise-recursive Kalman filter. It should be pointed out that in all of the figures of this section (for Case 3) the filter was allowed to operate as a fully implemented Kalman filter for the first 10 iterations; this operation serves as an initialization for the piecewise-recursive Kalman filter. The estimation errors obtained through simulation for Case 3 are exhibited in Figs. 44 through 49. Figures 44, 45, and 46 show the estimation errors for $\Delta \tau$ = 20, 50, and 100 sec, respectively, when the sample interval is $\Delta \tau$ = 2.0 sec and there is no data presmoothing. The estimation errors exhibited in Figs. 44 through 49 indicate that, for Case 3, the piecewise-recursive Kalman filter has acceptable performance for $\Delta \tau$ as large as 100 sec, with Δt = 1.0 or 2.0 sec.

Recall that the error magnitudes plotted in Fig. 37 for the fully implemented (extended) Kalman filter with a sample interval of Δt = 1.0 sec show that after 30 sec of filtering, the error in estimated position is less than 6,000 ft and the error in estimated velocity is less than 200 ft/sec. Figures 44 through 49 indicate that for Case 3, the
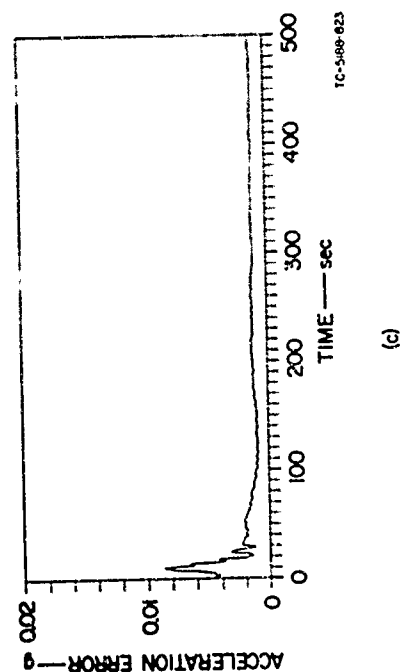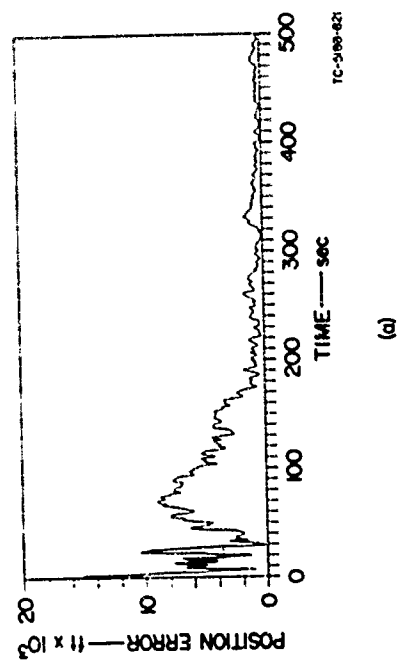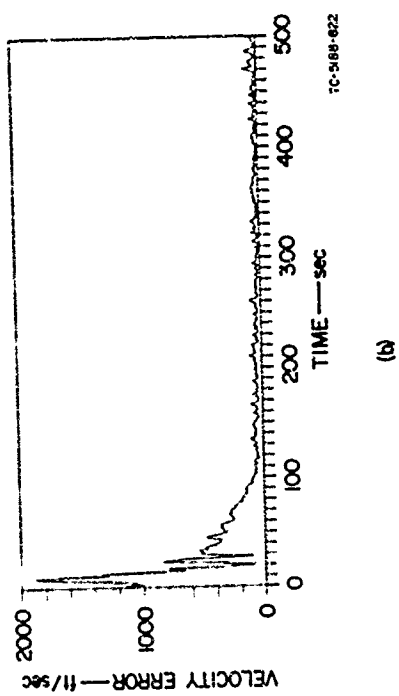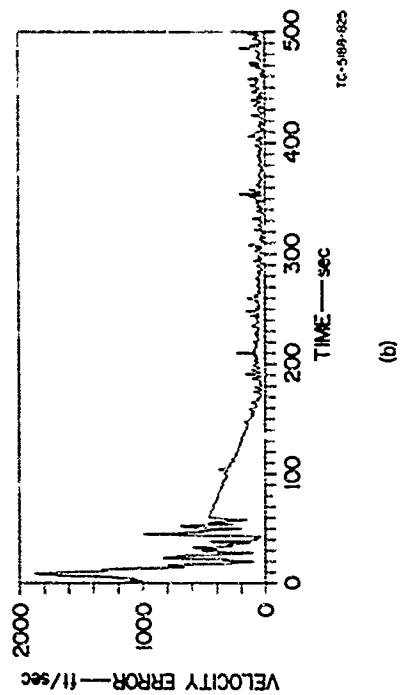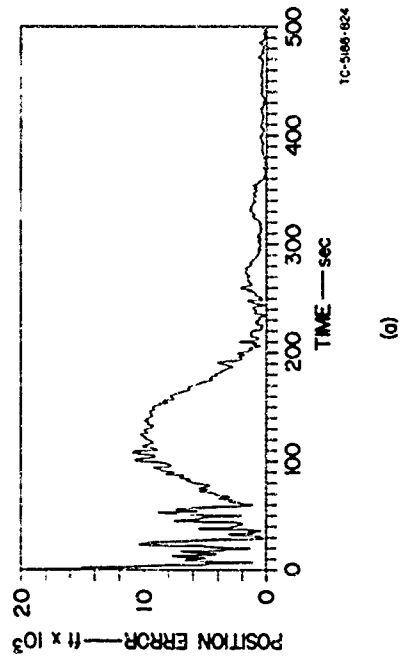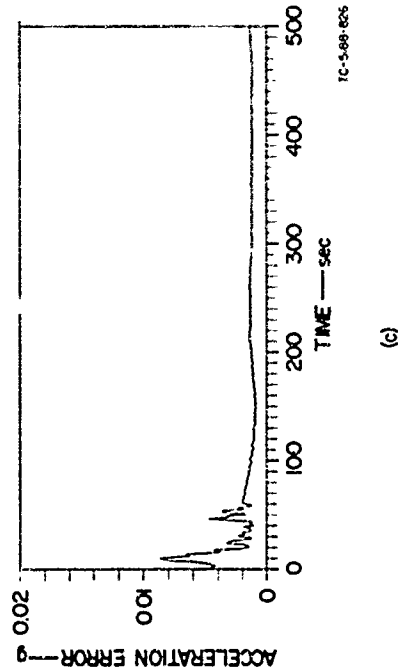
83

FIG. 44   ESTIMATION ERRORS FOR PIECEWISE–RECURSIVE KALMAN FILTER — CASE 3,
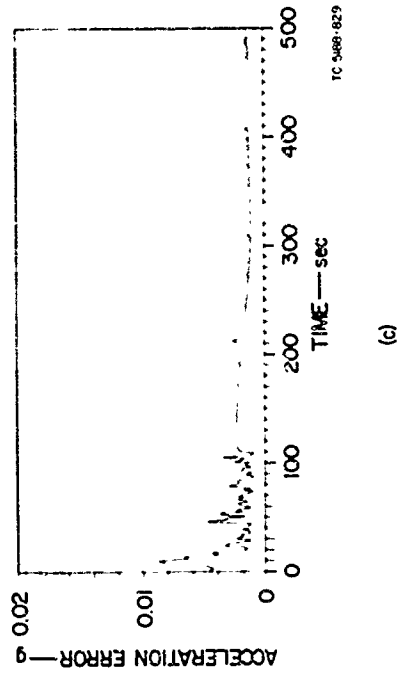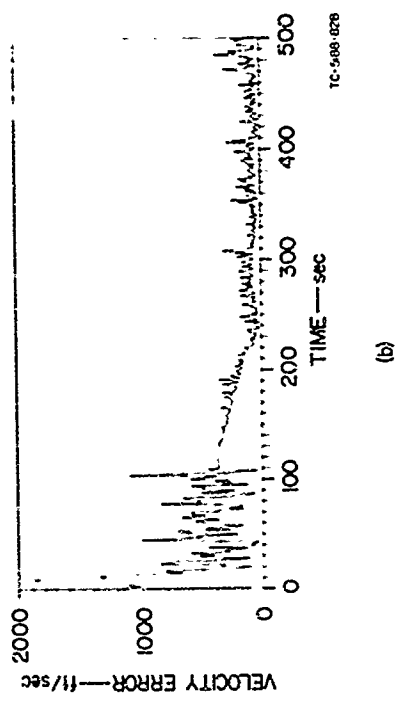$\Delta t = 1.0$ sec   AND $\Delta \tau = 20$ sec

84

FIG. 45 ESTIMATION ERRORS FOR PIECEWISE-RECURSIVE KALMAN FILTER — CASE 3,
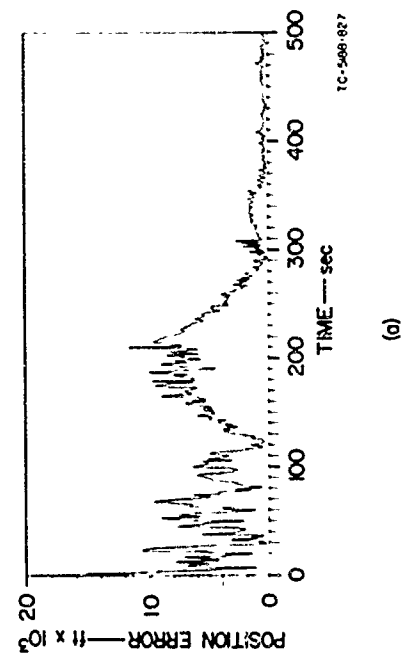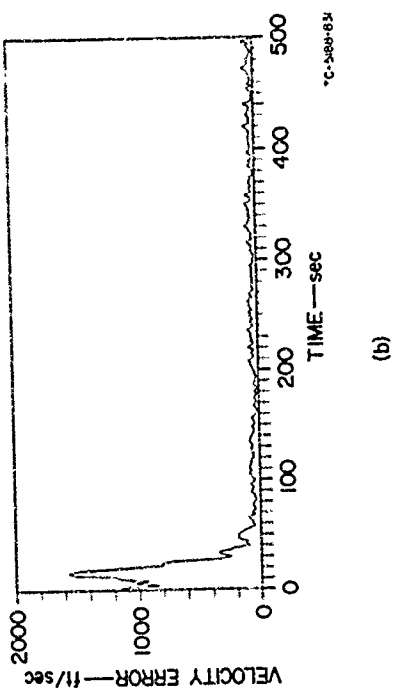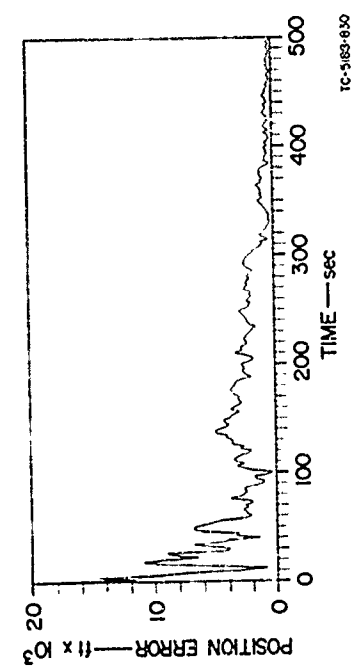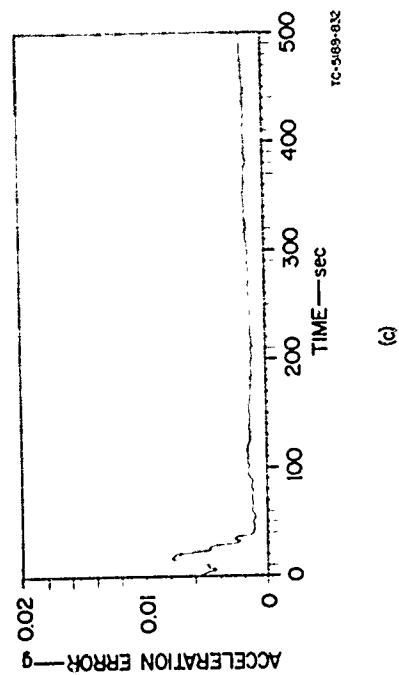Δt = 1.0 sec AND $\Delta \tau$ = 50 sec

FIG. 46 ESTIMATION ERRORS FOR PIECEWISE-RECURSIVE KALMAN FILTER — CASE 3,
$\Delta t = 1.0$ sec AND $\Delta \tau = 100$ sec

86

FIG. 47 ESTIMATION ERRORS FOR PIECEWISE-RECURSIVE KALMAN FILTER — CASE 3,
$\Delta t = 2.0$ sec AND $\Delta \tau = 20$ sec

87

FIG. 48 ESTIMATION ERRORS FOR PIECEWISE-RECURSIVE KALMAN FILTER — CASE 3,
$\Delta t = 2.0$ sec AND $\Delta \tau = 50$ sec

88

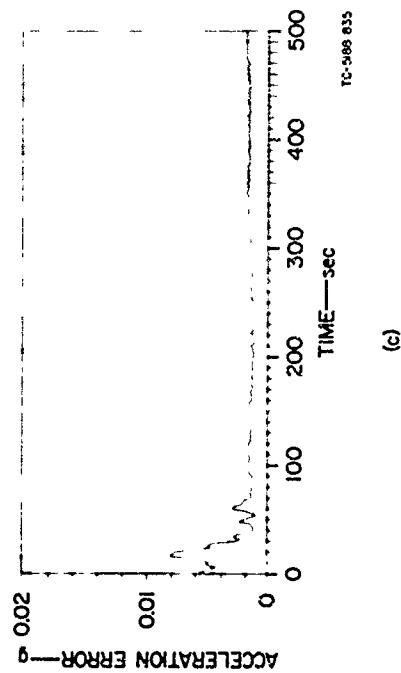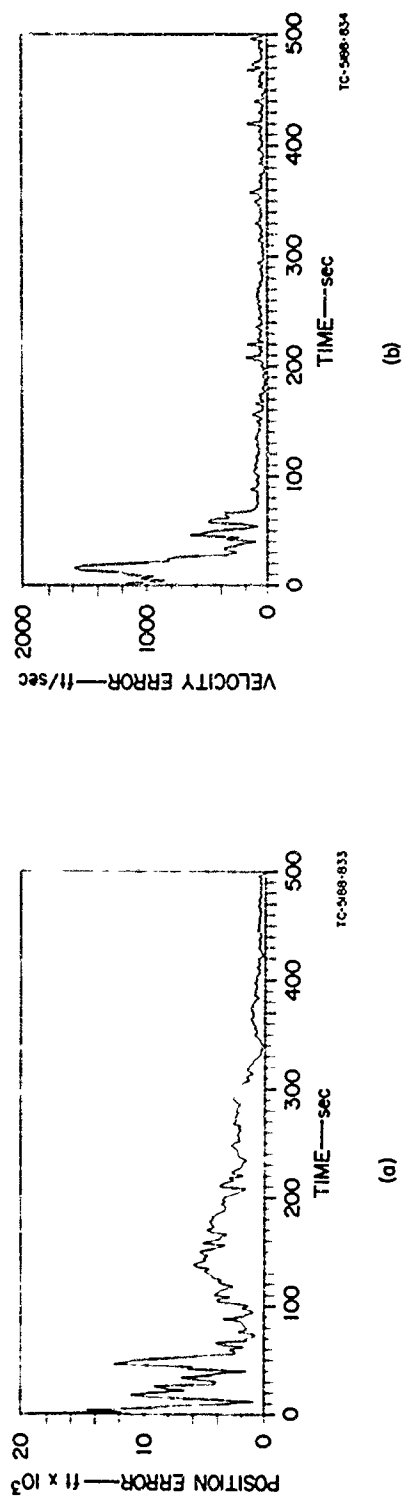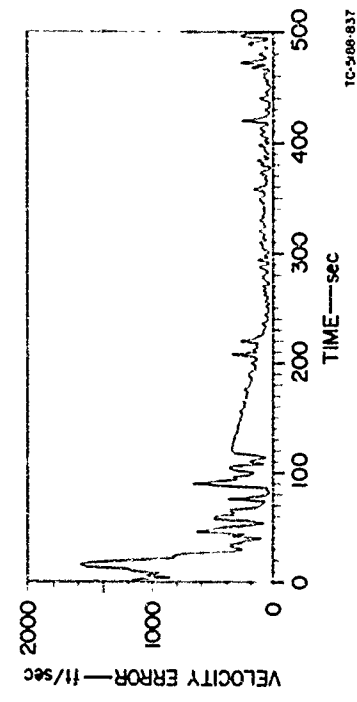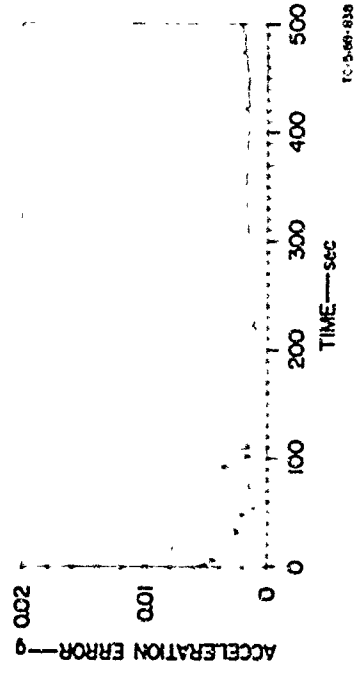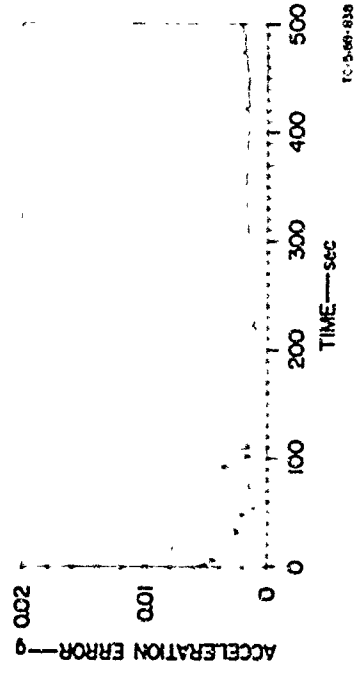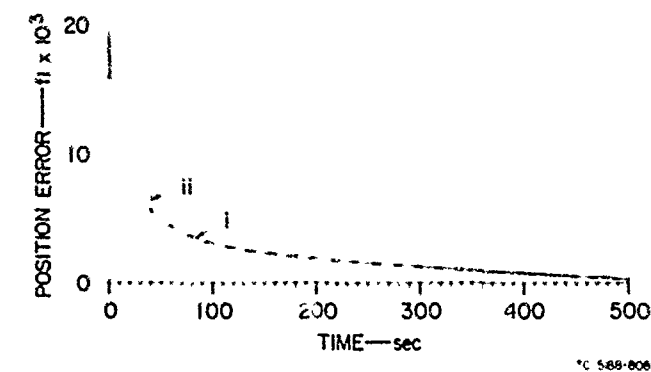FIG. 49 ESTIMATION ERRORS FOR PIECEWISE-RECURSIVE KALMAN FILTER — CASE 3,
Δt = 2.0 sec AND Δτ = 100 sec

piecewise-recursive Kalman filter estimation errors do not converge as rapidly as those of the fully implemented Kalman filter; however, in the worst case (Δt = 1.0 or 2.0 sec and $\Delta\tau$ = 100 sec) the position estimation errors are less than 6,000 ft after 230 sec and the velocity estimation errors are less than 200 ft/sec (except for infrequent excursions) after 200 sec.

Figure 50 shows the standard deviations (for Case 3) of position and velocity estimation errors [as calculated from $P(k/k)$] for (i) the fully implemented Kalman filter with a sample interval, Δt = 2.0 sec, and (ii) the piecewise-recursive Kalman filter with Δt = 2.0 sec and $\Delta\tau$ = 20 sec. These two curves indicate that the assumption made in Eqs. (36) and (37) of Sec. IV concerning the approximation of the filtering done by the piecewise-recursive Kalman filter is valid. Specifically, we had considered the filtering done with a fixed weighting

(a)

(b)

FIG. 50 STANDARD DEVIATIONS FOR PIECEWISE-RECURSIVE KALMAN FILTER — CASE 3, Δt = 2.0 sec: (i) $\Delta\tau$ = 2 sec, (ii) $\Delta\tau$ = 20 sec
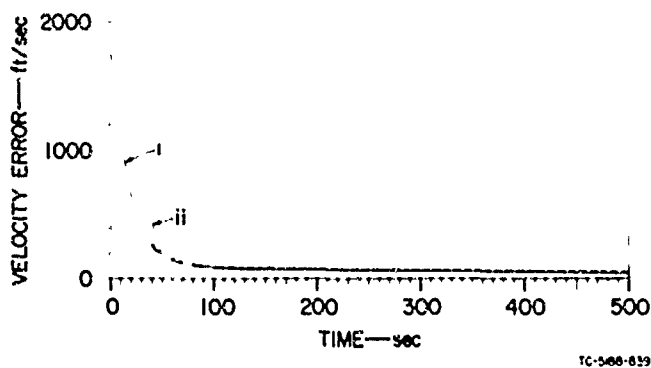
90

matrix as being equivalent to measurement presmoothing, so that when the estimation error covariance matrix was updated [see Eq. (37)], the calculation used a measurement noise covariance reduced to $R(k) \, \Delta t / \Delta \tau$. The validity of this assumption is verified in Fig. 50, since each new calculation of the estimation error covariance at intervals $\Delta \tau$ sec gives a decrease to nearly the value of the covariance matrix obtained with the use of the fully implemented Kalman filter when it is calculated at intervals of Δt sec.

In summary, the computer simulations indicate that for exoatmospheric estimation the accuracy of the piecewise-recursive Kalman filter is comparable with that of the fully implemented Kalman filter, and that it offers significant savings in computation time.

VII   CONCLUSIONS AND RECOMMENDATIONS FOR FUTURE STUDY

This study has addressed itself to the problem of real-time implementation of the Kalman filter for estimating ballistic trajectories. As shown in this study and Ref. 1, the Kalman filter is an extremely effective algorithm for estimation of ballistic trajectories, although the computational requirements of the fully implemented Kalman filter are quite severe. On the Univac 1108 Computer, the fully implemented Kalman filter runs about five times faster than real time for the endoatmospheric cases and about 100 times faster than real time for the exoatmospheric cases.

In this report, several approaches that may be used to modify the Kalman filtering algorithm in order to reduce the computational requirements are described. The most promising approach of those considered is the piecewise-recursive Kalman filter, which is described in Sec. IV. As shown by the numerical results obtained from extensive computer simulations (see Secs. V and VI), the piecewise-recursive Kalman filter can process measurements of a single target at a computational speed (on the Univac 1108) that is about 20 to 25 times faster than real time for the endoatmospheric cases and about 500 times faster than real time for

the exoatmospheric cases, and yet obtain estimation accuracy approaching that of the fully implemented Kalman filter. This increased filter capability is invaluable for the real-time estimation of multiple targets.

Other investigations that should be performed in order to further reduce the computation time of the piecewise-recursive Kalman filter are:

(1) Use a piecewise-linear weighting matrix in the filter, rather than a piecewise-constant weighting matrix as described in Sec. IV. This approach can be readily incorporated into the existing computer program and should yield significant reductions in computation time for comparable filter performance by allowing larger values of $\Delta\tau$.

(2) Vary Δt and/or $\Delta\tau$ over different portions of the estimation interval. This approach can be placed upon a rigorous basis by applying the sensitivity results obtained in Ref. 6, and it also should reduce the filter's average computation time per iteration.

(3) Simplify the model of the system equations that is used in the filter's covariance calculations. As shown in Table I of Sec. III C, these covariance calculations comprise the major portion of the computation time per filter iteration.

REFERENCES

1. R. E. Larson, R. M. Dressler, and R. S. Ratner, "Application of the Extended Kalman Filter to Ballistic Trajectory Estimation," Final Report, Contract DA-01-021-AMC-90006(Y), SRI Project 5188-103, Stanford Research Institute, Menlo Park, California (January 1967).

2. R. E. Larson, R. M. Dressler, R. S. Ratner, and B. L. Ho, "Applications of the Extended Kalman Filter to BRV and MRV Trajectory Estimation (U)," Final Report, Contract DA-01-021-AMC-90006(Y), SRI Project 5188-203, Stanford Research Institute, Menlo Park, California (December 1967), CONFIDENTIAL.

3. Y. Kashiwagi, "Prediction of Ballistic Missile Trajectories," Menoramdum 37, Contract DA-01-021-AMC-90006(Y), SRI Project 5188-305, Stanford Research Institute, Menlo Park, California (June 1968).

4. R. Kalman, "A New Approach to Linear Filtering and Prediction Problems," Trans. ASME, J. Basic Engineering, pp. 35-45 (March 1960).

5. J. Peschon, R. M. Dressler, L. Meier III, and R. E. Larson, "Research on the Design of Adaptive Control Systems," Final Report, Contract NAS 12-59, SRI Project 5578, Stanford Research Institute, Menlo Park, California (July 1966).

6. B. L. Ho, "Sensitivity of Kalman Filter with Respect to Parameter Variations," Memorandum 33, Contract DA-01-C21-AMC-90006(Y), SRI Project 5188-305, Stanford Research Institute, Menlo Park, California (March 1968).

7. G. McGlone, "Comparison of the Accuracy of the Kalman-Bucy and Second-Order Filters," Memorandum 254, Stanford Research Institute, Huntsville, Alabama (October 1966).

8. J. D. McHenry and P. K. Whalen, "NIKE-X MSR Error Equations (U)," Technical Note SED 140, Stanford Research Institute, Menlo Park, California (September 1966), SECRET.

9. R. S. Ratner, "Noise Model of NIKE-X MSR for Implementation in Extended Kalman Filter (U)," Technical Memorandum 22, Contract DA-01-021-AMC-90006(Y), SRI Project 5188-203, Stanford Research Institute, Menlo Park, California (February 1967), SECRET.